Ref. Ares(2024)9287128 - 31/12/2024

HVDC-WISE

Deliverable 3.2

Control for AC/DC Architectures

Document Properties

Funding Program	Horizon Europe and UK Horizon Europe funding guarantee
Grant Agreement Number	101075424 (UK 10041877 and 10051113)
Project	HVDC-WISE
Deliverable Id	D3.2
Title	Deliverable 3.2
Distribution Level	SEN
Due Date	31/05/2024
Date Submitted	
Status	***Draft*** */ Submitted / Final*
Version	1
Work package / Task	WP3, Task 3.2
Authors	Monika Sharma (TU Delft) Robert Dimitrovski (TenneT TSO GmbH) Sophie Coffey (Strathclyde University) Ying Pang (Supergrid Institute) Lars Osterkamp (RWTH Aachen University) Lampros Papangelis (Engie) Antoine Knockaert (Engie) Diego Cirio (RSE) Juan-Carlos Gonzalez (Supergrid Institute) Jose Rueda Torres (TU Delft)

Version History

Version	Date	Comment
0.1	12/07/2024	First version for review
0.2	19/08/2024	Revised after review
0.3	01/10/2024	Revised after review

Approval Flow

Title	Person	Date	Comment
Reviewers	SSE SGI TENNET	21/10/2024	
WP Lead	Robert Dimitrovski	21/10/2024	
Coordinator	Juan Carlos GONZALEZ	21/10/2024	

HVDC-WISE is supported by the European Union's Horizon Europe programme under agreement 101075424.

UK Research and Innovation (UKRI) funding for HVDC-WISE is provided under the UK government's Horizon Europe funding guarantee [grant numbers 10041877 and 10051113].

Contents

List of Figures

List of Tables

Executive Summary

This report presents the main outcomes of Task T3.2 related to Control for AC/DC Architectures, which is part of Work Package WP3 within the HVDC-WISE project. Task T3.2 aims to introduce innovative control concepts tailored to future AC/DC architectures to increase the reliability and resilience (R&R) of large-scale hybrid AC/DC systems. The proposals aim to strengthen system resilience and reliability by enhancing the grid's ability to respond effectively to events and disturbances, focusing on both core and supplementary control layers.

Key findings include:

- **Core Control Functions**:
    - An enhanced control strategy is proposed to combine grid-forming (GFM) with DC voltage droop control. With two simple modifications, GFM can integrate with DC voltage droop control to improve small-signal stability and DC voltage security during N-1 contingency ride-through. Additionally, the proposed control can provide inertia support by redistributing power from other AC areas, without requiring communication and without causing significant disturbances to the DC voltage.
    - Small-signal models assess the "firewall" capability of GFM converters, highlighting the role of key parameters impeding disturbances to propagate between grid regions.
    - A fuzzy logic-based controller is introduced to mitigate DC oscillations during post-fault recovery, demonstrating better performance over traditional methods.
- **Supplementary Control Functions**:
    - A coordinated control layer for active power-based services—such as power oscillation damping, AC line emulation, and frequency reserve sharing—is proposed, effectively reducing interactions with DC voltage control. Among these services, the AC line emulation function shows particular potential to enhance system resilience by automatically redistributing power to prevent cascading failures following disturbances.
    - A proposed supervisory control system enhances DC voltage stability and manages unbalanced conditions, supporting reliable operation across varying grid states.

Using adapted simulation tools, the implementation and performance of these proposals are analysed. The numerical analyses demonstrate the feasibility and effectiveness of these strategies in enhancing the resilience of HVDC-HVAC architectures. These findings lay a foundation for future work packages that will test these strategies in practical scenarios.

1. Introduction

The future of the electric power grid demands a transformation to accommodate large-scale renewable energy integration. High-Voltage Direct Current (HVDC) technology, with its rapid development, is increasingly seen as a critical solution. HVDC grids offer distinct advantages over traditional AC systems, enabling cost-effective and secure transmission of renewable energy over long distances. This technology not only facilitates the connection of remote offshore wind farms but also promises higher transmission capacities, particularly when compared to cable-based AC connections. As HVDC integration grows, the need for a comprehensive understanding and control of these combined AC/DC systems increases to ensure their resilient operation.

This report presents the main outcomes of Task T3.2 related to **Control for AC/DC Architectures**, which is part of Work Package WP3 within the HVDC-WISE project. Task T3.2 aims to introduce innovative control concepts tailored to future AC/DC architectures, addressing the Transmission System Operators' (TSOs) requirements for a reliable and resilient (R&R) hybrid AC/DC system. These efforts are closely aligned with the project's overarching objectives.

The controllers proposed in this report are designed not only to ensure the operation of HVDC systems as an integral part of the transmission grid but also to fully exploit their potential to enhance the R&R of the entire AC/DC system. Our proposals aim to bridge the existing gaps identified in current systems and provide advanced functionalities for improved system performance.

For the different proposals in this report, a state-of-the-art review is presented to highlight the gaps addressed by our investigations. Then, the proposed controls are detailed. Finally, to evaluate the performance of our proposals, comprehensive simulations in simple and representative test systems are performed. These innovative proposals form the basis for defining the functionalities that will be included and tested in subsequent work packages.

1.2 Objective of T3.2

The main objective of this report is to propose enhancements to existing HVDC control systems to increase the resilience and reliability of the system. These control enhancements span different control layers, starting at the converter level and extending to higher control levels that may require coordination between stations via communication. Given the limited experience with MTDC systems, there is currently no consensus on the demarcation and definition of these control layers. Therefore, to provide structure to this report, we adhere to the guidelines set forth in IEC TS 63291-1:2023 [1], which proposes a hierarchical control structure. This structure, illustrated in Figure 1.1, will be followed throughout this report. Although the definitions of the different control layers, their included functions, and the associated response times are still under discussion (see references [1] [2] [3]), we will use this framework to differentiate between **core control functions** and **supplementary control functions**, thereby providing a clear structure for this report.

The **core control functions** are implemented inside each converter and rely on information and measurements that are locally available to each converter. These functions are critical for the operation of each converter (valve switching and internal converter controls) and of the HVDC grid (DC node voltage control) and have very fast response times up to some tens of milliseconds. On the other hand, the **supplementary control functions**, are functions that might involve coordination via communication (e.g., from a central HVDC grid controller to HVDC stations or remote measuring points). Consequently, they have longer response times compared to core control functions. If communication between this supplementary control functions layer and a part of the HVDC grid, such as an AC/DC converter station, is lost, the supplementary control functions might not be fully operational, depending on the architecture of the control implemented (centralized, distributed, with or without backup). This differentiation between control layers will serve as the basis for structuring this report.

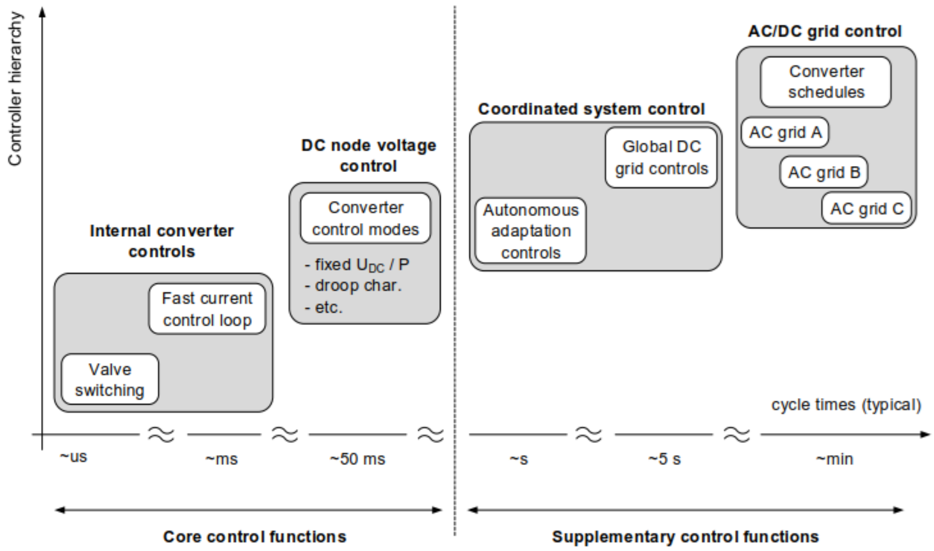

FIGURE 1.1: IEC STANDARD GUIDELINES (FIGURE FROM IEC TS 63291-1:2023).

In this deliverable, the objective is to propose a variety of enhancements to known controls in the literature at the different control layers. These enhancements are tested separately in the different sections of the report, the combination of the controls belonging to the core control layer and to the supplementary control layer will be discussed in future WPs.

1.3 Outline of report

The structure of this report is as follows:

- Chapter 2 focuses on **core control functions.** It begins with a brief recall on the mechanisms to achieve **DC voltage control and synchronization with the AC grid**, essential functions for the normal operation of the HVDC grid. Following this, we discuss our **new proposals for implementing and combining these functions**, e.g., DC voltage control and AC grid synchronization under various grid conditions. The chapter concludes with an examination of **power oscillation damping on the DC** side of the converter, highlighting innovative solutions to manage these oscillations.

- Chapter 3 explores the **supplementary control functions.** It starts by introducing new control concepts designed to provide **active power-based services to the AC grid**. These services include power oscillation damping, frequency control, and AC line emulation, achieved through coordinated efforts across HVDC stations. Next, we detail a **new supervisory (secondary) DC grid control** concept aimed at securely redistributing the DC grid in response to DC events.

- Chapter 4 summarizes our contributions, summarizes also how the different controllers can affect the R&R levels of the system and provides some insights on how these results can impact the following work packages.

Additionally, Appendices A offer details about simulations of post-fault recovery process.

1.4 Outcomes of T3.2 and relation with other tasks (e.g. T3.3, WP4, etc.)

The outputs of T3.2 include the design criteria, implementation, and tuning recommendations for control functionalities, which are disseminated across WP4, WP6, and WP7. These contributions significantly advance their respective tasks. The control functionalities introduced in T3.2 not only provide guidance for individual components in WP4 but also serve as foundational elements for use case development in WP6 and WP7, where they undergo evaluation.

2. Core functions

This chapter addresses the functions that can be achieved via controllers implemented at the "Core Functions" layer, as defined in IEC TS 63291-1:2023. These functions are implemented within each converter and rely on locally available information and measurements.

This chapter firstly presents a brief review on DC voltage control and AC grid synchronization. In the second part of the chapter, we introduce our first proposals through control concepts designed to fulfil these functions under different grid conditions. The final part of this chapter addresses a specific optional function: damping oscillations on the DC side following a DC fault.

2.1 Minimum Requirements for System Normal Operation

This section recalls the basics of **DC voltage control and AC grid synchronization**, essential functions for the operation of HVDC grids to operate as an integral part of the AC transmission system.

2.1.1 Control of DC voltage

To achieve its primary goal of power transmission, an HVDC system must first ensure continuous and secure operation. Preventing power flows and DC voltages from exceeding the physical limits of system components in case of disturbance is therefore crucial, since if these fluctuations exceed system limits, the entire system may be jeopardized. Therefore, AC/DC converters must respond rapidly and collaboratively to restore energy balance through DC voltage control mechanisms, ensuring the HVDC system's secure operation. Effective DC voltage control strategies are essential for operational reliability, maximizing power transmission efficiency, and enhancing the grid's ability to handle dynamic changes in load and generation. A deviation in DC system voltage reflects an imbalance of the pre-disturbance power flow. Primary DC voltage control is essential for correcting this imbalance and restoring system stability.

This section provides a brief overview of the two main control strategies used to manage voltage levels across multi-terminal DC (MTDC) networks, beginning with the general principles of voltage control in larger DC systems.

Master-Slave Control

The master-slave control strategy is traditionally used in point-to-point HVDC systems. In this configuration, one converter, known as the *Master* (or the converter in fixed DC voltage control mode), is responsible for maintaining the DC voltage at its connection point at a desired setpoint specified by the operator or a higher control layer. The *Master* converter achieves this by automatically adjusting its active power injection or absorption. Meanwhile, the other converters, known as *Slaves* (or converters in fixed active power control mode), are set to follow fixed active power references defined by the operator or higher control layers.

In this setup, the Master converter is solely responsible for compensating any active power imbalances in the HVDC system. This arrangement has two main drawbacks: (a) the ability to compensate for imbalances is limited by the maximum HVDC active power transmission capacity of the Master converter (which can be particularly problematic in multi-terminal configurations), and (b) having only one converter in charge of DC voltage control creates a single point of failure, which could result in a network shutdown if the *Master* converter fails [4]. Therefore, when implementing the master-slave configuration, failure changeover mechanisms are necessary to handle potential Master converter outages. The Voltage Margin Method, subcategory of a pure master-slave control, employs a backup Master converter to the master-slave control [5]. This backup Master operates as a Slave under normal conditions but can take over as Master if the primary Master fails or if voltage deviations or rather predefined voltage thresholds are exceeded, ensuring continuous and stable power delivery [4].

DC voltage droop Control

The concept of DC Voltage Droop Control (DVD) is widely recognized in both industry and academia and is one of the most cited methods for voltage regulation in multi-terminal DC (MTDC) systems. The principle behind this method allows multiple converters to **autonomously adjust their active power output, working collaboratively to stabilize the network's voltage in response to power disturbances**. DVD is analogous to frequency droop control in AC systems and is particularly useful for systems that operate without a centralized communication infrastructure [4].

Despite its widespread recognition, there are still different definitions of DC voltage droop control, as it can be defined in various ways using different measured variables or control outputs (e.g., based on active current or active power). In this report, we adopt the definition from [2]: The DC voltage droop (DVD) refers the ***"change of active power in response to a deviation of the DC voltage from its reference value".***

Following the definition, the DC voltage droop can be expressed in the following manner:

$$\Delta P = P - P^* = K_P(V_{DC} - V_{DC}^*) \tag{2-1}$$

Where, ΔP is the change of active power defined as the difference between the measured active power P and the Active power set-point P^*. V_{DC} is the measured DC voltage at the DC point of connection and V_{DC}^* is the DC voltage set-point. Finally, K_p is the droop characteristic (also referred to as the droop gain in this report), which defines the relationship between changes in active power and deviations in DC voltage. Figure 2.1 illustrates a classical proportional droop characteristic following the proposed definition. In this case, a higher value of K_p leads to a greater variation in active power output in response to changes in DC voltage.

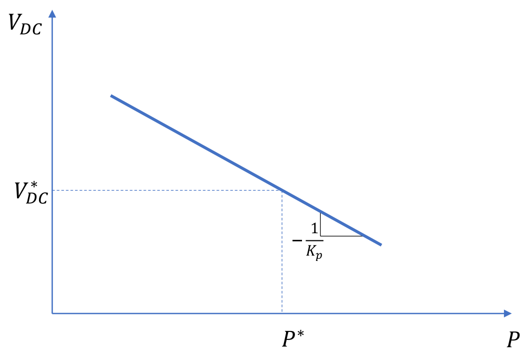

FIGURE 2.1: EXAMPLE DROOP CHARACTERISTIC OF A CONVERTER

It is important to note that droop characteristics can follow different forms; for example, recent collaborative projects have proposed for example a piecewise representation of this characteristic [3].

The key advantages of DC voltage droop control are that it promotes redundancy and resilience by distributing control across multiple converters, while also enhancing the flexibility and scalability of grid operations. Although this method is generally considered the most appropriate for multi-terminal HVDC, there are still some locks and challenges for its application in real projects [3] [6].

Both described methods “master-slave” and “DC voltage droop control” will be used in the following chapters of this report.

2.1.2 AC grid synchronization

Synchronization of grid-connected power converters is essential for stable operation alongside other devices in the AC grid. Unlike synchronous generators, which naturally remain synchronized with the grid during normal operation due to inherent synchronizing torque, converters rely on dedicated control actions to achieve and maintain synchronization and restore it after disturbances. This section reviews the grid-following and grid-forming converter control philosophies, including their mechanisms for achieving grid synchronization.

Grid-following and synchronization via a phase-locked loop (PLL)

Grid-following control (GFL) refers to a generic control concept of grid-connected converter by which the **converter is controlled as a current source** (See Figure 2.2) typical via vector current control. The controlled current source aims to fulfill the system active and reactive power setpoints given from higher level controller of the grid by injecting active and reactive current relative to the phase and magnitude of the voltage the point of connection. These phase and magnitude measurements are typically made by **synchronization units, such as phase-locked loops (PLLs)**. By tracking the voltage phase, the PLL enables the control to lock the reference rotating frame of the converter—usually the d-axis—to the terminal voltage.

Historically, GFL has been widely adopted in transmission power systems, particularly for power converter-interfaced resources. This control approach initially focused on efficiently feeding maximum power into a robust grid, with less emphasis on supporting grid characteristics. In systems such as wind, solar, and high-voltage direct current (HVDC) applications, where DC voltage regulation is also required, the vector current control also follows additional current references needed to maintain the DC voltage, alongside fulfilling the PQ setpoints [7] [8].

Grid-forming and self-synchronization of converters

Grid-forming control refers to a generic control concept of grid-connected converter by which **the converter is controlled as stiff voltage** source behind impedance (See Figure 2.2). **The voltage source synchronizes with the AC grid typically via an active power control** that defines the converter internal angle necessary to stabilize the active power injections [9]. GFM converter can be controlled to only fulfill PQ setpoints by the system or in the case where energy storage is available, can be controlled to provide **additional services to the AC grid, such as frequency support in the form of inertial response—a service that will receive special attention in the following sections**. During disturbances like AC faults, the stiff voltage source behavior can be limited by the converter overcurrent protection.

As grid strength and short-circuit power decline due to the decommissioning of conventional voltage sources, the emphasis on converters’ ability to “form” the grid voltage, rather than simply “follow” it, has increased. Consequently, operators are now beginning to require grid-connected converters to incorporate grid-forming capabilities.

In the literature, several grid-forming control structures have been proposed, including droop control [10], power-synchronizing control [10], (equivalent to droop), virtual oscillator control (VOC) [11] ,and virtual synchronous machines (VSMs) among others. In subsequent sections where grid-forming control is discussed, the VSM structure is used, with a description of this structure shown in Figure 2.6 in the next section. [12], power synchronising control (equivalent to droop [10]), virtual oscillator control (VOC) [11] [13], and virtual synchronous machines [10], [14], [15], [16] [17] [18] [19] [20]. In the further sections, where grid forming control is used, the topology is that of the VSM, and a description of the structure used is shown in Figure 2.3.

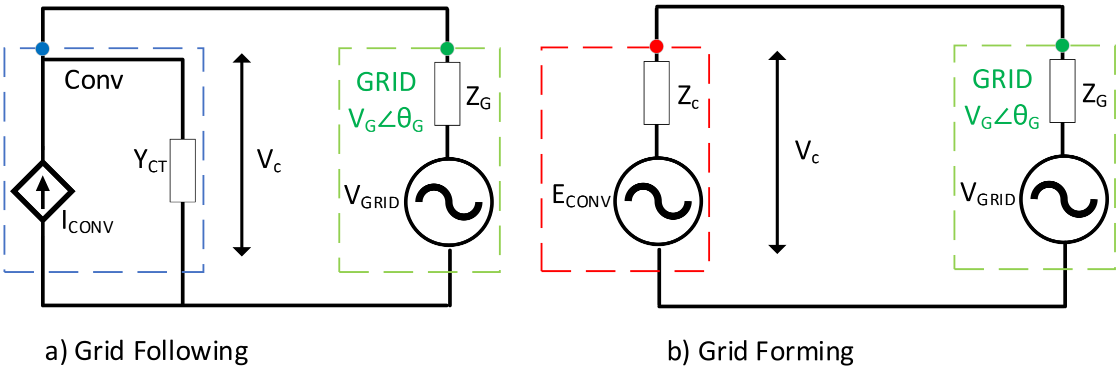

FIGURE 2.2: GRID FOLLOWING AND GRID FORMING EQUIVALENT REPRESENTATIONS.

To summarize and for the sake of clarity, in the context of this report, grid-forming behaviour will refer to a converter operating as a voltage source behind an impedance, while grid-following control will describe a converter functioning as a current source.

2.2 Fulfilling DC voltage control and AC grid synchronization

This section describes possible options and solutions to achieve the constraint functions via the control of the converter, i.e., what are the options to provide Vdc control and synchronization with the AC grid. Some of them are well known as grid following + Vdc droop, others are part of our contribution, i.e., grid forming + Vdc droop. The below sections state which combinations are feasible for the next steps of the project, why we believe they are important, and what are the associated challenges.

2.2.1 Innovation Focus

Section 2.1 has recalled the relevant information to this section. Based on this, the authors derive open research questions that have not yet been answered and research gaps that need to be addressed, which form the resulting innovation focus of this work package.

Innovation focus regarding core functionalities

It has been shown in 1.2 that there are already several investigations regarding the topic of the core functionalities for converters in the transmission system acting under weak grid conditions and the necessity of new requirements regarding grid stabilization control-schemes. So far research focuses heavily on single converter station or rather Point-to-Point (PtP) links. So far there is only very few publications dealing with the topic of this kind of converters acting under the influence of a bigger MTDC system behind. Especially **there is a gap in the interplay of DC side restrictions and AC side requirements** and how these interplay with the services that the system behind the converter station can deliver. For a high GFM active power delivery the power needs to be drawn either out of the DC-system or rather there need to be the headroom provided to buffer it from the converter.

In a Multi-Terminal Direct Current (MTDC) system, variations in inductances and line lengths on the DC side impact the system's dynamic response and stability. Coordinating different Transmission System Operators (TSOs) adds complexity, affecting power flow and voltage regulation. Maintaining an adequate voltage margin is essential for the system's reliability, ensuring control range for Grid Forming (GFM) converters, especially during transient conditions. The distribution of DC voltage control (Vdc) across terminals is crucial for balanced power flow and efficient MTDC network operation, which is vital when integrating variable renewable energy sources. In strong AC grids with a high Short Circuit Ratio (SCR), GFM converters face challenges in voltage control, necessitating advanced control strategies for stability and power quality. **Managing an MTDC system under GFM control involves coordinating diverse elements, maintaining voltage stability, optimizing Vdc share, and ensuring effective GFM operation in strong AC grids**. Developing robust GFM control algorithms and a standard test system for new controls is essential for system reliability.

There are two outlooks to be considered, for the focus on the core functionalities of converters in this work package, especially on the role of grid forming inverters in MTDC systems. The first focus is on the capabilities of the grid forming converter and the benefits they can provide to interconnected TSOs. This is based on the assumption that there is available reserve in other AC areas, allowing for TSOs to support other grids. Additionally, DC voltage droop control with grid forming control can be utilised to ensure power sharing amongst networks. **The first set of studies presented here will investigate the conflict of DC voltage droop control with emulated inertia, and highlighting how one AC area can support another after a disturbance through the HVDC system**. However, the “firewall” capability of HVDC can also be a desired feature, preventing propagation of a fault, oscillation, or disturbance from one AC area to the other. Therefore, **the second study set** presented **here will assess**

when one grid will draw support from the other, but problem oscillations won't propagate and the GFM does not have a negative effect on the other grid. Similarly, we can identify the parameter limits of this and identify cases where a GFM drawing support from another AC grid will negatively impact the other grid too much.

Outlook 1: The Path to Reserve Sharing between AC Areas by GFM MTDC and the Existing Gaps

1. Inertia Provision by GFM control

One of the features of GFM converter is its capability to provide inertia to the AC system. The underlying logic is that GFM control, with the opportunity to introduce the virtual inertia term in the control loops, can emulate the rotating mass inertia in the traditional synchronous generator, which has been broadly verified in the configuration where DC storages (such as batteries) are available, and no DC voltage control (DVC) dynamics are present in the GFM converter.

Two recent studies [21] [22] **have shown that there exist conflicts between DVC and inertia provision (INP).** Generally, they point out that to keep the DC voltage stable, the DVC will attenuate the INP. In HVDC applications, due to the small time constant of the DC voltage, the inertia constant must be kept below a small value to achieve fast power angle dynamics and thereby DC voltage stability.

The first gap identified is that the existing studies on INP by GFM either ignore the DVC or only examining the magnitude of inertia power response, neglecting its phase related to the frequency fluctuations, which is critical in determining whether true INP and frequency stabilizing effects can be delivered by the virtual inertia.

The second gap identified is that no study has been found in the literature that offers an insight into the INP dynamics of multiple GFM converters employed in MTDC with DC voltage droop (DVD) primary control. In this report, the INP dynamics of GFM converters in this configuration are first examined and a practical design guideline is also formulated.

2. DC Voltage Droop (DVD) Interactions with GFM Control

DVD is commonly used in MTDC to ensure power sharing between stations at the steady-state and ensure safe ride-through during active power contingency in the DC network. To achieve the second goal, the droop gain must be rather steep. Even though such droop gains have been used in studies where GFL are employed [23]. **Few studies have been done where such droop gains are combined with GFM control.** In our studies, it has been identified that that such droop gains when applied to GFM, introduces a great challenge into the system small-signal stability. Detailed analysis of such small-signal stability is provided to understand its mechanism, based on which new control methods are proposed to overcome this issue [24].

Outlook 2: The Path to HVDC Firewall and the Existing Gaps

Although it is of common understanding that GFM can provide benefits to the grid, there are some cases, especially when using GFM for transmission systems, where the benefits provided by the GFM to the connected AC grid result in unwanted propagation to the other AC grids.

Firewall capability has been described as "inherent" to HVDC systems due to the controllability of grid following power converters [25]. However, when replacing grid following with grid forming controllers, this inherent effect might be limited due to the role of the GFM in its support to the AC grid to which it is directly connected to. If the GFM support the AC grid during a disturbance, it will draw power from the HVDC link, and so will affect the AC grid on the other side of the link. This could lead to propagation of disturbances, such as sub and super synchronous oscillations [26]. The effect of different system and control parameters needs to be studied to highlight the conditions where this is worsened.

One identified gap in this outlook is that studies allowing to analytically analyse the propagations in HVDC systems using Modular Multi-level Converters (MMC) in GFM mode, are quite rare, particularly for more than one converter, that are not connected to a constant DC source. There are research items on the modelling of GFM-MMC converters connected to HVDC systems focusing solely on the stability of the directly connected AC grid, such as [27] and [28]. However, they do not assess the impact of the GFM on the propagation of oscillations to the AC grid on the other side of the HVDC link. Reference [29] provides a good analysis of energy-based control structures in grid-forming converters connected through an MMC-HVDC link to a connected grid following converter by assessing the eigen properties of the system. However, they focus on the energy balancing control, and do not vary the parameters of the system. The parametric limits of a GFM-MMC-HVDC to GFL-MMC system have not been assessed in the literature to assess what situations the GFM-MMC significantly affects the firewall capability of the system.

Therefore, in this work, we aim to address this gap by developing small-signal models of HVDC systems with MMCs under GFM control. These models will facilitate understanding of disturbance propagation through the HVDC system and allow for evaluating the impact of key parameters without the computational burden associated with non-linear time-domain simulations.

The key parameters investigated for their small signal impact on firewall capability are GFM inertia, GFM damping, DC voltage droop control (on GFL side) and circulating current control in GFM controller. The effect of SCR on converter stability has been extensively researched however the combination of the control parameters with varying SCRs needs to be investigated also. Small-signal modelling will be a useful tool to investigate the eigenvalue stability of the system under these parameters, as well as giving information of the participation of the system states and their influence on modes that are unstable, poorly damped, and of frequencies of concern.

2.2.2 Outlook 1: The Path to Reserve Sharing between AC Areas by GFM MTDC

Grid forming control results in the converter acting as a voltage source with low series impedance. Additionally, many grid forming controls provide ancillary services to support the AC grid they are connected to, by drawing support from the DC link. This is a desired benefit in many cases and will be the focus of the first set of results in this section. However, "firewall" capability is also a desired characteristic of HVDC applications, where the inherent controllability of the DC link prevents unwanted propagations from one AC grid to another. Seeing as many GFM controls aim to directly draw power from the DC link, this could affect this desirable feature. Therefore, the second set of results will in this section focus on this.

Proposed Control Method 1: Enhancing DC voltage stability in GFM MTDC and enabling inertia sharing between AC areas

The proposed control overcomes the instability problem identified by gap 2 but at the same time does not hinder the real INP properties that is enabled by DVD, as pointed in the discussion around gap 1.

1. The Phase compensator cascaded with DVD
    - From the small-signal modelling, it can be understood that the low-bandwidth nature of GFM in terms of active power control, leads to a significant phase lag even at around 1~5 Hz. This phase lag plus the aggressive droop gain leads to instability.

- Therefore, we apply the phase compensator (Pcom) to compensate for the phase lag around these frequencies.

2. The virtual power system stabilizer.
   - From the passivity analysis, it can be understood that Pcom introduces negative resistance at higher frequency (around 10 to 100 Hz), which could risk of amplifying the resonance formed by the DC reactors (DCRs) and DC capacitors.
   - To address this problem, the VPSS in is introduced which essentially imposes a positive DC current response to a positive DC voltage disturbance by increasing the AC voltage magnitude and thereby the active power from DC to AC. Equivalently, this introduces a positive resistive behaviour on the DC side and pacifies the DC side admittance around 10 to 100 Hz.

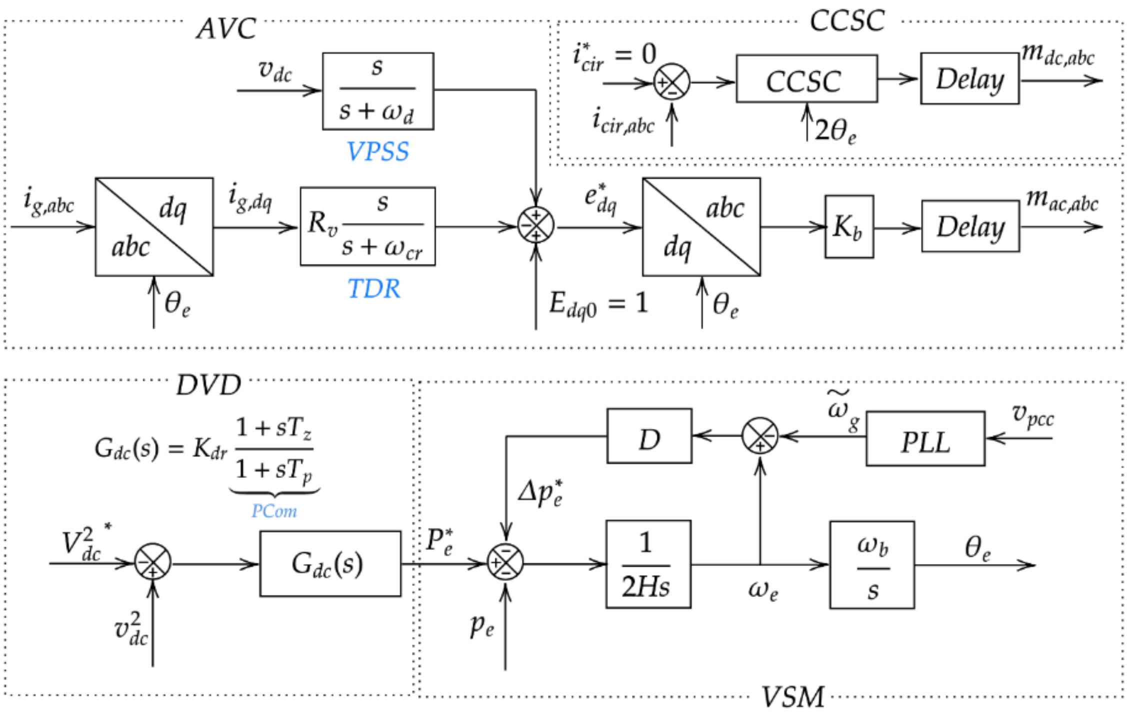

FIGURE 2.3: THE STRUCTURE OF THE PROPOSED CONTROL METHOD 1 FOR IMPROVED STABILITY WHEN COMBING GFM WITH DC VOLTAGE DROOP IN MTDC.

Test System for Control Method 1

To study the problem of low-frequency harmonic instability induced by interactions between DC voltage droop and GFM control, a 3-terminal MTDC grid with monopole Modular Multilevel Converters are modelled in EMTP-rv as the test system as shown in Figure 2.4. All MMC station models comprise 400 modules per arm with its total DC-side time constant designed as 40 ms. They share same control strategy as in Figure 2.3, with circulating current suppression control (CCSC) [30] as the internal control of MMC. Other types of internal control of MMC, such as energy-based control, will have an impact on the stability of the system, which is planned to be studied in future work package 7 of the project. DC reactors needed for DC protections are also included in the EMT simulations since they have a strong influence on the DC voltage harmonic stability. Wide-band DC cable models are also used in the simulations. The DC grid is rated at 525 kV and the AC grids is rated at 400 kV (line-to-line, RMS, connected by 320 kV / 400 kV transformers). The AC grids are assumed to be infinite AC buses.

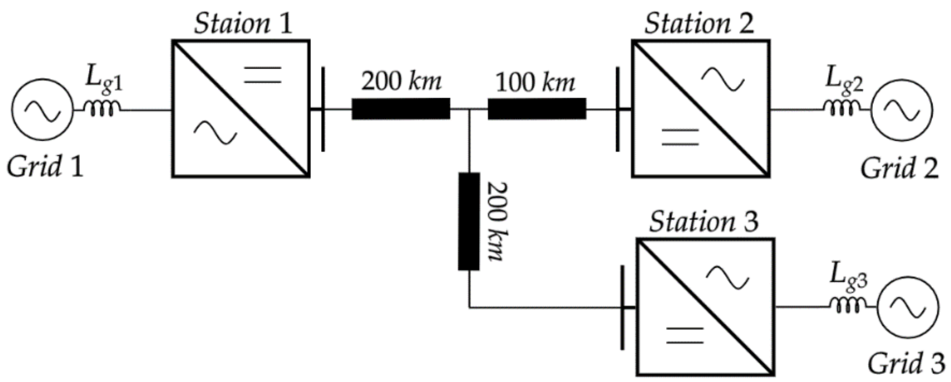

FIGURE 2.4: THE UNDERSTUDIED 3-TERMINAL SYSTEM.

Case Study 1 for Proposed Control Method 1: Low Frequency Harmonic Instability and its Inhibition

An in-depth study of N-1 contingency ride-through of MTDC has been done in [23] based on GFL control in each station. It shows that the aggressive DC voltage droop gains (e.g., 1 p.u. of DC voltage deviation translates to 5 to 20 p.u. of active power reference modification) are needed to secure DC voltage during contingencies. Through the study in [23], no harmonic instability was reported with GFL stations. However, when combining GFM with such droop gains, as shown in Figure 2.6, low-frequency harmonic instability is excited when there is PCom by-passed. The mechanism of such instability can be intuitively understood from Figure 2.5, where in the case of simple DC voltage droop control $G_{dc}(s)$ simply reduces to the droop gain. The core of the problem resides in the large-time-constant high-order low-pass filter nature of the VSM, which with the typical tuning practice, renders the phase of $G_{VSM}(s)$ to be below -90° around 1 to 5 Hz, at which frequency the DC capacitance impedance is large and introduces another -90°. If this is combined with a large droop gain, it would result in the open loop gain larger than 1 at low frequencies where the open loop phase shift is larger than -180° and thus instability occurs. Whereas with GFL control, since it comes with a much faster bandwidth (typical in the range of 200 Hz to 400 Hz for MMC), its phase crosses -90° at much high frequencies where the DC capacitance impedance decays significantly, rendering the open loop gain far smaller than 1 even with aggressive DC voltage droop gain and hence the risk of such instability is low.

It should be emphasized that such harmonic instability is different from the typical power-angle oscillations seen in traditional power systems induced by AC transients like faults or device disconnections [31]. It is induced by converter control dynamics that amplify small-signal disturbances of certain frequencies during steady-state operations. The detailed mechanism of such instability and why this issue does not appear when combing DVD with GFL is discussed in [24].

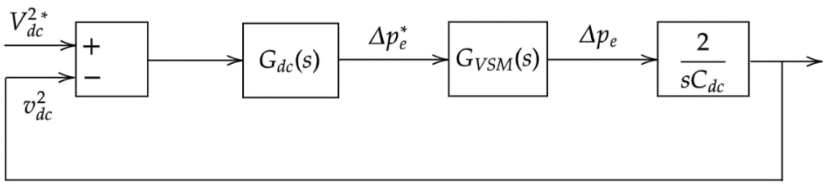

FIGURE 2.5: SIGNAL PATH FOR INTUITIVE UNDERSTANDING OF THE ROOT CAUSE OF THE HARMONIC INSTABILITY WHEN COMBING AGGRESSIVE DC VOLTAGE DROOP GAINS WITH GFM.

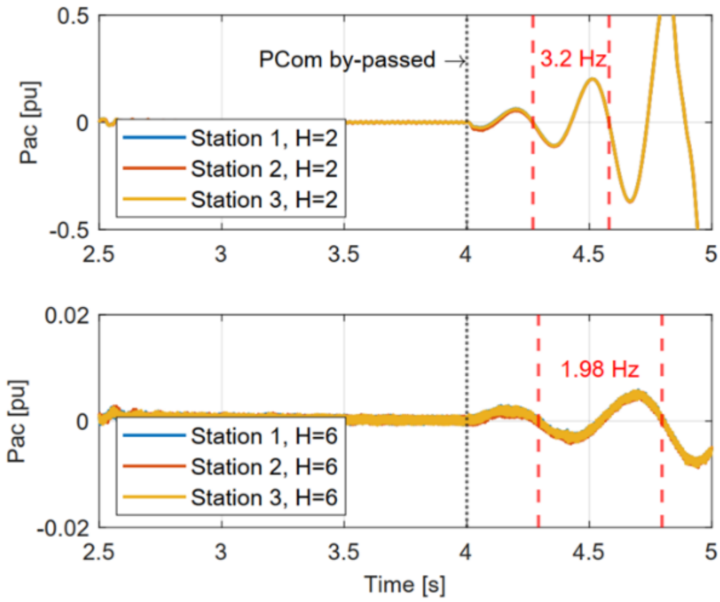

FIGURE 2.6: THE EFFECTIVENESS OF THE PHASE COMPENSATOR IN SUPPRESSING THE HARMONIC INSTABILITY DUE TO DVD/GFM INTERACTIONS.

However, as mentioned above, adding the PCom introduces strong non-passive behavior to the converters input admittance on the DC side around 10 to 100 Hz (See [24] for more details), which risks amplifying the resonances formed by the DC capacitance of the MMC and the DC reactors. With the VPSS introduced in proposed Control Method 1, the input admittance around this range of frequencies becomes passive again (See [24] for more details). The fundamental mechanism of the passivity enhancement introduced by the VPSS can be understood as in Figure 2.8 – if there is a positive disturbance on the DC voltage, it will increase the magnitude of the AC voltage magnitude through the high-pass filter, which leads to an increase of active power injection into the AC that translates to an increase of DC current and the resistive behavior on the DC admittance is thus increased.

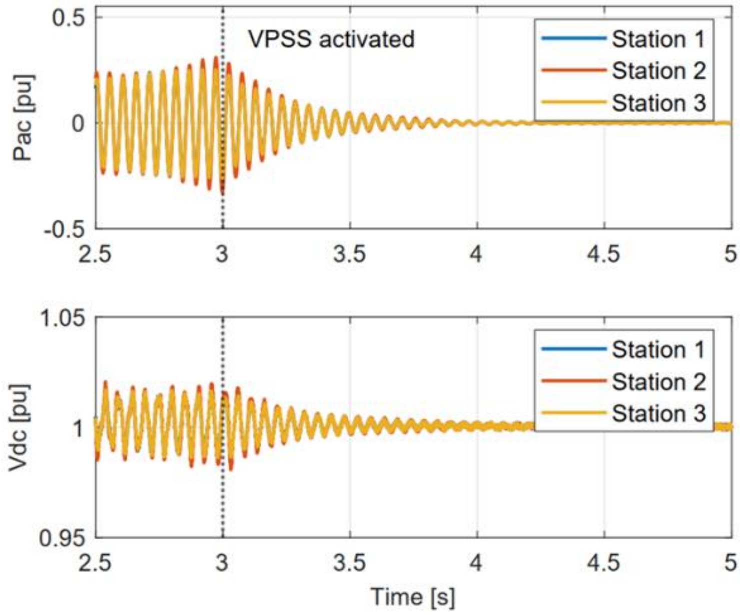

FIGURE 2.7: THE EFFECTIVENESS OF THE VPSS IN SUPPRESSING THE HARMONIC INSTABILITY DUE TO CONVERTER DYNAMICS THAT AMPLIFIES THE DC SIDE PASSIVE RESONANCE.

Figure 2.7 shows the effectiveness of the VPSS, where it can be seen that with the PCom but without the VPSS, resonance formed by the DC capacitance and the DC rector at 18 Hz are amplified by the negative resistance behavior of the converter and once the VPSS is activated, this resonance is suppressed by the enhanced resistive behavior.

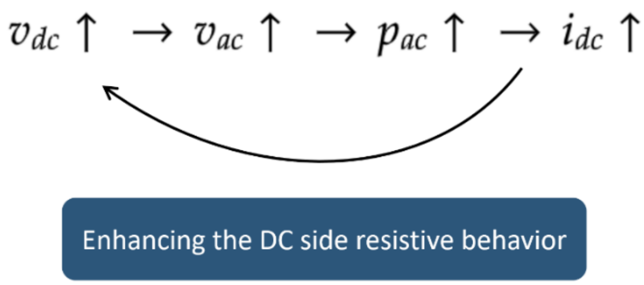

FIGURE 2.8: ILLUSTRATION OF THE PASSIVITY ENHANCEMENT BROUGH BY THE VPSS.

Design of the PCom

The main reason for the low-frequency oscillations was the large phase lag introduced by GFM VSM control at low-frequency. Therefore, the PCom should directly aim for compensating its phase around 1 to 5 Hz. A typical phase compensation technique is to introduce a zero to increases the phase by +90° and then cancel it with a pole at high frequency to avoid any high-frequency noise amplification by the zero. Based on this logic, it is recommended that the zero is placed around 1 Hz and the pole is placed around 500 Hz, which leads to $T_z = 0.2$ and $T_z = 3 \times 10^{-4}$ in Figure 2.3.

VPSS, TDR and VSM frequency separation

As mentioned above, the VPSS enhances stability by modifying the AC voltage magnitude. Yet, it is generally undesirable to have strong angle-magnitude (P and Q) coupling within the control since it might further induce other modes of oscillation or instability. Therefore, the key to designing the high-pass filter in the VPSS is to make sure that the VPSS is only active above the control bandwidth of the

VSM, e.g., $\omega_d = 10\pi\ rads/s$ is recommended for the VPSS high-pass filter. Similarly, when it comes to designing the high-pass filter for the transient-damping resistor (TDR) in Figure 2.3, the same logic applies and $\omega_d = 20\pi\ rads/s$ is recommended.

Case Study 2 for Proposed Control Method 1: Inertia Provision with a Single DC Voltage Station

As discussed previously, there lacks a proper examination of the true inertia power provided by a GFM station that controls DC voltage. In this section, inertia power is first examined by modifying the control in the system in Figure 2.3 as in Figure 2.9, where on Station 2 is controlling the DC voltage with a PI controller, and Station 1 and 3 are in constant power mode. Then, a frequency disturbance is introduced in Grid 2 and the active power response of Station 2 to that disturbance will be analysed to determine its characteristics in inertia provision.

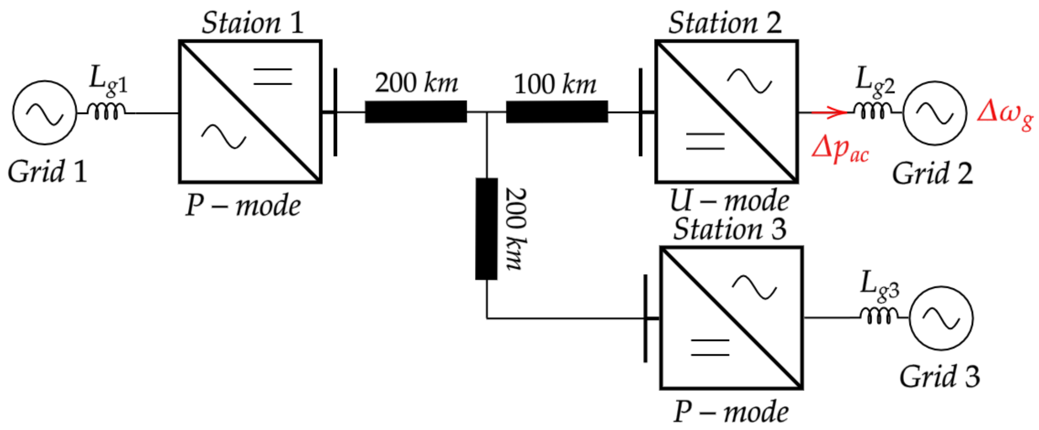

FIGURE 2.9: ILLUSTRATION OF THE CONFIGURATION FOR CASE STUDY 2.

All AC grids are modelled by ideal AC sources. Grid 1 and 3 operates with constant frequency. Since the purpose of introducing the virtual inertia effects is to compensate active power imbalance when there are frequency fluctuations in the grid, Grid 2 are modelled with an ideal AC source with controllable frequency. Two test signals are then introduced to its frequency to examine the inertia provision:

- **Test signal 1:** Constant rate of change of frequency (RoCoF), at 0.5 or 1 Hz/s.
- **Test signal 2:** A sinusoidal perturbation in the frequency around its nominal value, which is defined as $\Delta f(t) = \sin(0.2\pi t)$.

By the definition of inertia power response in eq. 1, it should be proportional to the change of frequency (linearly scaled with the first derivative of the frequency). Therefore, when there is a constant RoCoF in Grid 2, Station 2 is expected to respond with a constant power; while there is a sinusoidal perturbation in the frequency of Grid 2, it should respond with a sinusoidal power with its phase leading the frequency oscillation by 90 degrees.

Figure 2.10 shows the power response of Station 2 to constant RoCoF in Grid 2. It can be clearly seen that when there is DVC combined with GFM, the active power response converges to 0 after some initial oscillation, in contracts to the constant power response produced by a reference test with battery connected to the DC side and no dynamics of DVC are introduced to Station 2. This suggests that when there is only one U-station in the system, the U-station cannot provide any inertia power even if virtual inertia is introduced to the VSM. Although at the very first moment of oscillation the active power response is in the correct direction, within short time, it oscillates to the opposite direction. This means that when the U-station is connected to an AC grid with frequency characteristic (finite AC bus), during a frequency event, it might help reducing RoCoF at the initial moment of the event, but then it deteriorates it. Plus, since the total energy exchanged during the oscillation averages to 0, its total energy exchange to the AC grid during the constant RoCoF is zero.

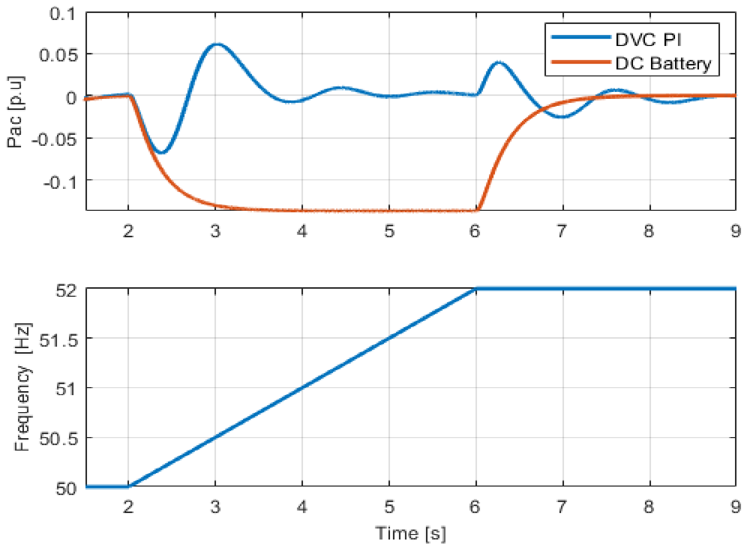

FIGURE 2.10: THE ACTIVE POWER RESPONSE OF MASTER STATION TO TEST SIGNAL 1.

Figure 2.11 shows the power response of Station 2 to a sinusoidal frequency perturbation in Grid 2. It can be observed that even though the power response is also sinusoidal, it is lagging the frequency perturbation by 90 degrees as opposed to the expected leading 90 degrees produced with batteries connected on the DC side. In other words, the phase of the power response is modified by the DVC in a manner that it is in fact introducing negative inertia to the system and therefore tend to worsen the RoCoF and frequency nadir in a frequency even.

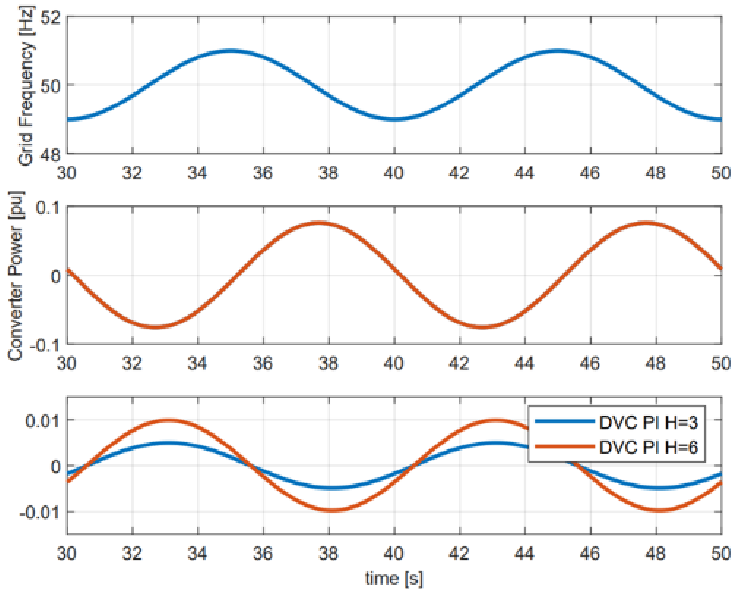

FIGURE 2.11: ACTIVE POWER RESPONSE OF A MASTER STATION TO TEST SIGNAL 2.

Case Study 3 for Proposed Control Method 1: Inertia Provision with GFM + DC Voltage Droop Control

In this case study, we resume the system in Case Study 1 in Figure 2.4, with all MMC stations controlled as in Figure 2.3, with the variation between 2 and 3 terminal configuration to demonstrate how the number of terminals affects the effective inertia provision and DC voltage fluctuations during these transients.

The two test signals defined in Case Study 2 are applied to Grid 2 as well in this case. First, during the constant RoCoF test of 1 Hz/s, it can be seen in Figure 2.12 that with the proposed control, the active power response of Station 2, after its rise time, reaches a constant power steady-state, namely, the inertia provision with the proposed control and plural stations participated DC voltage droop control is recovered. This is because during this transient, the DC voltage droop control functions as a dynamics active power dispatcher, that by allowing a certain deviations of DC voltage, modifies the active power references of the other stations and dispatches it from other AC areas to the one where the frequency event occurs.

It is also interesting to note that the effective inertia power that Station 2 can provide is not solely determined by its inertia constant defined in the VSM, but is also re-shaped by the droop gains, which follows the relation in the 3-terminal case:

$$H_{e2} = \frac{K_{dr1} + K_{dr3}}{K_{dr1} + K_{dr2} + K_{dr3}} H \tag{2.2}$$

Since in this case study, we assume all droop gains are the same, a.k.a, $K_{dr1} = K_{dr2} = K_{dr3}$, the effective inertia formed in Station 2 is $H_{e2} = \frac{2}{3}H$ and with $H = 6$ implemented, the effective $H_{e2} = 4$, which matches simulation results in Figure 2.12 where the active power reaches a constant value of 0.16 p.u. at RoCoF = 0.02 p.u./s.

If we change the number of terminals from 3 to 2, i.e., by removing Grid 3, Station 3 and its DC connection components to the DC grid, the effective inertia form by Station 2 reduces to:

$$H_{e2} = \frac{K_{dr1}}{K_{dr1} + K_{dr2}} H \tag{2.3}$$

which means that $H_{e2} = \frac{1}{2} H$ and is validated in Figure 2.12 with the active power at the steady-state reduced to 0.12 p.u.

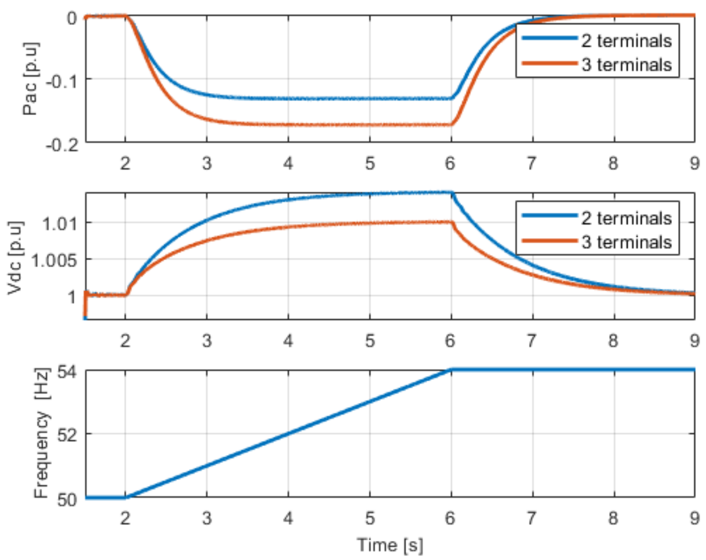

FIGURE 2.12: ACTIVE POWER RESPONSE OF STATION 2 TO TEST SIGNAL1 APPLIED IN GRID 2 WITH DIFFERENT NUMBER OF TERMINALS.

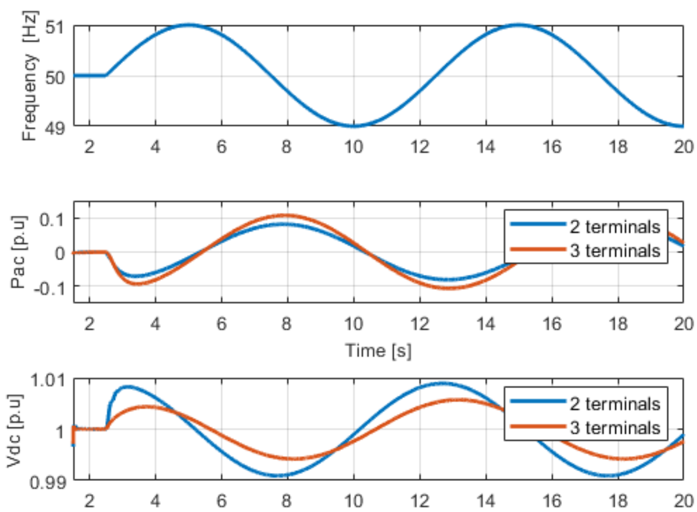

FIGURE 2.13: ACTIVE POWER RESPONSE OF STATION 2 TO TEST SIGNAL2 APPLIED IN GRID 2 WITH DIFFERENT NUMBER OF TERMINALS.

In general, the effective inertia of a certain GFM i^{th} station in an MTDC grid can be derived as:

$$H_{ei} = \frac{\sum_{j=1}^{n} G_{dc,j}(s) - G_{dc,i}(s)}{\sum_{j=1}^{n} G_{dc,j}(s)} H_i \tag{2.4}$$

Where $G_{dc,j}(s)$ is the DC voltage controller, which as shown in Figure composes of the droop gain and the phase compensation:

$$G_{dc,j}(s) = K_{drj} \frac{1 + sT_z}{1 + sT_p} \tag{2.5}$$

If the phase compensation is assumed to be the same in all stations, the effective inertia is reduced to a simpler form:

$$H_{ei} = \frac{\sum_{j=1}^{n} K_{drj} - K_{dri}}{\sum_{j=1}^{n} K_{drj}} H_i \tag{2.6}$$

with K_{drj} being the droop gain of the j^{th} station that participated in DVD, and n being the total number of stations that participates in DVD. The inertia of the other stations (not the i^{th} station) has no influence on the effective inertia form at the i^{th} station. Further, this relationship holds even if some of the stations who participate in DVD are in GFL mode, since they provide inertia to the i^{th} station only by following their active power references modified by the DVD.

On the other hand, the DC voltage fluctuation that is required to form the inertia power, is related to the droop gain, the inertia constant of VSM and the RoCoF as the following:

$$\Delta \mathrm{v}_{dc} = \frac{2RoCoF}{\sum_{j=1}^{n} G_{dc,j}(s)} H_i \tag{2.7}$$

It can be seen that increasing the number of stations proportionally reduces the DC voltage fluctuations needed to form the inertia power, which can be seen in Figure 2.12 and Figure 2.13.

Case Study 4 for proposed control method 1: Comparison of Single DC voltage Station with Proposed Control Method 1

To further demonstrate the negative inertia exhibited by the single DC voltage station and the positive inertia provided by the proposed control structure, a load jump test is performed by modifying Grid 2 from an ideal voltage source to a simple grid model with a frequency to power primary droop control and a simplified governor plus turbine dynamics, shown in Figure 2.14. Then a GFL constant power load is applied by a step-in power from 0 to 0.5 GW, which creates an imbalance of active power in the AC area form by Grid 2 and Station 2.

It can be observed in Figure 2.15 that with the single DVC station based on a PI controller, the frequency nadir is actually slightly worse when increasing inertia from 2s to 6s while paying a much larger DC voltage penalty at the same time. In other words, within this control configuration, increasing inertia deteriorates stability on both AC and DC side at the same time. Therefore, if GFM is applied to the Master station, there exists no trade-off between AC frequency stability and DC voltage stability and the optimal choice of inertia is not the maximum value that can fulfil DC voltage stability, but rather the smallest inertia that can avoid noise issues and the harmonic instability analysed in Case 1. Additionally, this also suggests that only voltage stiffness should be expected if GFM is applied to a Master Station.

Yet, if the proposed control method 1 is applied to the same test, the frequency nadir is prominently improved yet with almost no disturbance on the DC voltage, as can be seen in Figure 2.15. Further, it can also be observed that whether Grid 1 and 3 are modelled by an ideal AC source (infinite grid) or by the same frequency dynamics as in Grid 2, produces no impact on the inertia synthesized on Station 2 and the frequency responses are identical. This is because the INP in Station 2 is synthesized by using DC voltage deviation to dispatch power from Grid 1 and 3. Since a PLL is included in the GFM control, frequency variation in Grid 1 and 3 has little impact on Station 1 and 3 following their power references and therefore does not influence the INP in Station 2.

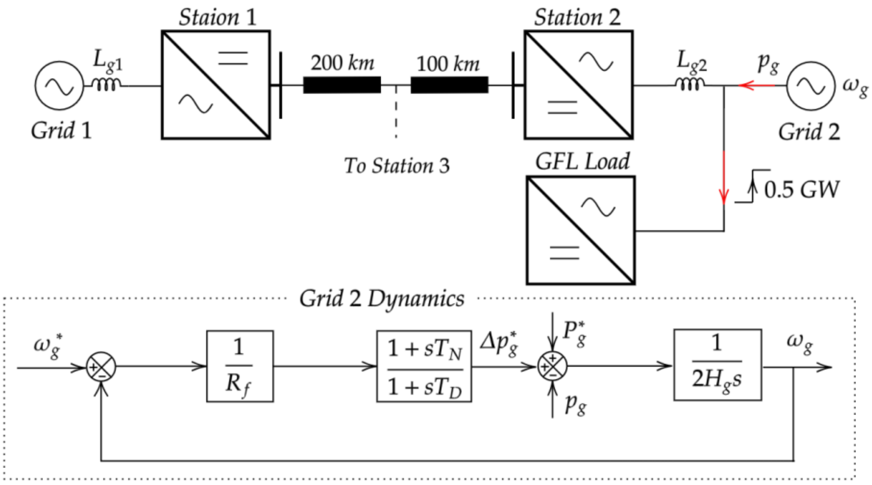

FIGURE 2.14: A LOAD JUMP TEST APPLIED TO GRID 2 WITH A SIMPLIFIED GRID MODEL.

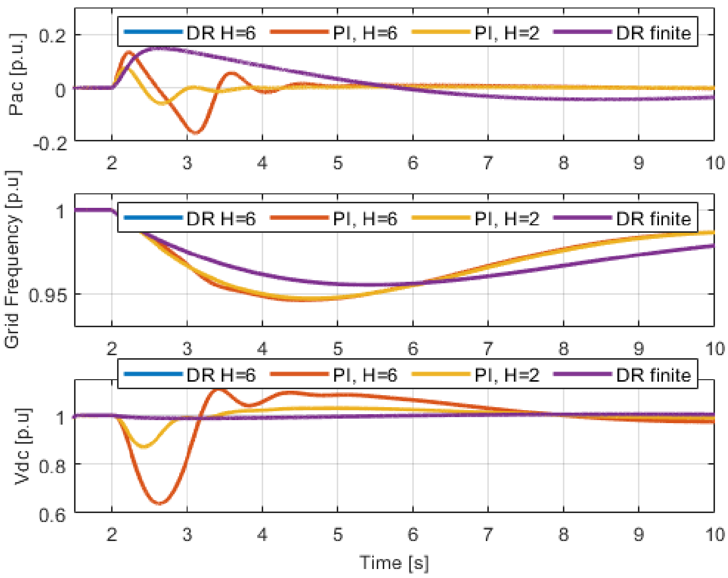

FIGURE 2.15: LOAD JUMP TEST RESULTS. COMPARISONS BETWEEN MASTER STATIONS WITH DIFFERENT INERTIA VALUES AND TO THE PROPOSED CONTROL.

Case Study 5 for proposed control method 1: N-1 Contingency Ride-through with Proposed Control Method 1

As discussed in the core functions, the primary control MTDC is responsible for securing the system during N-1 contingency, namely, loss of one station during operation. Since the DVD is responsible for modifying the active power references in each station immediately after the contingency and it has been modified by the addition of the Pcom, it is necessary to evaluate the proposed control during a N-1 contingency.

Figure 2.16 shows the results of such a ride-through transients, where all stations are rated for 1 GW and before the contingency, Station 1 operates at 1 GW in rectifying mode while Station 2 and 3 operate at 0.5 GW in inverting mode. Then at t = 8s, the DCCB at Station 1 is opened introducing a severe change of power flows on the DC side. With the proposed control, for both remaining Station 2 and 3, the powers, DC voltages at the terminal and the internal arm capacitor voltages of the MMC are well regulated during the contingency and converge to a new operating point of DC voltage solely determined by the droop gain.

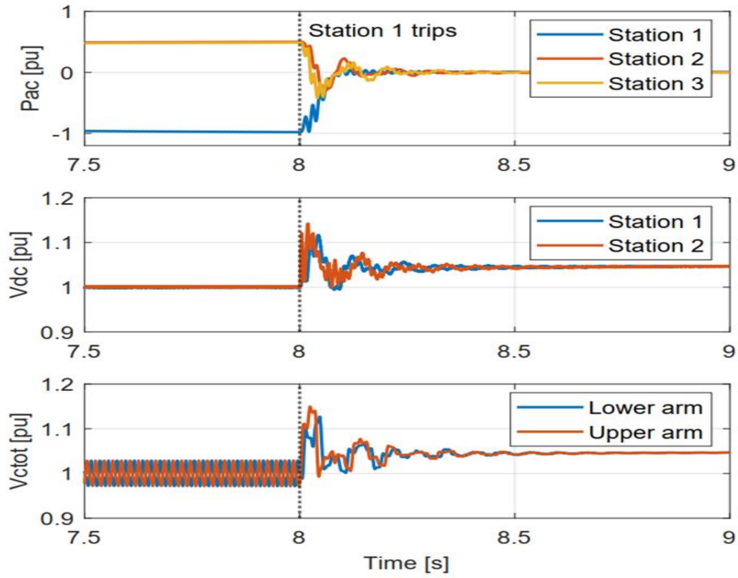

FIGURE 2.16: PERFORMANCE OF THE PROPOSED CONTROL DURING N-1 CONTINGENCY RIDE-THROUGH.

Conclusions and recommendations of Outlook 1

Combining GFM with DC voltage droop control in MTDC is a challenge that has been barely discussed before the project. It is more common today to combine GFL with DC voltage droop due to its fast power response. To fill this gap, in this section, the capabilities of Grid Forming Converters have been analysed and an improve GFM-based DC voltage droop control has been proposed for enhanced DC voltage stability while retaining the functionality of inertia support by sharing reserves across different AC areas.

Some conclusions and important remarks can be derived from these studies:

- **On the GFM control vs. DC voltage droop control:**
  - The report demonstrates that by two simple modifications, GFM can be combined with DC voltage droop control reliably with enhanced small-signal stability and DC voltage security during N-1 contingency ride-through.
  - At the same time, the proposed control can deliver inertia support by dispatching power from other AC areas without the need for communication and without introducing noticeable disturbances to the DC voltage.
- **On inertial support in stations controlling the DC voltage:**
  - The virtual inertia support from DC voltage stations in HVDC systems is commonly regarded as a design trade-off problem – larger virtual inertia leads to better frequency stability but deteriorates DC voltage stability. Given the limited capacitive energy stored on the DC side, the optimal inertia constant should therefore be the maximum value that can still guarantee DC voltage stability.
  - However, if there is only one DVC station in a HVDC system, such as the Master Station in a Master-Slave control configuration, then applying GFM control to this station cannot improve AC frequency stability. On the contrary, increasing the virtual inertia

in this station brings increased negative inertia effects, or a combination of negative inertia and negative frequency damping effects, which deteriorates the frequency stability and the DC voltage stability at the same time. This issue is not originated only from the limited capacitive energy stored in the DC system, but more importantly from the dynamics of the DC voltage control that modifies the phase of the active power response to a frequency oscillation. The design of the virtual inertia value in this case is therefore not a trade-off problem, since the optimal value of the virtual inertia should be the smallest value that still avoids noise problems and harmonic stability problems.

- Yet, the conclusion would be very different if DC voltage droop control is applied, since in this case the droop acts as a dynamic power dispatcher to bring energy from the other areas to form the inertia in one of the terminals. The effective inertia is defined by the inertia constants, the droop gains and the number of terminals that participate in the droop control. This provides a clear indication of how reserves from different areas are shared since the active power contribution from each terminal is deterministic.

- **On virtual inertia vs. actual inertia:**
  - It is also worth noting that virtual inertia is control dependent with a certain response time. When a frequency event starts with a constant RoCoF, it would take a certain time before the active power from the GFM converters can properly respond, which is not the case with the actual inertia from the synchronous machines, since in that case the energy stored in the rotating mass will be immediately released to compensate for the active power imbalance in the system. Consequently, virtual inertia will not be as effective as a synchronous machine in limiting RoCoF in the first 100 ms. This response time constant from the VSM can be reduced by reducing the inertia constant or reducing its damping coefficient. But it then leads to less effective inertia or worst damping of the system.

2.2.3 Outlook 2: The Path to HVDC Firewall

The previous section has described inertia provision when accounting for the DC voltage dynamics and understanding true capabilities of GFM under such conditions. The following section considers the impact when the inherent firewall effect of HVDC control is inhibited by these additional control services. The control methods and proposed tests are described in the following sections along with key results to highlight conditions that most significantly affect the firewall capability of the HVDC link.

The overall system architecture used for these studies can be observed in Figure 2.17, showing the two system architectures to be investigated. The initial system is AC Grid$_{jj}$ connected through a GFL-MMC, through a DC link to a second GFL-MMC to AC Grid$_{kk}$. The second system consists of the controller at Grid$_{jj}$ being replaced with a GFM, with the topology of a VSM (described in the previous section). In these tests, the grid following converter will have DC voltage control, implemented as a Power-DC Voltage droop at Grid$_{kk}$.

The systems will be implemented using small signal modelling (SSM), which is the linearization of a non-linear power system around the specified operating point. The system equations are represented in their state space form and linearized, shown below:

$$\dot{x} = Ax + Bu$$

$$\Delta \dot{x} = A\Delta x + B\Delta u \tag{2.11}$$

This enables the application of classical control theory to power electronics systems. Large signal models use numerical methods to solve nonlinear equations, which can fail to converge, and take a long time to run. Obtaining a SSM around a set operating point allows for fast iterations of parametric sweeps. Additionally, stability and mode participation can be assessed from the model.

From the full state space system, the modes where the system go unstable can be observed for each parametric condition. These modes, and underdamped modes can have the participating states identified by the participation factors. Once the participating states and frequencies of the modes have been identified, this information can be used to obtain relevant bode responses of the states and observe differences between the two models.

From the Bode plots it will be identified when the grid following only system is more effective as a "firewall", and when the system with the GFM negatively impacts this, and vice versa. The system parameters and tunings for these conditions will be highlighted.

Test systems description

The equivalent model of the full system can be observed in Figure 2.17 showing the full system to be represented in state space form and linearized around the operating point. The equations of the full system detail the AC grid to AC side of MMC equivalent model, the DC side of the MMC model, to the DC link and then the second MMC. The dynamics of the MMC are included in this model, which are often not included in small signal studies. The impact of the included internal MMC dynamics (particularly around 50 Hz and 100 Hz) under the varying parameter conditions will be highlighted and if the GFM control has an impact on interacting with these dynamics.

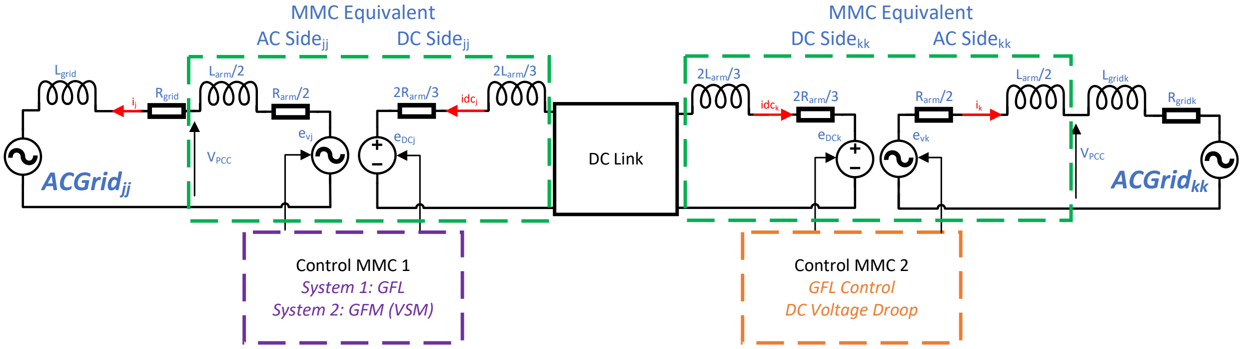

FIGURE 2.17: EQUIVALENT MODEL OF MMC-HVDC CONNECTION.

The representation of the small signal model of the two systems is shown in Figure 2.17, with the first system being two GFL-MMC converters connected by the HVDC link, and the second system having the converter at Grid$_{jj}$ replaced with the VSM.

Key parameters under evaluation

The parameters varied in the systems are:

- SCR of AC grid 1 (1 to 10)
- SCR of AC grid 1 (1 to 10)
- GFM Inertia, *H* (1s to 10s)
- GFM Damping, *D* (100 pu to 3000 pu) (MMC 1)

- MMC 2 DC voltage droop, *Droop* (0.2 to 0.001) (equivalent to the inverse of the proportional gain *Kp* in equation (2-3)).
- Circulating current control gains, *Krp*, *Kpp (Both MMCs)*

Methodology description and results

For the two tested systems, over these parametric sweeps, the eigenvalues of the system were analysed to highlight instability in the system, and then obtain the participation factors of the states in the system modes. A participation factor is the sensitivity measure of an eigenvalue to a diagonal entry of the full system A matrix [32]. If for matrix A, l_i is the i^{th} eigenvalue in the system, p_{ki} is the participation factor of the k^{th} state variable to the i^{th} eigenvalue. p^{ki} is calculated with w^{ki} and v^{ki}, k^{th} element of the left and right eigenvector for the i^{th} eigenvalue.

$$p_{ki} = \frac{|v_{ki}||w_{ki}|}{\sum_{k=1}^{n}|v_{ki}||w_{ki}|} \tag{2.13}$$

Over the parametric sweeps of the two systems, were the GFL only and GFM system had modes that diverged from each other significantly, or that were poorly damped or unstable, the participation factor of each state was calculated and the states with the highest value were highlighted. From this, the states for the bode plot could be defined and the frequency response of the system highlighted. This allows for the parameters where each system has reduced firewall effect to be highlighted. From the small signal model, the conditions of instability, and oscillatory modes, from the eigenvalues can be identified. In Figure 2.18, the dashed lines show the limit of a damping ratio of 0.1. Anything above this line has a damping ratio of less than 0.1 and so these modes that are poorly damped are investigated.

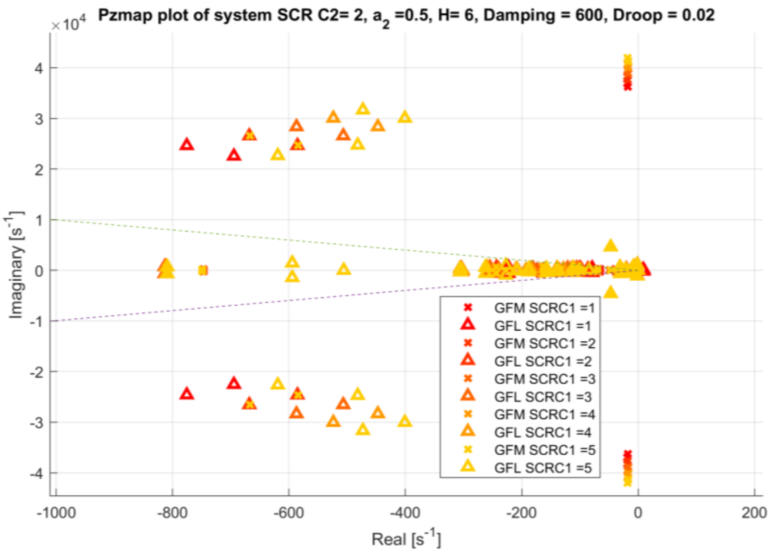

FIGURE 2.18: PARAMETRIC SWEEP OF POLES OF SYSTEM ALTERING SCR.

Several parameter iterations have been tested, and there are limits that the system has to be operated within. The value *2ωζ* (a_2) of the circulating current bandpass filter needs to be limited to around 0.5s for GFM to maintain good stability at lower SCRs due to current limitations.

From the small signal model and the eigenvalue and state analysis, we can obtain the most relevant input/output responses to observe the magnitude response of across the range of frequencies. There are many combinations of parametric sweeps that could be performed on the systems however, the most relevant parameters must be chosen. Therefore, a series of combinations of variations of the

SCR on Grid 1, SCR on Grid 2, Damping and inertia values of VSM, circulating current controller gains, and DC voltage droop of the GFL on the Converter 2 (in both systems). For the pertinent identified input to state combinations, the bode responses can be observed across the parametric sweeps.

For each system, a disturbance of current or voltage on the AC grid 1 will be observed for the effect on the variables at converter and $Grid_{kk}$. Some key bode plots are highlighted in the following section. However, first the subjective concept of firewall limit needs to be discussed. The system has been represented entirely in the *dq* frame components, and so the fundamental components are now DC variables [33], meaning that in the bode plots, the very low frequencies (≈0) will be equivalent to the magnitude of the component at the synchronous 50 Hz. At the fundamental frequency (represented in the *dq* frame at the very low frequencies, approximately equal to 0), the response is passed through and for Power at terminal 1 to terminal 2, the 0 dB gain is as expected. As the frequency increases from ≈0 Hz the magnitude of the components of the signal at these frequencies can be seen, and for the input to output responses shown, the level of propagation of one side to the other. For example, in Figure 2.19, it is expected at the synchronous frequency, that if the converter at $Grid_{jj}$ controls the power, then the power will respond with the same magnitude on the opposite side. However, at around 0.1 Hz, a spike in the bode plot can be seen resulting in a larger response in power at $Grid_{kk}$. This effect occurs when the damping is very large, 3000 pu).

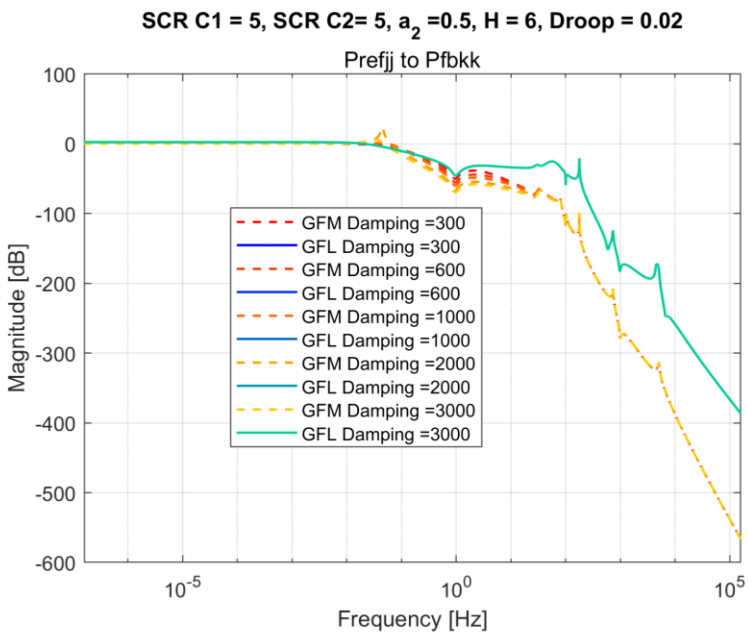

FIGURE 2.19: PARAMETRIC SWEEP OF POLES OF SYSTEM ALTERING

The previous example was of the same input to output variable (power to power) so it can be assumed that 0 dB is the expected firewall limit. Anything above 0 dB can be seen as amplifying the response from one grid to the other with unwanted gain, and anything below (specifically -3 dB), won't affect the response on AC $grid_{kk}$. However, for an input voltage to current, and vice versa, the desired magnitude response needs to be reassessed. The magnitude level of a 1 pu input resulting in a 1 pu output therefore must be calculated, by calculating the gain that results in the same pu output as pu input. This can be calculated by equation (2.14 – 2.15) and then calculating the decibel magnitude.

$$V_{to_i} = \frac{V_{nom}}{I_{nom}} \tag{2.14}$$

$$i_{to_v} = \frac{I_{nom}}{V_{nom}} \tag{2.15}$$

From this, anything above -43 dB is a “significant” oscillation from an input voltage disturbance to current. For current to voltage, anything above 43 dB is a 1:1 oscillation. Any oscillation that is below a 1:1 gain will be deemed as acceptable, but anything above will be highlighted as a cause for concern. Therefore, for variables of the same type, 0 dB is limit, for voltage to current, -43 dB, and current to voltage, 43 dB.

The injected disturbances are from one AC grid$_{jj}$ to AC grid$_{kk}$, and the response of system 1 and system 2 are compared. The inputs for the following bode plots are current and then voltage disturbances in AC Grid jj. The outputs are the identified states that were identified are participating highly in poorly damped modes. In general, for “non extreme” parameters, both System 1 and System 2 do not have significant propagation at unwanted frequencies. The aim of this research is to identify parameters and tuning that have adverse effects and so primarily figures where parameters cause a response that could inhibit the firewall effect of HVDC are shown.

For many of the plots, there were variations in the responses between the GFL and GFM based systems. The GFM frequently had a slightly larger magnitude response at “undesirable” frequencies, however they were often limited to below the magnitude of having significant impact. The first set of figures are the bode plots of an input disturbance of the current on AC Grid$_{jj}$ to the identified states that participate in poorly damped modes. Figure 2.20 (a) and (b) show the response of the grid current on AC Grid$_{kk}$, both sweeping through the droop coefficient of the DC voltage control. Figure 2.20a has medium damping (600 pu), SCR on both grids of 5, and Figure 2.20b increases the damping on the GFM to 1400 pu but reduces the SCRs to 2. The first set of parameters results in a peak at around 1 Hz however the magnitude is not significant enough to cause a serious effect. In figure b, the magnitude does peak past 0 dB and is a wider peak, but again is not that significant.

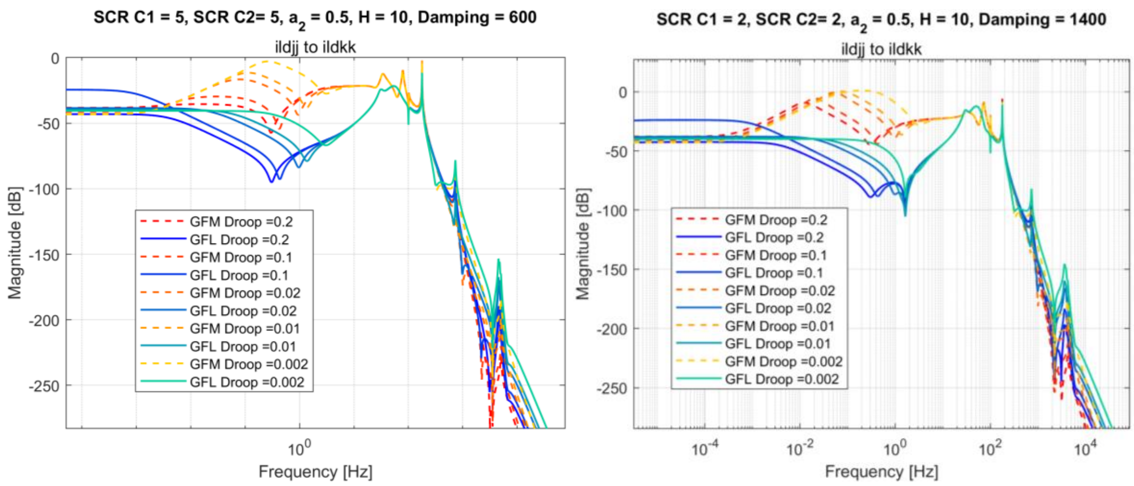

FIGURE 2.20: BODE PLOT OF INPUT CURRENT DISTURBANCE TO AC GRID KK CURRENT. A) DAMPING 600, SCRS=5, H=6 B) DAMPING 1400, SCRS=2, H = 10.

However, the response to the circulating current and to zero component saw an impact, mainly due to changes in droop. The zero component of the circulating current has a larger response around 0.1 Hz when the damping is increased, and when the DC Voltage droop is increased. This is most prevalent at damping 1400 and very high droop of 0.2, shown in Figure 2.21.

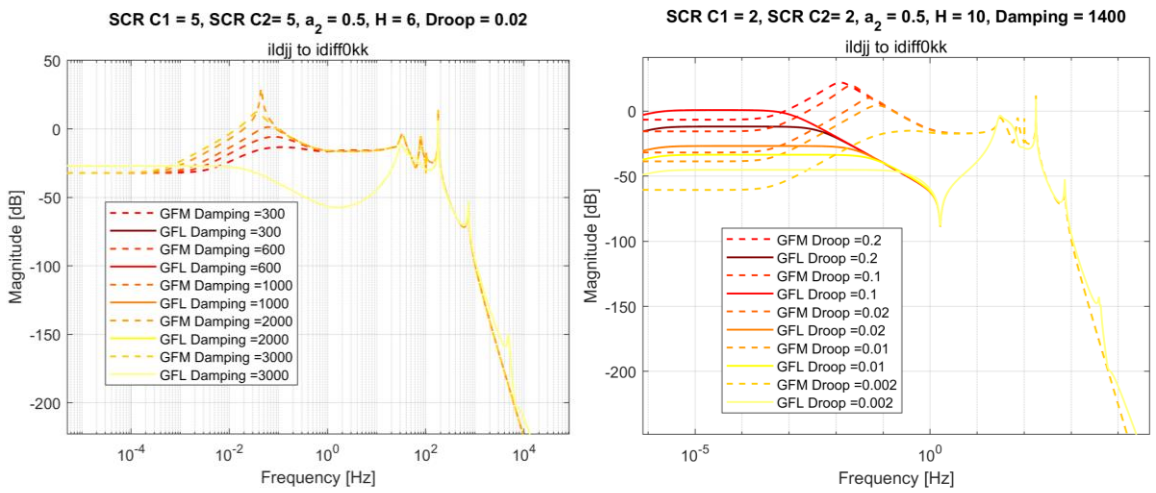

FIGURE 2.21: BODE PLOT OF INPUT CURRENT DISTURBANCE TO AC GRID KK ZERO COMPONENT CURRENT. A) VARYING DAMPING. B) VARYING DROOP.

For the 100 Hz component of the current, again increasing the droop and damping have the most effect, but only when the damping is excessively high, peaking at 2000 pu.

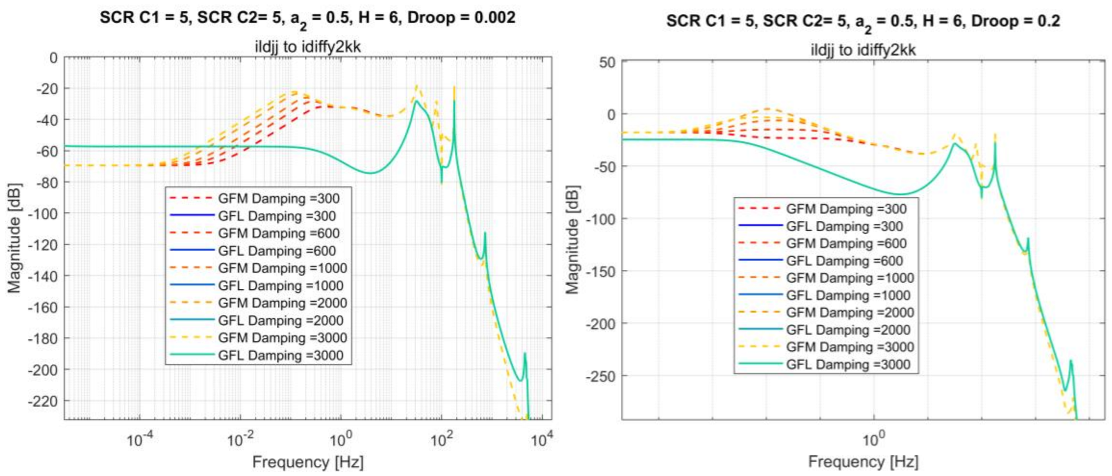

FIGURE 2.22: BODE PLOT OF INPUT CURRENT DISTURBANCE TO AC GRID KK CIRCULATING CURRENTS. A) VARYING DAMPING AT 0.002 DROOP. B) VARYING DAMPING AT 0.2 DROOP.

Looking at current to voltage responses, there were limited situations where the values would have caused a significant response. However, for current to the zero component of the MMC dynamics, a significant peak in magnitude frequently occurs, for example in Figure 2.23. The response to the MMC circulating voltages is generally greater in the GFM system and is impacted by the damping and droop significantly. The current to zero component voltage has a peak at 1 Hz, which is above 43 dB so will have an effect on the current to voltage. Increasing the DC voltage droop results in an increased peak for higher damping values.

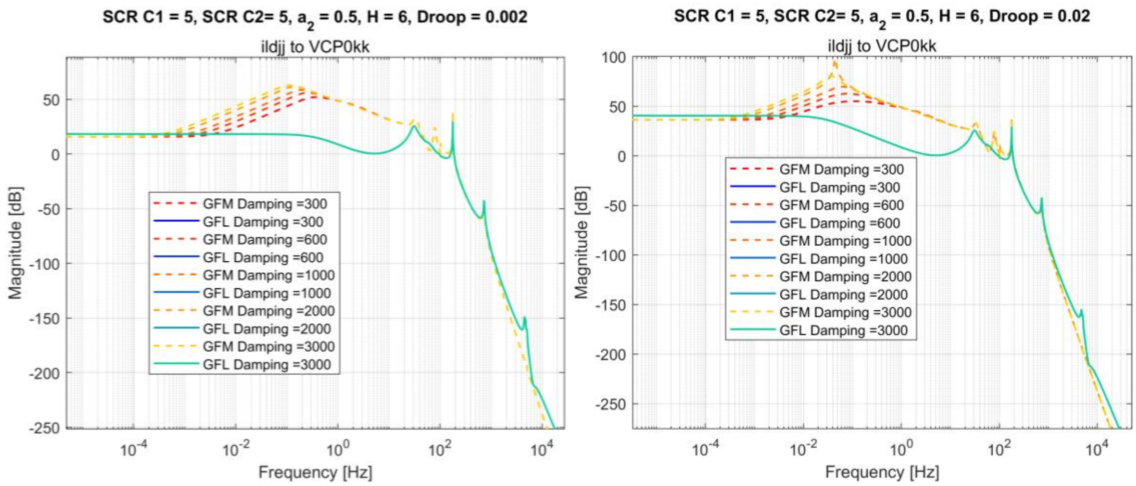

FIGURE 2.23: BODE PLOT OF CURRENT TO MMC VOLTAGE DYNAMICS WITH INCREASING DAMPING (300 PU TO 3000 PU).

For a voltage disturbance to voltage output, the “firewall limit” is again 0 dB. Anything above this magnitude level could cause an unwanted propagation at an undesirable frequency. In the bode plots of Figure 2.24, the response can be seen of the zero component of the MMC voltage dynamics of AC grid$_{kk}$. The first two responses in Figure 2.24C in the GFL system are unstable.

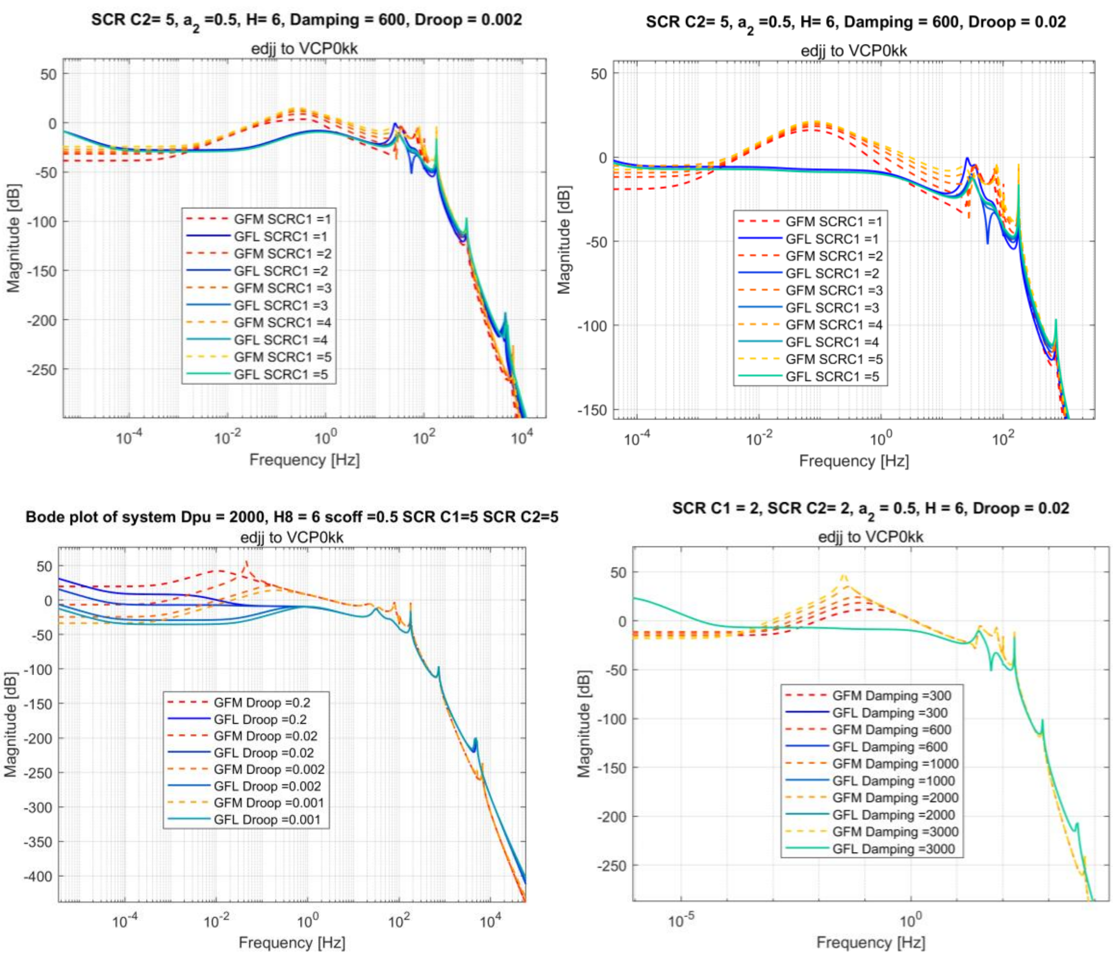

FIGURE 2.24: BODE PLOT RESPONSE TO MMC DYNAMIC VOLTAGES IN AC GRID KK. A) B) C) D)

Increasing the damping increases the response onto the other side (provides more damping power). In general conditions, the input voltage to MMC dynamic voltage has limited affect, but some situations have higher responses. However, those shown in Figure 2.25 are the extent of the oscillation peaks, which is at an incredibly high per unit damping.

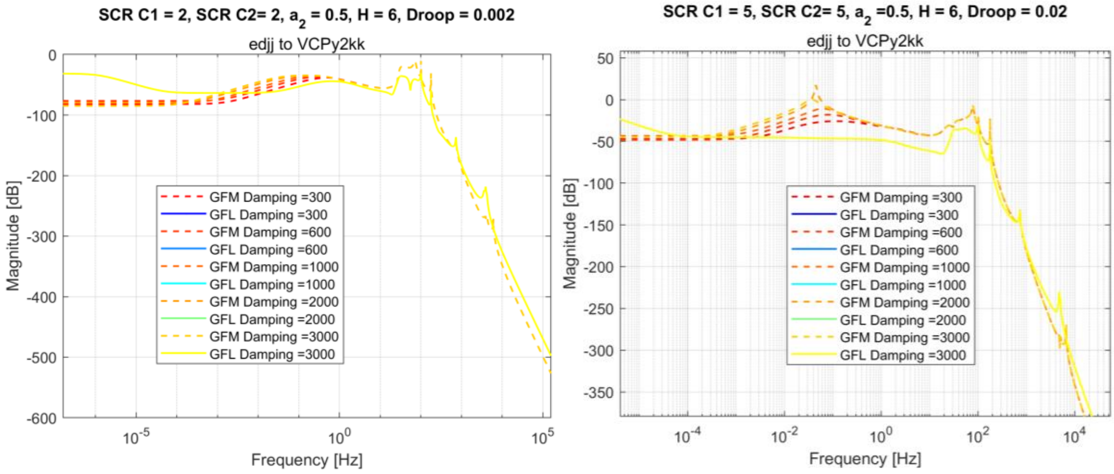

FIGURE 2.25: BODE PLOT RESPONSE OF MMC DYNAMIC VOLTAGES.

Now for a voltage to current disturbance, anything above -43 dB could be a cause for concern (as described in the previous section). For instance, the oscillations shown Figure 2.26, however, this is only at the very high damping in VSM, particularly when the droop is increased.

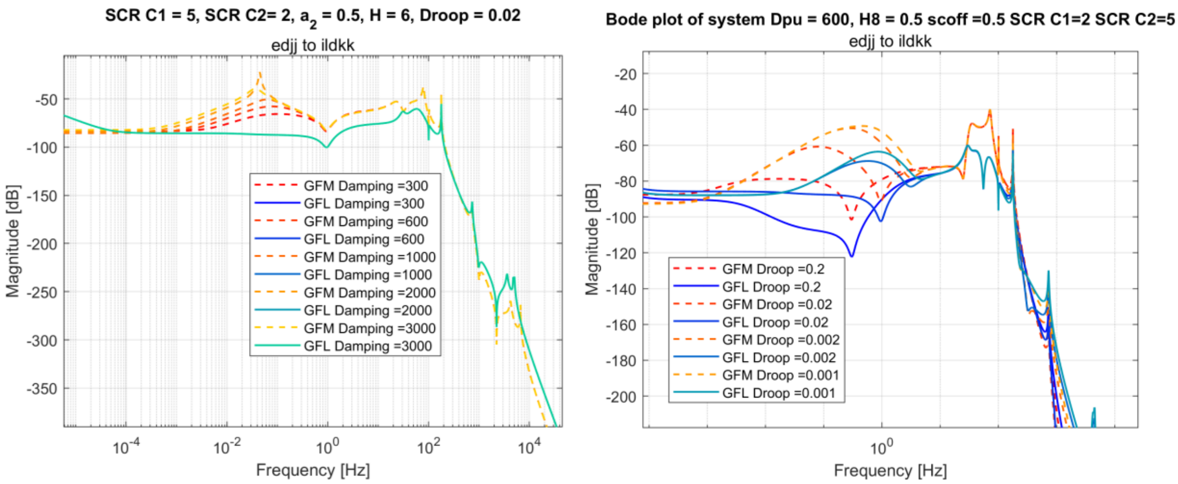

FIGURE 2.26: BODE RESPONSE OF AC GRID$_{KK}$ CURRENT, A) INCREASING DAMPING, B) DECREASING DC VOLTAGE DROOP.

For the response to the circulating currents, the peak shown in Figure 2.27 is more significant, especially as the *y* component. However, this is again with extreme damping, and with SCR of AC Grid$_{kk}$ being weak (<2).

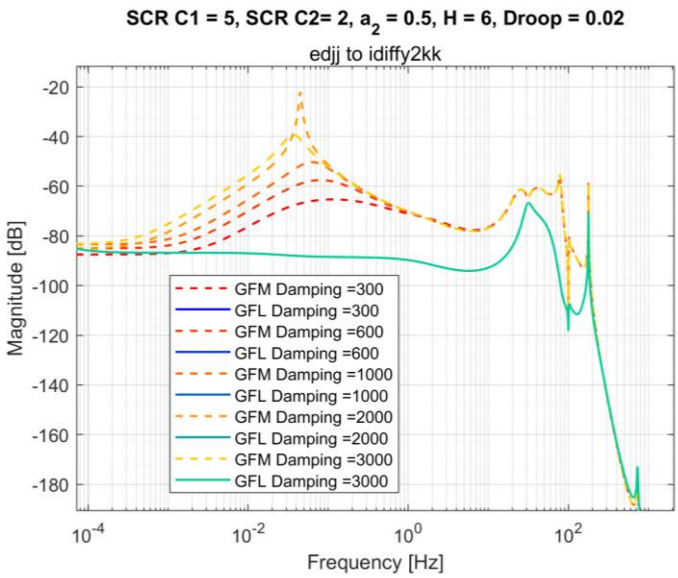

FIGURE 2.27: BODE RESPONSE TO CIRCULATING CURRENT OUTPUT.

Conclusions and remarks of Outlook 2

In this section, an HVDC link with solely GFL converters was compared to a link with the first converter switched to a GFM, with the two systems tested shown in Figure 2.17. For each, a disturbance of current or voltage on the AC Grid$_{jj}$ was injected to observe the effect on the variables at converter and AC Grid$_{kk}$, across a series of parameters.

The effect of the grid forming converter on the system is heavily affected by the parameter conditions of the grid and controller tunings. The Bode plots in Figure 2.20 to Figure 2.27 show that there are undesirable magnitude responses from one AC grid, through the HVDC link, to the other AC grid. This is due to the response of the grid forming converter actively supporting the AC grid it is directly connected to, and drawing power through the HVDC link. The recommendations for future tests are to verify the effect of these parameters on the system described in Figure 2.17, and it is advised to confirm the following findings.

Firstly, the SCR of each grid affects how much active power the grid forming converter draws from the HVDC link to support its connected AC grid. The SCR of GFM connected grid, Grid$_{jj}$ is more significant than that of Grid$_{kk}$. The SCR of Grid$_{jj}$ results in an increase in the peak of the magnitude response, by increasing the value from 1 to 5. Changing SCR of Grid$_{kk}$ from 1 to 5 has a minimal effect on the peak magnitude response.

Additionally, the damping coefficient of the grid forming converter has an even more significant effect on the magnitude response. Increasing the damping results in the grid forming system having a much larger peak than the grid following system in the Bode response, specifically between 1800 pu to 2200 pu. Damping above this level also shows an undesirable high magnitude response.

In combination with the effect of the damping, the DC voltage droop control of the grid following converter connected to Grid$_{kk}$ affects the propagation of the response. Increasing the DC voltage droop from 0.002 to 0.2, coupled with a damping value between 1800 pu to 2200 pu results in a significant unwanted propagation from AC Grid$_{jj}$ to AC Grid$_{kk}$.

2.3 Other Optional Core Functions

The previous section primarily focused on the essential core functions required for future MTDC networks. The work meticulously examined grid-following with Vdc droop and grid-forming with Vdc droop control, both of which are crucial for maintaining grid stability during normal operation. However, when unforeseen events such as DC faults occur, the focus shifts to post-fault recovery.

2.3.1 Focus on damping of DC-side post-fault oscillations

As detailed in other deliverables, a key characteristic of future systems is their resilience, including the ability to recover from fault events quickly. This section addresses the measures and analyses necessary for stabilizing the DC system and the recovery process following a DC fault.

During a DC fault, the smooth operation of the grid is disrupted. The primary goal during post-fault recovery is to minimize disruptions and promptly stabilize the DC side, which is crucial for enhancing the grid's overall resilience.

This section explains the occurrence of post-fault oscillations and proposes supplementary controllers for damping these oscillations on the DC side of the converter. These measures will strengthen the grid against disruptions and contribute to a more resilient power system.

Literature Review and Innovation Focus

The post-fault recovery process is crucial for ensuring the reliability of the HVDC network, especially in the event of DC faults. A DC fault refers to a temporary or permanent interruption in the normal operation of the HVDC system, which can occur due to various factors such as insulation failure, short circuits, or equipment malfunction. To mitigate the adverse effects of these faults, the DC-side fault current should be cleared within the millisecond range (e.g., tens of milliseconds). This clearing time should be at least ten times faster than in an AC protection system to minimize the impact of DC-side faults on the connected AC systems and restore power flow.

The Post fault recovery strategy is tasked with the stable restoration of DC voltage to levels closely resembling pre-fault values. This necessitates the swift recovery of voltage (and consequently, power flow) while effectively managing oscillations, preventing over-currents, and averting over-voltages.

The post-fault recovery process highly depends on whether any of the converters in the HVDC grids are in a blocked state due to a fault. Various fault conditions and sequences affect the HVDC network in different ways. The extent of the resulting power flow disturbance largely depends on the specific fault scenario being considered, including factors such as the fault's severity and duration.

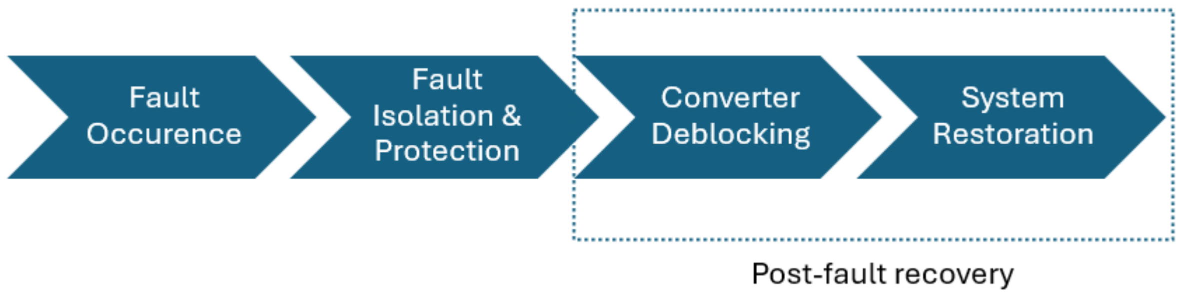

FIGURE 2.28: TIMELINE OF ACTIONS FOR POST-FAULT RECOVERY IN AN HVDC NETWORK

Figure 2.28 illustrates the timeline of actions in an HVDC network during a severe fault near the DC side of a converter, which disrupts normal operations. The protection system identifies the fault and takes corrective actions, potentially including temporarily blocking the converter to isolate the fault. Once the fault is cleared, , if the converter was temporarily disconnected from the DC network, it is deblocked and reconnected. This reconnection triggers voltage oscillations, current imbalances, and power fluctuations in the network when the system is restored to normal operation. The post-fault recovery involves converter deblocking and system restoration. During this phase, supplementary control strategies are employed to dampen the oscillations and ensure the stable reintegration of the network.

The sudden changes in converter operation, such as reconnecting the affected converters, can introduce transient oscillatory behavior in the DC voltage and current. These DC-side oscillations can have various frequencies depending on the characteristics of the system and the control strategies employed. To facilitate analysis and control design, these frequencies are often categorized in relation to the AC system's fundamental frequency as sub-synchronous or super-synchronous.

Several control techniques and strategies can be employed to mitigate and stabilize DC-side oscillations during the deblocking process, including damping control, DC-side filtering, and control system design.

- Supplementary damping control: Damping control methods can be implemented to suppress oscillations and improve system stability. It may involve adjusting the control parameters of the damping controller or applying supplementary damping control schemes.
- DC-side filtering: The use of DC-side filters, such as DC-line reactors or capacitor banks, can help dampen the oscillations and their effects on the network.
- Internal controller tuning: Careful design and tuning of the converters' control system can significantly mitigate DC-side oscillations. The control system should be designed to respond appropriately to transient events and maintain stability during the deblocking process.

Fast and stable post-DC-side fault recovery is essential to a fault-clearing strategy to achieve continuous operation in meshed HVDC grids. Various studies have been conducted to analyze the recovery process of a single converter [34] [35] [36]. However, the post-DC-side fault recovery of the multi-terminal HVDC systems and the interactions between the converters and the grid during system recovery has yet to draw much attention in the literature. As the post-DC-side fault recovery involves converter restoration, unwanted poorly damped oscillations may be triggered.

The post-fault grid recovery strategy has the task of restoring the DC voltage to a value close to the pre-fault value in a stable manner. This implies that the voltage (and consequently, power flow) must be recovered with adequate speed while limiting oscillations and avoiding over-currents and over-voltages. The capacitive and inductive components (e.g., converters, cables, line inductors, etc.) in the HVDC network will result in resonant frequencies. During the switching or deblocking of converters at voltage levels different from the grid voltage, oscillations with these resonant frequencies may be triggered.

Before discussing the methods to improve damping, understanding the origin of oscillations that occur during post-fault recovery is important. During the de-blocking of a converter, uncontrolled oscillations can be seen, which occur due to the interaction between the converters and the HVDC network during the recovery process, where the magnitude of these oscillations depends upon the damping characteristics of the network unless the converter controller is able to control and suppress a wide range of non-DC component frequencies. These oscillations occur due to poor damping characteristics, which are highly influenced by interactions between converter and the HVDC network or by DC side inductors, some DC faults etc. and lead to overvoltage's or overcurrent's on the DC side of the network.

The work focuses on the DC side oscillations or Sub-Synchronous Oscillations (SSO), which can be seen during the de-blocking of the converter at the DC side of HVDC grids, which stem from the interaction between the converter and the DC network. These oscillations can be excited by different factors such as faults, disturbances, and system parameter variations, which result in significant power fluctuation and voltage variation on the DC side.

DC side oscillations can endanger the operation of the entire power system by causing instabilities, and hence systems' electrical equipment may be severely damaged [37]. The frequency of these oscillations is below the fundamental frequency. Depending on where the resonance occurs, the conventional power system SSO can be categorized into various types, including sub-synchronous resonance (SSR), sub-synchronous torsional interaction (SSTI), and sub-synchronous control interaction (SSCI) [38]. Damping of these SSOs is required to ensure reliable operation, as these oscillations lead to reduced power transfer capabilities, potential system failures, and increased stress on components.

During post-fault recovery, damping of DC side oscillations can be achieved using appropriate control strategies, including active and passive damping methods. Active damping methods for oscillation damping during post-fault recovery can be categorized based on the performance metrics of the controller, such as overshoot, settling time, and damping ratio. Higher damping achieved through modulated signals, such as model predictive control or DC-side voltage regulator, indicates a faster decay of oscillations and better damping performance [39].

However, damping control in HVDC networks may face challenges due to system complexity, limited observability, parameter variations, coordination issues, and emerging oscillatory modes. These factors can limit the effectiveness of damping techniques, highlighting the need for continuous improvement. Enhanced control strategies, improved measurements and monitoring, accurate modelling, and coordinated control can address these challenges and improve damping to ensure system stability.

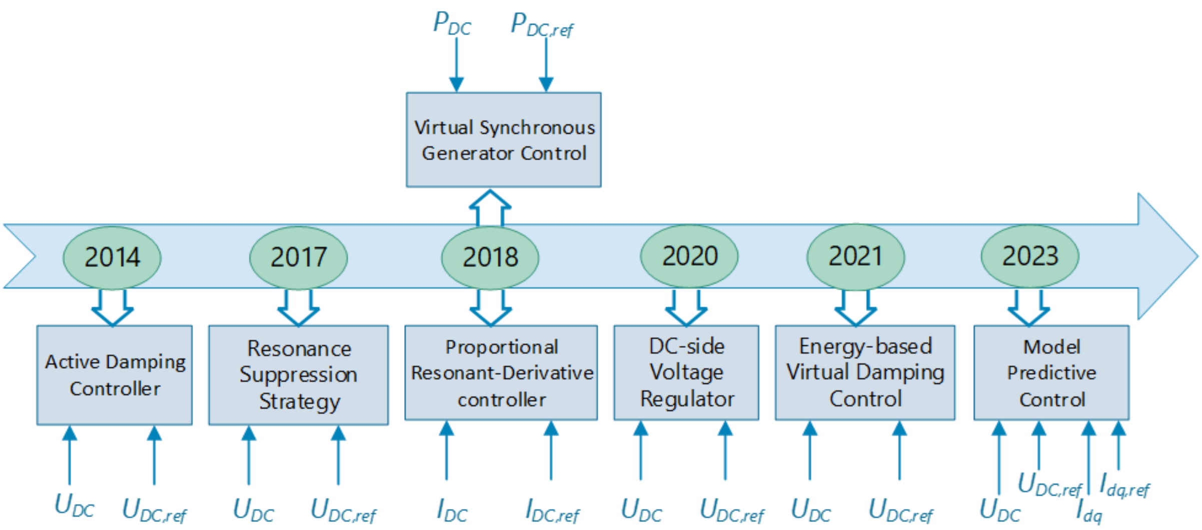

FIGURE 2.29: VARIOUS DAMPING CONTROL TECHNIQUES AVAILABLE FOR SSOS DAMPING.

Various supplementary controllers are available in the literature to suppress voltage/current oscillations to improve damping at DC side of HVDC networks. Figure 2.29 illustrates the different damping control methods used for SSO damping at the DC side of HVDC networks. However, adding a damping controller requires an extra control loop in the outer loop of VSC-HVDC control, as shown in Figure 2.30. The modulated signal utilizes damping methods for HVDC networks, where an additional signal is injected into the converter current control loop to modulate the DC current/voltage and enhance the damping of sub-synchronous oscillations. The state-of-the-art methods applied are illustrated in Figure 2.34, including:

- Proportional-resonant derivative controller [40]
- Active damping controller [41]
- Model predictive control [[39]]
- Virtual synchronous generator control [42]
- Resonance suppression strategy [43]
- DC-side voltage regulator [44]

Each damping control strategy has specific characteristics and benefits. The modulated signal improves the damping of DC side oscillations by increasing the damping coefficient and reducing overshoot and settling time. In [44], the authors use the *D-Q* CCSC method and the modulated signal to improve damping at the DC side through controls. They modified the *D-Q* type Circulating Current Suppression Control (CCSC) to suppress non-DC components in the zero-sequence current, resulting in a 2.59% reduction in overshoot and a 3.57% reduction in settling time compared to the conventional *D-Q* type CCSC.

In [39], the authors utilize CCSC with Model Predictive Control (MPC) to suppress circulating current and enhance damping. The performance of CCSC with MPC shows a 13.6% reduction in settling time compared to the PI control approach. In [43], the authors investigate DC-link voltages using a new active damping method known as virtual active damping or resonance suppression strategy. This method provides a resonance suppression effect similar to that of a passive damping controller and ensures DC-link voltages within the permissible range of ±10%. Virtual synchronous generators were proposed in [42], which use virtual inertia and virtual damping control with a proportional-derivative controller to enhance the damping and inertia of DC networks. The authors analyze the impact of time delays, illustrating that an increase in time delay is not beneficial to the stability of DC networks.

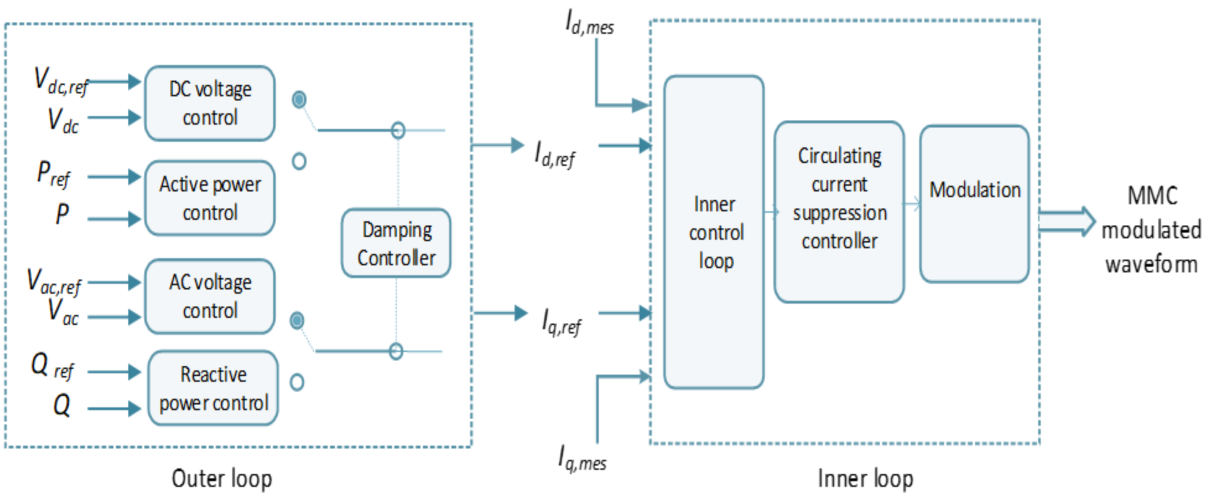

FIGURE 2.30: CONTROL LOOP STRUCTURE INSIDE MMC.

The post-fault oscillations propagate from the voltage loop and the grid currents to the inner current loop, as shown in Figure 2.30. Consequently, I_{dref} and I_{qref}, the reference currents, are distorted with oscillations without using damping controller. If the current loop provides sufficient damping for these oscillations, the SSO can be attenuated before propagating to the PWM block. Therefore, further investigation is conducted on the damping provided by the inner current loop, which regulates the current in each arm of the converter.

The CCSC modulates the DC current within the current control loop to dampen the oscillations. The output of the CCSC is a key factor in determining the behaviour of the DC current during post-fault recovery. CCSC works by detecting current instabilities, such as changes in current direction or magnitude, and applying corrective measures to dampen the oscillations and maintain stable operation [45][[30]]. It eliminates undesired circulating current in the Modular Multilevel Converter (MMC) cells that may occur during converter operation.

Various CCSC algorithms are available in the literature, including:

- Methods based on energy control [45]
- Method based on double line-frequency D-Q coordinate [30]
- Method based on model predictive current control [46]
- Method based on Proportional-Resonant (PR) controller and repetitive controller [47] [48]

The CCSC method based on the *D-Q* coordinate is a typical method widely used in the literature. This method uses two Proportional-Integral (PI) controllers to directly suppress circulating current in the *D-Q* frame by setting the reference value to zero [30]. The energy control method aims to reduce circulating current from the source by controlling the total energy and balancing the energy difference between the upper and lower arms, as circulating current is caused by the energy difference [45]. The method based on the PR controller or repetitive controller can eliminate high-order harmonics in the circulating current and can be used as compensation for other control methods [48].

Commonly applied CCSC is used to eliminate the double-frequency circulating currents. However, recent studies have demonstrated poorly damped oscillations or even instabilities associated with the DC-side current can occur with conventional *D-Q* type CCSC [49]. In [50], authors proposed a new Fast Circulating Current Controller (FCCC) controller. The difference lies in controlling the DC component of the circulating current. FCCC directly defines the DC reference of the circulating current based on the AC-side power. In contrast, in D-Q type CCSC, the DC component of the current control loop is naturally defined based on converter dynamics. The modified CCSC shows a 7% reduction in overshoot and a 12% reduction in settling time compared to conventional *D-Q* CCSC [51]. Therefore, from the literature, it can be concluded that by utilizing modulated signal with CCSC, the damping of oscillations can be enhanced, leading to improved stability and performance in HVDC networks.

The next sections elaborate on the system model and discuss the performance of the voltage regulation method and the modified D-Q type CCSC for an MTDC network, aiming to enhance the post-fault recovery of HVDC networks.

Parametric Sensitivity Analysis

Test system and assumed parameters

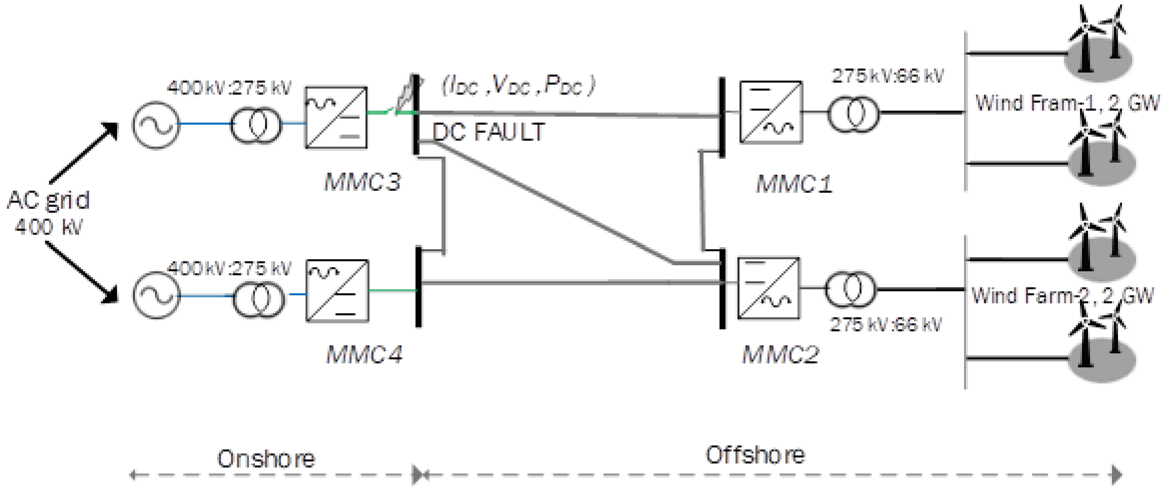

FIGURE 2.31: A FOUR-TERMINAL ±525 KV HALF-BRIDGE MMC-BASED MTDC NETWORK.

The test system is a four-terminal MMC-based MTDC network with a DC voltage rating of ±525 kV, with bipolar dedicated metallic return (DMR) configurations. The converter is a half-bridge topology. The system can be divided into two subsystems: the onshore system, and the offshore system as depicted in Figure 2.31.

The onshore AC system consists of Thevenin's equivalent circuit (static voltage source) of a strong grid; the grid impedance is computed based on the short circuit current level—a series resistor connection of a parallel resistor and inductor models it. By adjusting the values of the inductance and resistance, the short circuit current value and the damping angle at fundamental and Nth harmonic are controlled. The rated line-to-line (LL) voltage is 400 kV. The onshore converter station has two Y-D transformers, with ratings of 2 GVA each. The voltage ratio of this transformer is 400/275 kV. Onshore converters are labelled MMC3, and MMC4. The onshore converter stations use DC voltage control and AC voltage control, whereas *P-Q* control is used for the offshore converter stations.

For the four-terminal HVDC network, the length of the onshore cables is 12 km up to the point of common coupling (PCC), as indicated by the green-colored onshore DC cable. The land cables connect the onshore DC hub, which contains a DC switch. For simplicity and to reduce the computation burden, only one DC switch is employed. Furthermore, the DC system comprises five subsea cable links (300 km length of all the subsea cables). The cables are modelled with a frequency phase-dependent models. Furthermore, the cable link consists of three conductors (i.e., a positive, a negative, and metallic return per cable link) due to DMR topology [52]. More details about the four-terminal MTDC network and parameters are discussed in Appendix A.

Wind Turbine

The Wind Turbine model used for this study is a Type 4 model [53], It has a rating of 2 MW at a wind speed of 15 m/s. The Type 4 wind turbine model consists of four main components: the wind turbine model, a permanent magnet synchronous machine (PMSM), an AC-DC-AC Power electronic converter system, and a scaling transformer.

The wind speed data is uploaded to RSCAD /RTDS via co-simulation. The TCP/IP protocol connects RSCAD /RTDS to the Python script. In this script, live wind data is collected every second from two locations (i.e., Orkney and Shetland regions) in the North Sea via a website and then communicated to the wind speed slider in RSCAD /RTDS via TCP/IP protocol.

Approach for Parametric Sensitivity

The necessity for an active damping approach is critical for enhancing post-fault recovery in MMC-MTDC networks. This study highlights the importance of DC voltage regulation method, particularly when combined with the enhanced D-Q type CCSC controller. This combination shows promise in using modulated signals with CCSC to improve oscillation damping, thereby enhancing stability and performance in HVDC networks as discussed in state-of-the art [12]. The study employs parametric sensitivity analysis as a crucial means for system assessment.

Figure 2.32 illustrates the proposed approach for sensitivity analysis. The process commences with the preparation of the overall dynamic model. Initially, control parameters are configured using an RTDS script. Subsequently, an EMT simulation is conducted with the initial settings to pinpoint areas for improvement.

This study specifically addresses a FRT scenario pertaining to the blocking of converters when a severe fault (such as a DC short circuit) occurs near the converter terminal. The effectiveness of the post-fault recovery process hinges on whether any converters in the HVDC network are in a blocked state due to the fault. Converter blocking implies that they are no longer capable of controlling their active powers in post-fault conditions. To mitigate the impact of these disturbances, the blocked converter must be promptly deblocked and actively controlled.

The potential occurrence of poorly damped oscillations during post-fault recovery can be observed in current and voltage waveforms. The focus of the flowchart is on analyzing the Active Damping Controller (ADC) to improve post-fault recovery during deblocking, involving key parameter adjustments and evaluations until a satisfactory outcome is achieved to enhance the post-fault recovery of the HVDC network. Parameters are fine-tuned to ascertain the optimal set point from a wide range of values. A similar analysis is conducted for the enhanced CCSC loop once optimal set points for the ADC are determined. Finally, the optimal values obtained after key parameter adjustments of the ADC and enhanced CCSC are verified to ensure that all key parameters are configured optimally, thereby concluding the process.

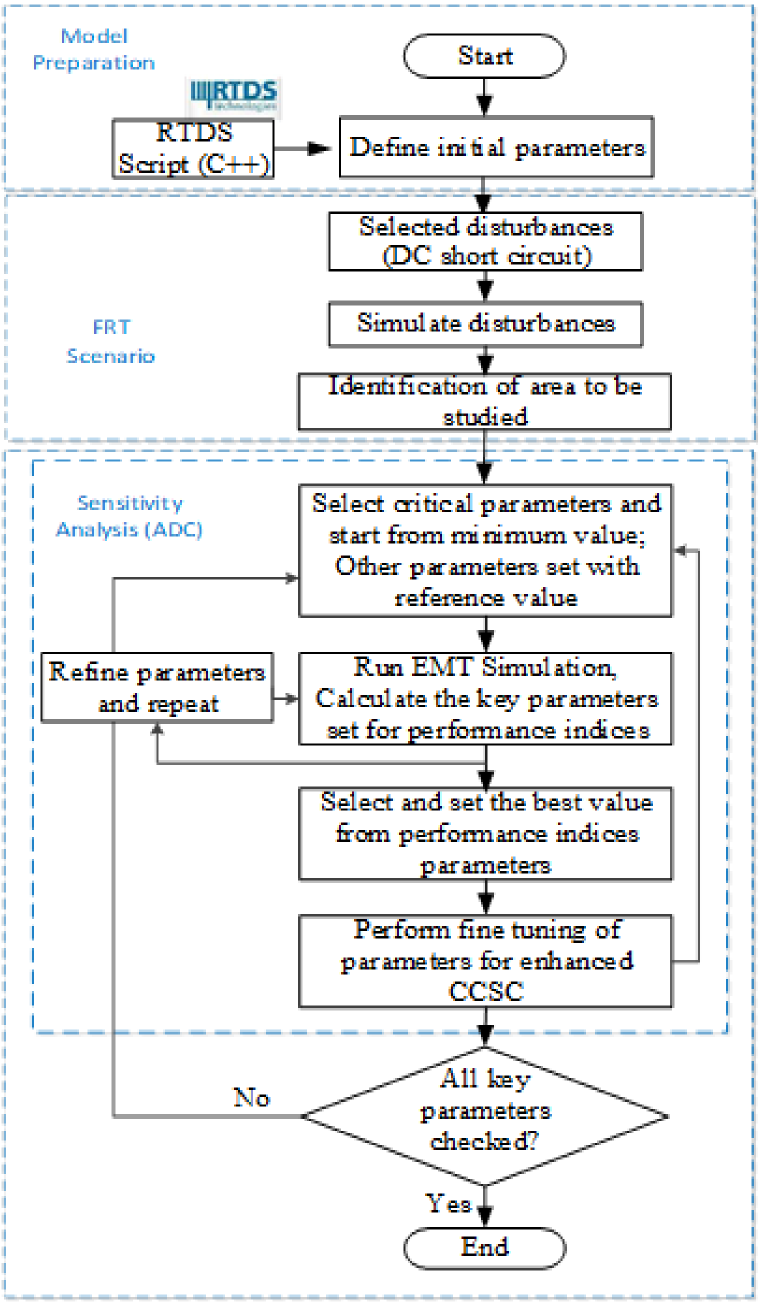

FIGURE 2.32: PROCEDURE FOR SENSITIVITY ANALYSIS.

Performance of Active Damping Control and Enhanced CCSC

a) DC-voltage regulation method:

The primary focus of this study revolves around the control loop of the DC-voltage regulation method, as illustrated in Figure 2.33. Instances where the post-fault DC-side voltage consistently drops below the designated minimum threshold (V_{DC}^{min}) often lead to a disparity between the grid-side and converter DC-side voltage, attributable to the constraints of existing controls and voltage evaluation criteria. To rectify this discrepancy during the deblocking process, it becomes imperative to align the converter DC-side output voltage precisely with the grid-side voltage. This alignment is achieved by reducing the number of actively engaged sub-modules during the de-blocking moment, thereby effectively decreasing the converter DC-side voltage to closely match the grid-side voltage.

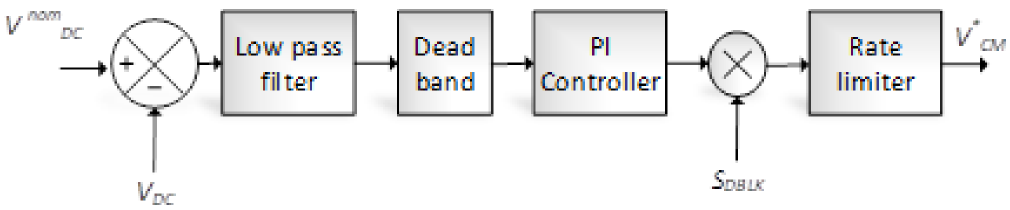

FIGURE 2.33: DC-VOLTAGE REGULATION METHOD CONTROL LOOP.

The DC-voltage regulation method achieves a reduction in submodule count during de-blocking by subtracting the control loop output from the internal voltage reference. The controller activation is specifically triggered solely at the deblocking instance through the signal S_{DBLK}. A rate limiter has been implemented to manage the rate at which submodules are adjusted. This limiter facilitates the acceleration of submodule reduction until the nominal DC-side voltage is reached, preventing sudden fluctuations while regulating the rate of submodule insertion. The voltage error, representing the deviation between the nominal DC voltage and the grid voltage, is integrated into the controller (G(s)) to fine-tune the system response during de-blocking. Typically, a proportional controller suffices for DC-side voltage regulation, with the inclusion of a low-pass filter to eliminate undesirable high frequency components. Under normal operating conditions, the controller output remains at zero due to the dead-band block, as the DC-side voltage closely aligns with the nominal value.

However, if the DC-side voltage falls below V_{DC}^{min} at the deblocking moment, leading to an error surpassing the predefined dead-band, the controller output is engaged to reduce the inserted submodules, thus aligning the system with the grid voltage [44].

b) Role of enhanced D-Q CCSC:

As highlighted in Section 0, converter de-blocking may generate uncontrolled oscillations. The magnitude of these oscillations depends on the damping characteristic of the HVDC network, unless the converter controllers are able to control and suppress a wide range of non-DC component frequencies. This section discusses the requirements of the CCSC to suppress the non-DC components, and proposed to use a modification to the standard DC-type CCSC to improve the system recovery [30]. The utilization of the modified D-Q type CCSC configuration serves to improve damping properties while maintaining the steady state DC current. This study involves a parametric sensitivity analysis of the enhanced D-Q type CCSC, illustrated in Figure 2.34.

The non-DC components infiltrate the zero-sequence component (i_{c0}) during post-fault recovery, which ideally should only contain a DC component during steady-state operation, as depicted in Figure 2.34. To handle these non-DC components within the zero-sequence current, a band-pass filter is used to effectively isolate them from the DC component. Additionally, a PI controller is employed to drive these non-DC components toward zero. The band-pass filter's bandwidth is carefully chosen to cover a wide range of resonant frequencies, identified through a comprehensive analysis of DC-side resonance.

The aforementioned study emphasizes the importance of carefully selecting appropriate parameters for DC-voltage regulation methods and enhanced CCSC in order to enhance the damping of post-fault oscillations during the de-blocking of the converter. The subsequent section will delve into the key parameters that need to be considered to improve post-fault recovery on the DC side of networks.

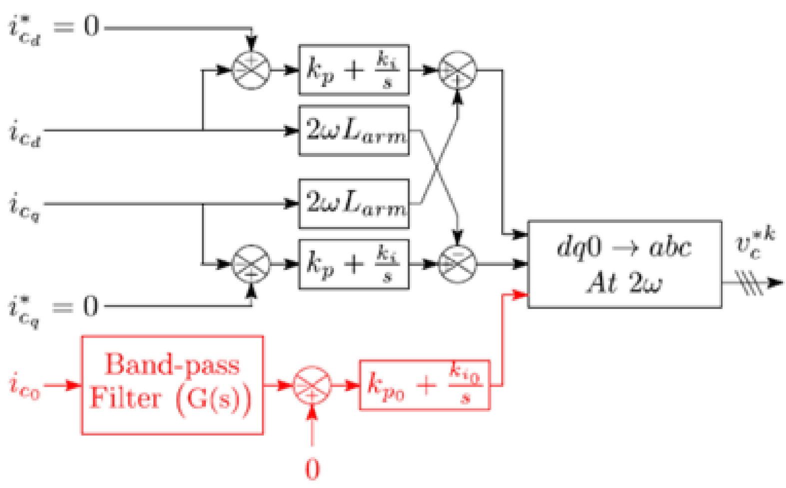

FIGURE 2.34: MODIFIED D-Q CCSC [30].

Fine Tuning of Key Parameters

This study investigates a four-terminal MTDC network (Figure 2.31) without DC circuit breakers. Figure 2.35 represents the initial voltages and currents at the DC side of the converters. During a severe DC fault (for instance, DC short circuit) near MMC3, the switch on the DC side is instantaneously opened to isolate the fault, effectively blocking MMC3. Upon fault resolution, MMC3 is deblocked.

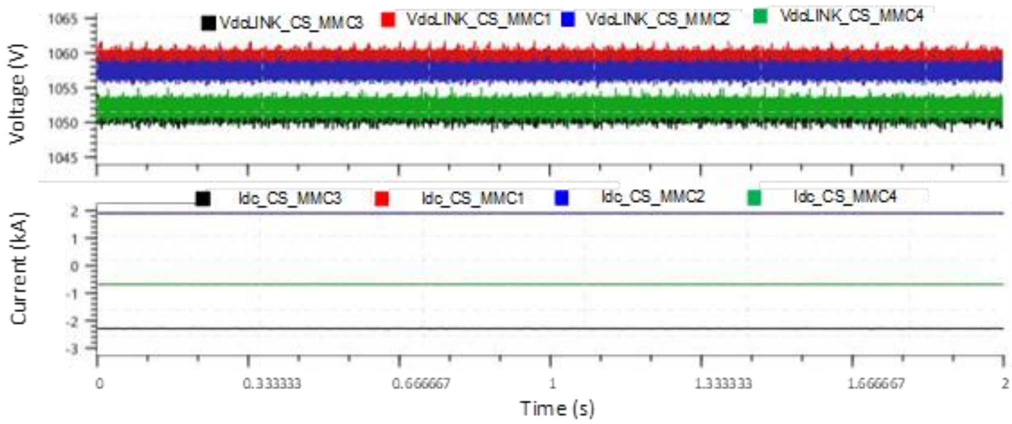

FIGURE 2.35: INITIAL CURRENTS AND VOLTAGES AT DC SIDE OF MTDC NETWORK.

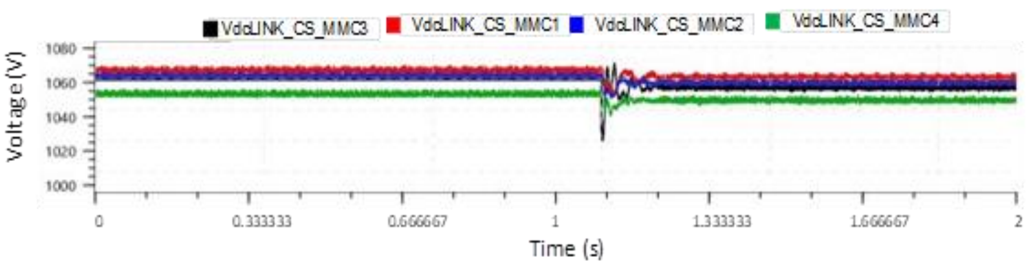

FIGURE 2.36: VOLTAGES AT DC SIDE OF CONVERTERS DURING DEBLOCKING EVENT.

Figure 2.36 provides an overview of the effects of deblocking Converter MMC3 at all DC terminals (MMC1-MMC4) when no active damping controller is employed. At the moment of deblocking, noticeable voltage dips are observed near the DC side of the converters. Likewise, Figure 2.37 illustrates the current at the Point of Common Coupling (PCC) near MMC3 converter during the deblocking of the converter, near MMC3. During this process, a peak overshoot of 1.1431 kA is observed, with a settling time of 0.15842 s.

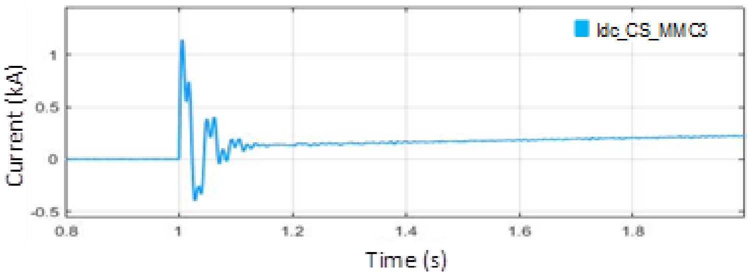

FIGURE 2.37: CURRENT AT PCC DURING DEBLOCKING OF MMC3 CONVERTER.

To facilitate improved postfault recovery, a DC voltage regulation method is adopted as an active damping controller in the MMC3 converter. Parametric sensitivity analysis is conducted on the crucial parameters of the DC voltage regulation method, specifically the Low Pass Filter (LPF), where stability relies on the relationship between the Gain (G) and the Time Constant (TC). Experimentation is employed to fine-tune the values of G and TC. Table 2.1(A) and FIGURE 2.38 (A) demonstrate the outcomes for various G and TC values at the moment the MMC3 converter is deblocked, subsequent to recovery from a severe DC fault. The results indicate the optimal values of a gain at 0.9 and time constant at 0.2. Furthermore, variations in G and TC lead to an increase in peak overshoot value and settling time.

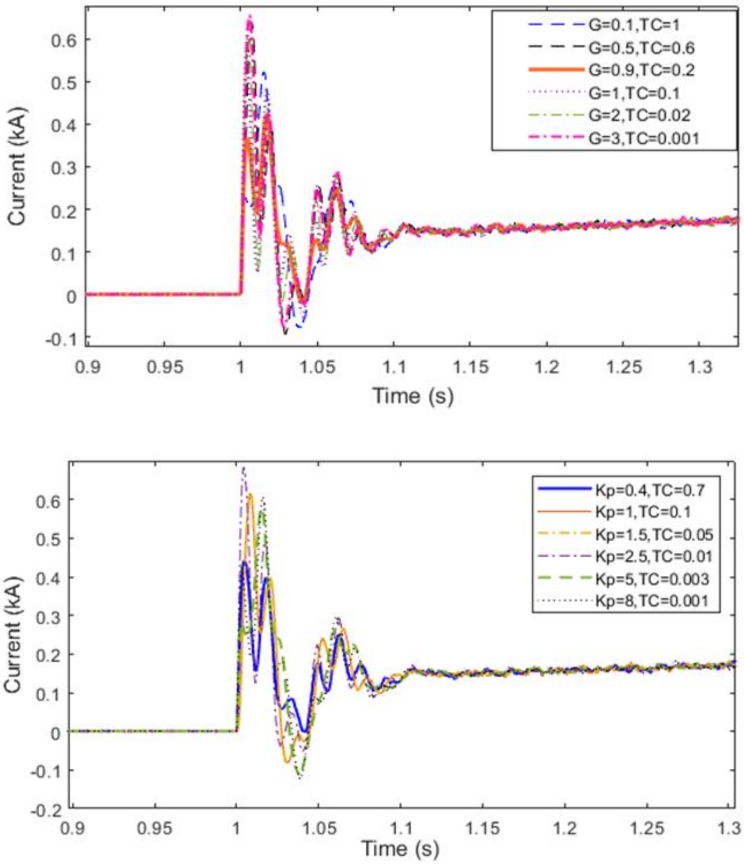

(A)

(B)

FIGURE 2.38: PARAMETRIC SENSITIVITY ANALYSIS DC-VOLTAGE REGULATION METHOD (A) LOW PASS FILTER (B) PI CONTROL COEFFICIENTS.

TABLE 2.1: OUTCOME OF THE VARIATION IN THE PARAMETERS OF ACTIVE DAMPING CONTROLLER (A) LOW PASS FILTER (B) PI CONTROL COEFFICIENTS

Gain (G)	Time Constant (TC)	Peak Overshoot Value	Settling time
0.1	1	0.508874	0.10448
0.4	0.7	0.462252	0.1164
0.5	0.6	0.627815	0.1277
0.9	**0.2**	**0.429801**	**0.11522**
1	0.1	0.561325	0.17504
1.1	0.09	0.613680	0.14924
1.4	0.06	0.605960	0.12354
2	0.02	0.591391	0.14258
2.5	0.01	0.752649	0.16358
3	0.001	0.649669	0.17627

Proportional Gain (K_P)	Integral Time Constant (ITC)	Peak Overshoot Value	Settling time
0.2	0.9	0.613245	0.11798
0.4	**0.7**	**0.435463**	**0.10706**
0.6	0.5	0.685091	0.12928
1	0.1	0.610438	0.1181
1.5	0.05	0.550054	0.1469
2	0.02	0.538552	0.17306
2.5	0.01	0.674545	0.1166
3	0.005	0.585054	0.126272
5	0.003	0.572539	0.11966
8	0.001	0.60384	0.12452

Following the LP filter is the dead-band controller, where values are chosen to prevent oscillations of the dead band controller output around the setpoint, ensuring the controller remains responsive to changes in the error signal. In this case study, the DC reference and measured DC voltage are considered in per unit. Consequently, the error becomes zero when the measured DC voltage equals the DC reference. For the study, high level and low-level thresholds are maintained at 1.05 and 0.95, respectively, while the slope of dead band block is set at 1pu/s. Optimizing the PI controller K_P (Proportional Gain) and Integral Time Constant (ITC) is critical to determine the controller's sensitivity to the error signal and eliminate steady state error. Different values of K_P and ITC are examined to achieve the desired response for the DC voltage to closely track the DC reference. Table 2.1(B) and Figure 2.38(B) present various combinations of KP and ITC, with the optimal values determined as 0.4 and 0.7, resulting in a notable reduction in overshoot time and settling time at the PCC point when the MMC3 converter is deblocked. Additionally, a rate limiter is incorporated to prevent the PI controller from making rapid and significant output changes, which could potentially lead to instability. The rate limiter's limits are set to control the rate of change of the PI controller's output. The optimal values derived from the parametric sensitivity analysis for the DC voltage regulation method are utilized and introduced as input to the inner control loop.

The modified D-Q CCSC is used in the inner control loop of the MMC3 converter. As detailed in above section, the modified D-Q CCSC involves the tuning of the band-pass filter and PI controller to minimize the influence of zero-sequence non-DC elements. The frequency of the bandpass filter should be carefully selected to permit the desired frequency components to pass through while suppressing frequencies beyond this designated range.

Table 2.2 presents the results of the frequency domain analysis, aiding in the selection of the band-pass filter's cutoff frequency based on the Gain Margin (GM) and Phase Margin (PM). For a cutoff frequency of 300 Hz, a GM of 0.42 and a PM of 47.36 degrees suggest that the system remains stable, offering some flexibility for adjustments in gain. However, the PM is a crucial indicator for stability. A PM within the range of 45 to 90 degrees is generally considered favourable for stability. For a 300 Hz cutoff frequency, it indicates a better filter response. With a cutoff frequency of 350 Hz, a GM of 8.23 signifies a comfortable gain margin, indicating favourable stability. A PM of 5.83 degrees further indicates the system is much closer to instability compared to 300 Hz. A small phase margin translates to a higher risk of oscillations and potential signal distortion within the filter's passband. However, at frequencies of 400 Hz, 500 Hz, and 600 Hz, GM are still very low, indicating that the system is susceptible to gain-related issues like unwanted amplification of noise. Nevertheless, the negative phase margins of -11.43, -161.06, and -116.79 degrees raise concerns. A negative phase margin of such magnitude implies that the system is likely to be unstable or highly underdamped, potentially leading to oscillations or poor transient response.

TABLE 2.2: FREQUENCY DOMAIN ANALYSIS TO SELECT CUT-OFF FREQUENCY OF BPF

Cut-off frequency	Gain margin	Phase margin
300 Hz	**0.42**	**47.36**
350 Hz	8.23	5.85
400 Hz	2.80	-11.43
500 Hz	3.34	-161.06
600 Hz	0.90	-116.79

TABLE 2.3: TUNING OF PI CONTROL COEFFICIENTS OF D-Q CCSC

Proportional Gain (K_P^{CCSC})	Integral Time Constant (ITC^{ccsc})	Peak Overshoot Value	Settling time
0.1	1	0.640762	0.1277
0.5	0.6	0.599984	0.147001
0.7	0.4	0.53367	0.11762
1	0.1	0.499549	0.14096
1.1	**0.09**	**0.411469**	**0.11174**
1.5	0.05	0.523293	0.1457
2	0.02	0.606246	0.1481
2.5	0.01	0.468817	0.16982
3	0.005	0.484841	0.15914

Moreover, the PI controller is meticulously adjusted while examining the response with varying values, as illustrated in Table 2.3 and Figure 2.39. An increase in KPCCSC from 0.1 to 1.1 correlates with decrease in the peak overshoot value. This reduction aligns with expectations, as higher KPCCSC values correspond to less overshoot, given the amplified control action of the proportional gain. Significantly, the settling time diminishes when ITCCCSC is reduced from 1 to 0.09. This shift occurs due to the smaller ITCCCSC value, enabling the integral action to promptly accumulate and rectify errors. However, further escalation of KPCCSC and ITCCCSC values would lead to increased peak overshoot and settling time. Consequently, the controller with KPCCSC = 1.1 and ITCCCSC = 0.09 strikes a balance, yielding relatively low overshoot (0.411469 kA) and a rapid settling time (0.11174 s). With the finely tuned parameters of the damping controller and CCSC, the reduction in overshoot and settling time amounts to 64.00% and 29.47%, respectively, compared to the MTDC network without the use of an active damping controller, as depicted in Figure 2.39 compared to Figure 2.37.

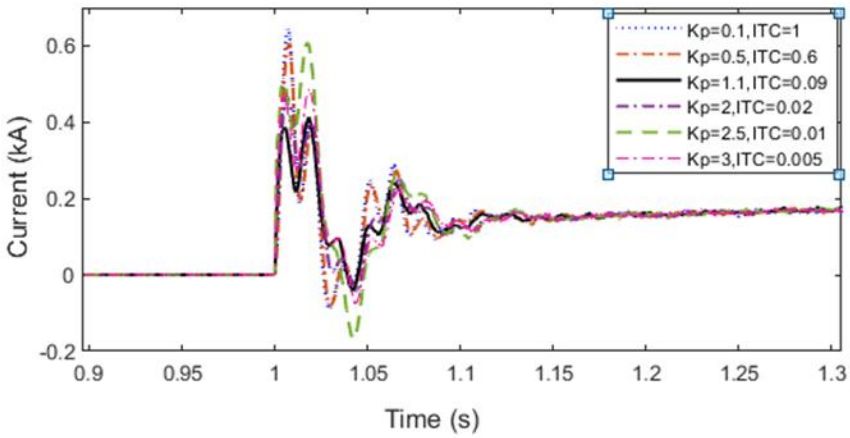

FIGURE 2.39: PARAMETRIC SENSITIVITY ANALYSIS FOR PI CONTROL COEFFICIENTS OF ENHANCED D-Q CCSC.

Proposed Control Method(s)

Traditional PI controllers are widely used for damping control due to their simplicity and effectiveness in linear systems. However, HVDC systems can exhibit non-linear behaviour under certain operating conditions (e.g., short circuit faults), which can limit the performance of PI controllers.

Modern control techniques offer promising alternatives for non-linear systems. Fuzzy Logic Controller (FLC) stands out among modern control techniques as one of the promising method, particularly in scenarios where system information is lacking or system complexity impedes comprehensive analysis [54], [55]. This is because FLC can handle imprecise or incomplete data effectively. The concept of fuzzy set theory, pioneered by Lotfi Zadeh, can be applied to control functionalities, particularly those related to damping oscillations at the DC side of HVDC networks. Unlike traditional methods that rely on crisp thresholds, fuzzy sets allow us to incorporate the inherent ambiguity or vagueness of system behaviour into the control strategy through mathematical framework [56]. A prime example is the intensity of oscillation, where the voltage/current fluctuations during deblocking event of the converter isn't always a clear-cut value like "high" or "low". These fluctuations can be gradual, transitioning from "somewhat normal" to "moderately severe" and so on it might vary. This enables the control strategy to adapt based on the degree of oscillation (encompassing both positive and negative deviation, as well as the magnitude of voltage fluctuations).

Moreover, FLC typically requires less computational resources compared to other intelligent control techniques. This translates to less computing power needed to implement the control strategy. FLC generally needs less complex calculations compared to other intelligent control techniques, making it more efficient for real-time control applications [57].

This study proposes a novel control approach for HVDC systems: a coordinated FLC and PI controller for improved damping performance. The FLC leverages its ability to handle non-linearities, such as changing power flow patterns, which can significantly impact oscillation behaviour. This allows the FLC to adapt the control strategy in real-time. The PI controller provides a well-established framework for achieving good overall system performance. By combining these strengths, the coordinated FLC-PI approach has the potential to lead to faster settling times and reduced overshoot compared to traditional methods.

The Active Damping Controller (ADC) circuit examined here is a DC voltage regulation method consisting of a PI controller and a fuzzy controller, as depicted in Figure 2.40. The fuzzy controller acts as a pre-processing stage for the PI controller, enabling it to handle nonlinearities (such as saturation in converter outputs) and effectively transforming the input for the PI controller. Thus, a coordinated approach, integrating fuzzy control alongside traditional PI controllers, offers a practical way to leverage the advantages of fuzzy logic without complete replacement [58].

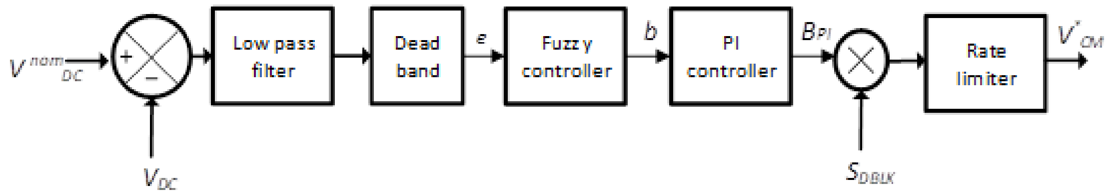

FIGURE 2.40: ENHANCED DC VOLTAGE REGULATION METHOD.

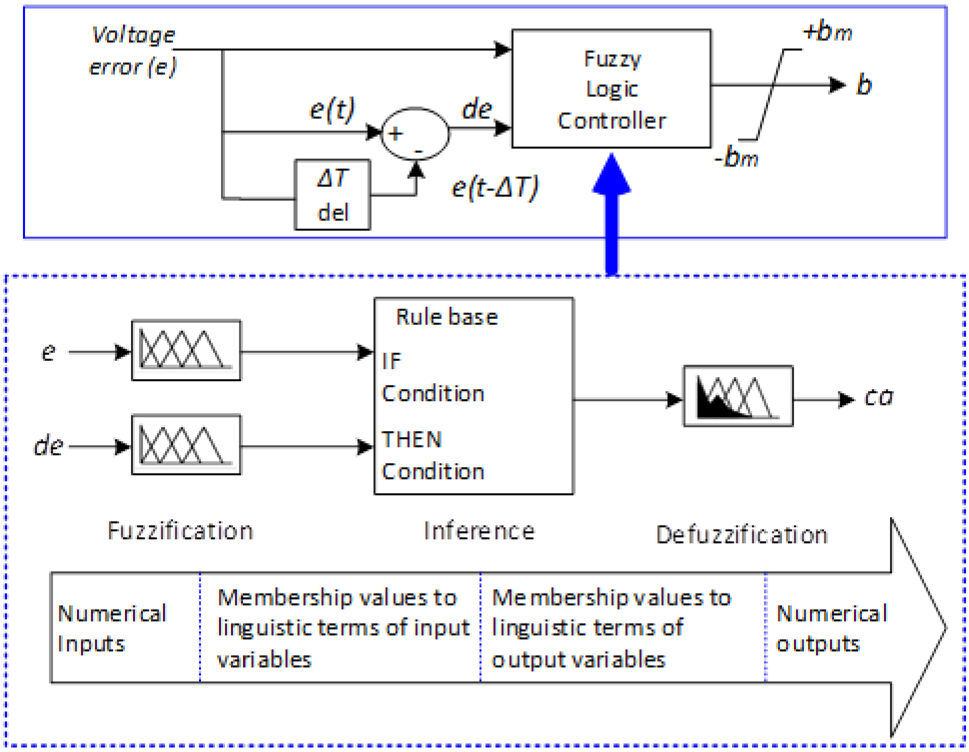

FIGURE 2.41: FUZZY LOGIC CONTROLLER WITH STRUCTURE OF A FUZZY SYSTEM WITH NUMERICAL INPUTS 'E', 'DE' AND NUMERICAL OUTPUTS 'CA'.

Further, designing a step of a fuzzy controller is a crucial step in this approach. A fuzzy logic controller requires appropriate ranges for input and output values, membership functions, a fuzzification method, a set of if-then rules, and a defuzzification method. The fuzzy logic controller is shown in Figure 2.41. The inputs to the fuzzy controller are derived from error signal (*e*) and the rate of change of error (*de*). A fuzzy logic controller consists of three stages [57]: Fuzzification, which converts crisp numerical inputs (e.g., error signal (e) and rate of change of error (de)) into fuzzy membership values; the inference mechanism, which uses linguistic if-then rules and logical operators like AND and OR to map fuzzy inputs to fuzzy outputs, with common models being Mamdani (fuzzy output membership functions) and Sugeno (weighted average of consequents); and Defuzzification, which transforms the aggregated fuzzy set into a single crisp output value (e.g., ‘ca’) using methods like the centroid method, bisector, or largest of maximum, influencing the FLC's control behaviour. The fuzzy interface process is illustrated in Figure 2.41.

A crucial aspect of this FLC design is finding the right balance between complexity and control effectiveness for damping DC-side oscillations in HVDC networks. This study utilizes five linguistic values for both the error (e) and the rate of change of error (de): "negative high (nh)," "negative (n)," "zero (z)," "positive (p)," and "positive high (ph)." This choice offers several advantages:

1) **Reduced Rule Complexity:** Complexity, in this context, refers to the number of fuzzy sets (linguistic values) and rules required for effective control. Using a larger number of values would necessitate a much more intricate rule base, increasing computational burden and potentially leading to overfitting. Five values provide a good compromise, offering sufficient granularity to capture the essential error dynamics that influence DC-side oscillations, while keeping the number of rules manageable.
2) **Effective Control for Oscillation Damping:** Too few linguistic values could limit the FLC's ability to differentiate between critical voltage deviations and minor fluctuations. The chosen five values allow the FLC to distinguish between:

- **Magnitude of Error:** The "nh," "n," "z," "p," and "ph" values represent different error magnitudes in DC voltage. This enables the FLC to tailor its response based on the severity of the oscillation. Significant deviations (nh) require a stronger corrective action compared to smaller errors (n).
- **Adapting to Error Dynamics:** Including the rate of change of error (de) provides crucial information about how quickly the voltage error is changing. This allows the FLC to adapt its response dynamically for more effective oscillation damping. For instance, a large negative error (nh) with a rapidly decreasing rate of change (de) might indicate a self-correcting transient. In this scenario, the FLC can apply a less aggressive correction to avoid unnecessary control actions. Conversely, a large negative error with a still-increasing rate of change (de) suggests a more sustained voltage drop, requiring a stronger corrective action from the FLC to prevent further oscillation buildup.

By effectively capturing both the magnitude and rate of change of the error signal, these five linguistic values empower the FLC to make fine-tuned adjustments that directly influence the DC voltage.

This design utilizes triangular (*trimf*) or trapezoidal (*trapmf)* membership functions (MFs) to represent linguistic values associated with control variables within the range of [-1, 1]. This range facilitates the normalization of input and output variables, which is crucial for effective fuzzy logic control. As demonstrated in Figure 2.42, Figure 2.43, and Figure 2.44, these MFs offer several advantages. Their simplicity contributes to computational efficiency, while their interpretability simplifies design and debugging. Additionally, the smooth transitions between membership levels prevent abrupt changes in the control outputs, leading to a more stable control system [59]. The width and slopes of these MFs influence the overlap and smoothness of the transition between fuzzified sets.

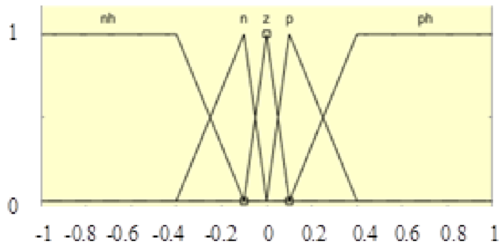

FIGURE 2.42: MEMBERSHIP FUNCTIONS OF INPUT VARIABLE, ERROR (*E*).

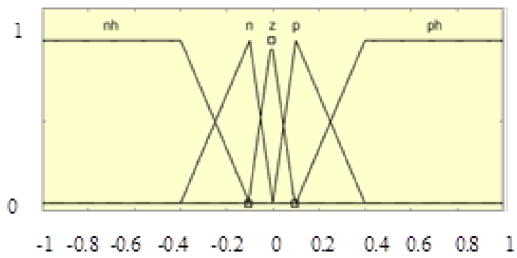

FIGURE 2.43: MEMBERSHIP FUNCTIONS OF INPUT VARIABLE, DIFFERENCE IN ERROR (*DE*).

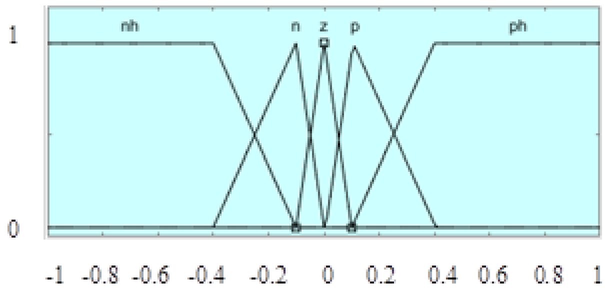

FIGURE 2.44: MEMBERSHIP FUNCTIONS OF OUTPUT VARIABLE, CONTROL ACTION (*CA*)

Once fuzzification is done, it translates precise data into fuzzy sets, enabling the system to reason with linguistic rules based on these sets. The fuzzy controller utilizes a set of if-then rules to determine the appropriate control action for regulating DC voltage. These rules consider both the error (*e*) and the rate of change of error (*de*) as illustrated by Table 2.4 which represent FLC decision making strategy.

Five linguistic values for the output (control action) are considered: "negative high (nh)," "negative (n)," "zero (z)," "positive (p)," and "positive high (ph)." This choice offers a range of control actions that translate into adjustments to the reference for active power injection. These adjustments, provided to the PI controller, ultimately influence the converter control system to regulate the DC voltage and effectively dampen oscillations.

Each rule maps a combination of error and rate of change values (e.g., "large negative error, *nh*" and "rapidly decreasing, *nh*") to a specific control action ("decrease output significantly, *nh*"). These values allow the FLC to make dynamic adjustments to the desired active power injection based on the system's behaviour.

For example, in Table 2.4, If the error is significantly negative(e=nh) (large voltage drop), the FLC increases active power injection (decrease control action (output)) to counter the voltage drop. Further, a rapidly decreasing rate of change (de = nh) alongside a significant negative error (e = nh) indicates a quickly worsening voltage drop. This is reflected in rule: "If e is 'nh' and de is 'nh,' then control action is 'nh'").

Further, if the error is significantly negative (e = nh) but the rate of change is positive (de = p), it suggests the voltage is decreasing but starting to recover. A fuzzy rule like: *If e* is 'nh' and *de* is 'p', then control action is 'n') reflects such case. For smaller errors (e= n, p), the FLC might adjust active power more moderately based on the error severity and rate of change (e.g. *If e* is 'z' and *de* is 'p', then control action is 'p'). When the error is zero (e=z) (desired voltage is achieved), the FLC aims to maintain the voltage by keeping the control action around zero (e.g. *If e* is 'z' and *de* is 'z', then control action is 'z').

TABLE 2.4: FUZZY RULES

de \ e	nh	n	z	p	ph
nh	nh	nh	nh	n	z
n	nh	nh	n	z	P
z	nh	n	z	p	Ph
p	n	z	p	ph	Ph
ph	z	p	ph	ph	Ph

The max-min inference operator, a popular method in fuzzy control systems, is employed to evaluate the if-then rules in this study. The inference engine incorporated the Mamdani fuzzy model. The well-known COG method is a popular defuzzification choice due to its computational efficiency and intuitive output generation [59]. This allows for the conversion of fuzzy outputs into crisp values for control decisions.

The PI controller takes the crisp control signal from the de-fuzzifier as its input. It combines the signal (*b*) with its proportional gain (*Kp)* and time constant (T_i) to adjust the final control output (*BPI*). The *Kp* and T_i values are considered 0.4 and 0.7 which is obtained after fine-tuning of PI controller using trial and error approach as discussed in parametric sensitivity section.

A user defined module for the FLC has been created using component builder (c-builder) facility available in RSCAD simulation tool and PI controller is added to it. The controller works as a coordinated Fuzzy & PI controller. The proposed Active Damping Controller (ADC) controller is tested using four-terminal terminal MMC-based MTDC network as discussed in detail in section 0(parametric sensitivity analysis), where proposed ADC shown in Figure 2.40 is used in outer loop for damping the oscillations at DC side of converter during post fault recovery. The current at the PCC during the deblocking of the converter is observed during deblocking of the converter (MMC3) after subsequent recovery from DC fault.

Table 2.5 and Figure 2.45 illustrate the outcomes of the advanced controller used in the Active Damping Controller (ADC), comparing the performance of ADC with fuzzy controller, PI controller, coordinated fuzzy PI controller, and without ADC (baseline scenario when no ADC is used) during the deblocking of the MMC3 converter following recovery from a severe DC fault. As discussed in the previous section, when no ADC is used, the current at PCC during the deblocking of the converter is depicted by the black dotted line in Figure 2.45.

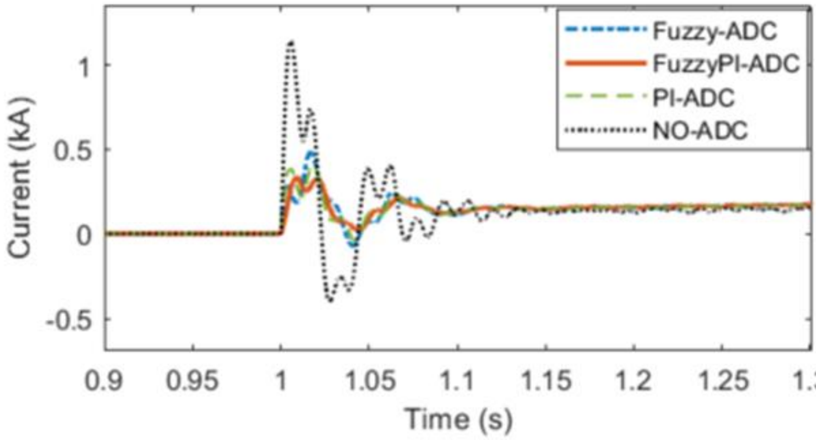

FIGURE 2.45: PERFORMANCE OF ADC USING FUZZY CONTROLLER, PI CONTROLLER, ENHANCED CONTROLLER AND WITHOUT ADC.

TABLE 2.5: OUTCOMES OF DIFFERENT CONTROLLERS USED IN THE STUDY

Controller	Peak-overshoot Value (kA)	Settling time (s)
PI	0.411468	0.11174
Fuzzy	0.429850	0.12421
Fuzzy +PI	0.330971	0.10016

During this process, a peak overshoot of 1.1431 kA is observed, with a settling time of 0.15842 s. With a fine-tuned PI controller used in ADC, a reduction in overshoot and settling time by 64.00% and 29.47%, respectively, is observed. When only a fuzzy controller is used in ADC, a reduction in overshoot by 62.40% and decrease in settling time by 21.57% are noted. For better post fault recovery after severe DC fault, the coordinated fuzzy PI controller achieves the best performance leading to reduction in overshoot by 71.05% and settling time by 36.78% compared to when no ADC is used. Further, the enhanced controller achieved a significant 19.56% reduction in overshoot and a 10.36% reduction in settling time compared to the fine-tuned PI controller used in the DC -side voltage regulator approach [44].

The enhanced ADC is compared to some key existing approaches from the literature review, as enhanced fuzzy-PI controller achieves a significant 19.56% reduction in overshoot, demonstrating exceptional transient response improvement and provides better damping of oscillations. This translates to faster settling time (10.36%), indicating a quicker reduction in steady-state error. The comparison with other key approaches is shown in Table 2.6 which shows the effectiveness of enhanced approach when compared with key performance indices such as overshoot time and settling time.

So, the coordinated Fuzzy-PI controller emerges as the most effective strategy for mitigating current fluctuations during the deblocking process of the converter (MMC3). This success hinges on its ability to leverage the strengths of both approaches: fuzzy logic component provides adaptability by handling the non-linearities and uncertainties inherent in the HVDC networks. This allows the controller to react swiftly to the initial change in operating point, minimizing overshoot and PI Control for precision as the controller component ensures precise adjustments and effective damping of system oscillations. This collaboration leads to a faster settling time and overall better performance.

TABLE 2.6: PERFORMANCE EVALUATION OF ENHANCED CONTROLLER

Method	Reference	Reduction in Overshoot (%)	Reduction in Settling Time (%)
Enhanced Fuzzy + PI Controller	-	19.56	10.36
D-Q CCSC with Modulated Signal	[12]	2.59	3.57
CCSC with MPC	[7]	---	13.6 (compared to PI)
Modified D-Q CCSC (FCCC)	[19]	7	12

However, it is crucial to remember that the effectiveness of the coordinated Fuzzy-PI controller is highly dependent on the design of the fuzzy logic component. The choice of linguistic values, membership functions, and rule base all significantly influence the controller's ability to interpret system states and generate appropriate control actions. Careful design and optimization of these fuzzy logic elements are essential to unlock the full potential of this powerful control strategy.

Conclusions

The section related to other optional core functions presents a thorough examination and a new control functionality for oscillation damping of an MTDC interconnected offshore-onshore system. The research is done by utilizing EMT-based simulations. Through a comprehensive literature review, it addresses research gaps concerning sub-synchronous oscillation damping on the DC side of HVDC networks. Specifically, it delves into a DC-voltage regulation method paired with a modified CCSC to enhance post-fault recovery of the converter. The study conducts meticulous parametric sensitivity analysis to evaluate system performance, resulting in a notable 34.46% reduction in overshoot and a 12.50% improvement in settling time compared to the initial controller parameterization. These findings contribute to the refinement of post-fault recovery mechanisms, bolstering the resilience of complex offshore-onshore HVDC networks.

Furthermore, the study extends its scope by introducing a coordinated fuzzy-PI controller to enhance controller performance. This approach offers an enhanced and adaptable strategy compared to traditional PI controllers in DC voltage regulation. The coordinated fuzzy-PI controller demonstrates significant improvements in post-fault recovery, evidenced by a 19.56% reduction in current overshoot. This enhancement translates to exceptional transient response improvement and better oscillation damping, resulting in a 10.36% faster settling time indicating a quicker reduction in steady-state error. Overall, this research underscores the potential of coordinated fuzzy-PI control in enhancing the dynamic performance and fault tolerance of MMC-based MTDC networks, thus contributing to the resilience of AC/DC networks.

3. Supplementary Control Functions

Moving to an upper layer of the structure proposed in the IEC TS 63291-1:2023 (See section 1.2), this section presents the investigations and proposals of the HVDC-WISE project regarding the functionalities that might be included in the "**Supplementary control functions**". The first part of the chapter will cope with control proposals that can go into the **"Coordinated control"** block**.** While the second part of the chapter focuses on the layer defined as "**AC/DC grid control"**.

3.1 Coordinated control: Primary Control for AC grid support

In [60] "HVDC Links in System Operations", ENTSOE, 2019, it is recognized that the use of advanced functionalities of HVDC links in system operation is essential for the secure and efficient operation of the AC/DC grid. These functionalities are summarized in Table 3.1.

TABLE 3.1: FUNCTIONALITIES OF HVDC LINKS IN SYSTEM OPERATION

	Functionality	Embedded	Non-embedded	LCC	VSC
1	Voltage control	x	x	–	x
2	Static and dynamic reactive power control	x	x	–	x
3	Active power control[4]	x	x	x*	x
4	Frequency control – FCR delivery	–	x	x*	x
5	Frequency control – FRR delivery	–	x	x*	x
6	Frequency control – RR delivery	–	x	x*	x
7	Power oscillation damping (POD)	x	x	x	x
8	Sub-synchronous damping (SSD)	x	x	x	x
9	Emergency Power Control (EPC)	x	x	x	x
10	AC line emulation	x	–	x	x
11	Special protection schemes (SPS)	x	x	x	x
12	DC Loop Flow	–	x	x	x
13	Operating an island	–	x	–	x
14	System restoration	–	x	x[5]	x
15	System Inertia (SI)	x**	x	–	x

[4] Active power control in normal operation (preventive congestion management, scheduling etc.)
* Minimum power transfer via converter needed
** only with additional storage equipment on DC side
[5] LCC can support system restoration, it cannot restore (black start capability) on its own

Although [60] focuses mainly on existing HVDC links, it can be expected that some or all of these functions might be applied in future HVDC multi-terminal systems. Starting from the presented list of functionalities, this section targets the functions that can be achieved within the **coordinated system** control layer. We are thus interested in the functions that can be performed or enhanced through coordination between stations within a timeframe **of hundreds of milliseconds to a few seconds**. Additionally, we will focus on coordinated (via communication) functions that require measurements available at all stations' location, as to ease the implementation of such controls. From the table below, we select and group the functionalities that meet these criteria for analysis in this section. These functionalities are: **Low-frequency power oscillation damping, AC line emulation, and**

Frequency control. In the following paragraphs, these functionalities are defined, current implementations on HVDC links and MTDC grids are discussed.

3.1.1 Low-frequency power oscillation damping

The term “low-frequency” is used to specify that the oscillations addressed in the following studies are of the electromechanical type, occurring within the range of 0.1 to 1 Hz. These should not be confused with sub-synchronous oscillations or converter-driven slow interactions. Low-frequency oscillations are inherent to large, interconnected power systems and pose significant challenges for power system operators. According to the “European network code on requirements for grid connection of high voltage direct current systems and direct current-connected power park modules,” it is stated that the HVDC system shall be capable of contributing to the damping of power oscillations in connected AC networks. The control system of the HVDC system shall not reduce the damping of power oscillations.

Implementations in HVDC links

Controllers designed to damp low-frequency oscillations using HVDC systems have been extensively studied in the literature. An extensive survey of both theoretical approaches and actual implementations in HVDC projects is presented in [61].

Power oscillation damping controllers (PODs) generally consist of a **controller** that processes one or more **measured signals** from the system and modulates a **control output signal** in the system. The **measured signals** analyzed in the literature include generator speeds, frequencies, voltages, and active power on AC lines, among others. The **control** laws embedded in these controllers range from simple proportional gains or PID controllers to more complex control laws, such as optimization-based methods. When HVDC links are used to damp oscillations, the **control outputs** can include various reference signals, such as active power reference, reactive power reference, DC voltage reference, active current reference, etc. The most common signals are active power references (these controllers are known as POD-P) and reactive power references (known as POD-Q). Depending on the topological situation of the HVDC system with respect to the targeted oscillations, active or reactive power modulations could be more or less effective. In embedded HVDC links active and reactive power injections are recommended. However, in the case of HVDC interconnecting asynchronous grids, POD-P is not recommended, as the modulated active power necessary to damp the oscillation in one grid will be injected in the second grid, thus disturbing it and potentially exciting electromechanical modes [62].

Implementations in multi-terminal HVDC systems

Compared to HVDC links, multiterminal HVDC grids offer more control outputs to damp the oscillations. Reference [61], also includes an extensive survey on research items in which the MTDC are used to damp oscillations.

The primary challenge in multi-terminal DC grids lies in the distribution of DC voltage control across multiple stations. Each station injects or absorbs active power to stabilize the DC voltage, typically employing a DC-voltage-to-active power (or current) droop control schemes. However, utilizing active power for damping inter-area oscillations within one asynchronous area can inadvertently transfer these oscillations to another synchronous area due to voltage droop effects, as shown later in this report.

To address this challenge, works such as those presented in [63] and [64] propose coordinating the active power references of two or more converters within the same synchronous area. This coordination, facilitated through communication, aims to target specific oscillations for damping. The concepts introduced in [63] and [64] serve as foundational ideas for the proposals outlined in this document.

Furthermore, reactive power injections offer an alternative method for oscillation damping. Reactive power does not interact with the DC voltage control system, preventing oscillation propagation via the DC voltage of the system to other areas. This unique advantage underscores the efficacy of reactive power modulation in dampening oscillations within MTDC grids [63].

3.1.2 AC line emulation

Embedded HVDC links can mimic the behavior of AC circuits or networks through AC line emulation. This feature proves invaluable during power disturbances, such as load changes or line trips, as it allows for real-time adaptation without manual intervention from operators.

Implementations in HVDC links

AC line emulation in HVDC links involves automatically adjusting the power setpoint of the link proportionally to the angle differences between the AC voltages at each converter station. Unlike certain frequency control implementations that rely solely on local measurements, AC line emulation necessitates communication between involved stations. This control method, also known as **Angle Difference Control (ADC)**, has been successfully utilized in projects like the INELFE link [65] where it effectively mitigated overloading on AC lines following significant power disruptions.

Implementations in multi-terminal HVDC systems

In [66] [64] and [67] authors propose a control strategy wherein the active power references of all dispatchable stations are adjusted based on a linear combination of voltage angles measured at connecting points. This approach effectively emulates the behavior of an AC network and forms the basis for subsequent discussions.

Challenges

However, challenges arise with AC line emulation controllers, as highlighted in [65] [68] and further analyzed in [69]. Depending on the topological configuration of HVDC links, these controllers may inadvertently impact the damping of certain electromechanical modes within the system. To mitigate this risk, careful consideration must be given to the controller's time response. Additionally, if adopting an AC line emulation controller, it is advisable for the HVDC link to provide some level of damping (via for example a POD) to ensure secure system operation [60]. In the following section, this report proposes a simple solution to overcome this issue.

3.1.3 Frequency control

When asynchronous AC grids are interconnected via an HVDC link, they can mutually support each other’s frequency stability by providing balancing power as needed. This capability is crucial not only for interconnected mainland grids but also for scenarios involving offshore wind farms connected to the mainland through HVDC systems or storage systems connected to the AC grid via HVDC. In such cases, the HVDC link facilitates the provision of balancing services.

An HVDC system can balance power through various mechanisms, each operating on different time scales: Fast Frequency Response (FFR), Frequency Containment Reserve (FCR), Frequency Restoration

Reserve (FRR), and Replacement Reserve (RR), as illustrated in Figure 3.1. For detailed definitions of these mechanisms, readers are encouraged to refer to [70].

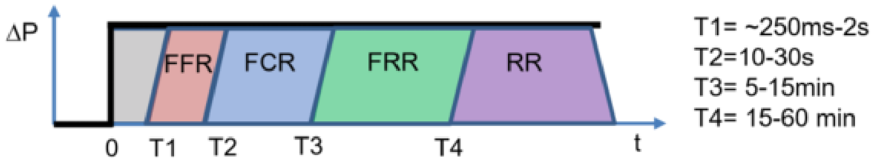

FIGURE 3.1: FREQUENCY SERVICES [70].

As the services encompassed between the hundreds of milliseconds to the tens of seconds are FFR and FCR, those are the ones considered in this section and will be encompassed in the term "Primary frequency control". **Therefore,** considered that the response of the converters under the FFR time-frame is managed at the local level (e.g., with the controls proposed in Section 2.1.2), while the FRR and RR are managed by higher-level layers of control.

Implementations in HVDC links

Traditionally, HVDC links implement this function by adjusting the active power reference proportionally to the frequency deviation at the receiving end or the difference between frequencies at both ends. This adjustment is achieved using a droop gain, similar to the method employed by synchronous generators. When the need for Frequency Containment Reserve arises, automatic initiation of balancing power transmission occurs by multiplying the frequency deviation difference with a droop factor. This calculation results in a change in the active power reference value in the converters. To prevent unnecessary activation of Frequency Containment Reserve during minor frequency deviations, a dead band may be incorporated.

While more complex implementations exist in the literature, such as utilizing center of inertia frequency measurements or coordinating multiple HVDC links, many projects opt for the simplicity of primary frequency control via droop gains. In the subsequent sections, we'll focus on analyzing coordinated droop-gain-based schemes.

Implementations in multi-terminal HVDC systems

As with the POD-P, the primary challenge in sharing primary frequency reserves via an HVDC system lies in the fact that the DC voltage control is distributed among dispatchable stations. The DC voltage droop control adjusts active power setpoints of several stations proportionally to DC voltage deviations measured by converters, which can lead to undesirable interactions between frequency and voltage control.

To address this challenge, coordinated controllers have been proposed to mitigate interactions between frequency and voltage controllers. In In [71] a comparison is drawn between simple droop-based schemes utilizing only local measurements and coordinated schemes coordinating active power references of converters. In subsequent sections, we'll adopt the control implementations proposed in In [71] for our investigations.

3.1.4 Identified challenges

It has been observed that the targeted services are provided via the modulation of active power (oscillation damping can be also achieved via POD-Q, but with different performances), while active power is also used for the DC voltage (identified in section 2.1 as a constraint function). Therefore, Coordination is necessary to provide the expected services while assuring minimal interactions with the DC voltage control.

3.1.5 Proposed framework and control

Therefore, to avoid interfering with the DC voltage control, it is proposed that the sum supplementary active power references provided by supplementary controls (frequency droop, ac line emulation controllers, POD or others) should be zero. **The "channel (or virtual link in** [64], [72]**)" concept can be used: If converter i modulates its power by ΔP_{ij}, converter j modulates the same amount of power in the opposite direction, thus $-\Delta P_{ji}$ (this coordination is achieved using communication).**

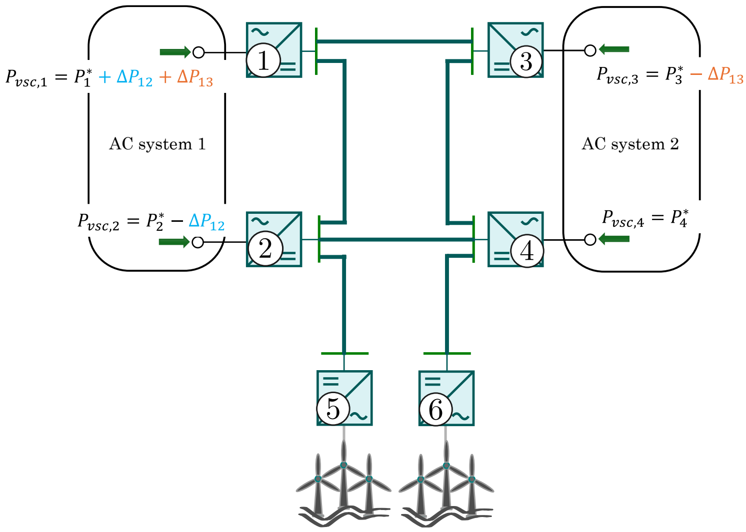

FIGURE 3.2: THE CHANNEL CONCEPT.

In Figure 3.2: The channel conceptFigure 3.2, let P_1^* and P_2^* be the power setpoints of stations 1 and 2 given by the dispatch center (or any other higher-level layer of control) and ΔP_{12} be the power variation generated by any supplementary control. As power absorbed/injected by station 1 to the DC grid is equal to the power injected/absorbed by station 2, the voltage of the DC grid will be almost not disturbed. It can be said that ΔP_{12} is the power modulation by a controller for channel 1-2. In Figure 3.2 the modulation of channel 1-3 (ΔP_{13}) between stations 1 and 3 is also represented. Note that there can be $\frac{m(m-1)}{2}$ number of channels, where m is the number of dispatchable stations.

Within this framework, the control inputs for the proposed supplementary controllers are no longer the modulated power of each station (ΔP_i), but the modulated power of each channel (ΔP_{ij}). This assures that the sum of active power modulations is always zero, so the interactions with the DC voltage control are minimized.

Adopted implementations for targeted functionalities

In Figure 3.3, an overview of the proposed control layer is illustrated. At the proposed control layer, an illustration of the possible channels is represented. Note that, as there are 4 dispatchable stations, 6 channels are possible (noted ch_{ij} in Figure 3.3). Measurements at the station level (voltage angles and frequencies as explained later) are sent by each station to the control layer, and the control layer sends back the necessary active power modulations to the stations.

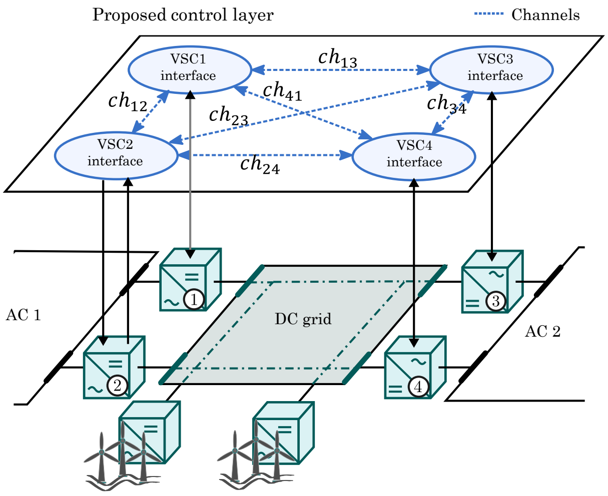

FIGURE 3.3: PROPOSED CONTROL LAYER.

In further works, different sorts of DC connected devices could be considered. Especially, **DC-connected energy storage converters can be introduced as additional dispatchable terminals.**

In the following paragraphs, the implemented controllers for providing different services are described.

Power oscillation damping

The proposed implementation is depicted in Figure 3.4. As proposed in [64], the POD in channel i-j achieved by applying a gain K_{POD} to the difference of the instantaneous frequencies f_i and f_j measured at the point of connection of the stations belonging to the channel. Additionally, as suggested [63] in a first-order filter is included to reduce the effect of noise in the measurements and communication delays. Also, a lead-lag filter is incorporated and can be tuned to target specific electromechanical modes.

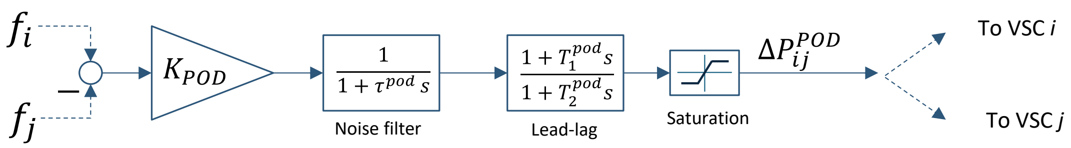

FIGURE 3.4: POD CONTROL IMPLEMENTATION IN CHANNEL I-J.

Note that this implementation only makes sense if stations i and j belong to the same synchronous area, otherwise the oscillation can be transmitted to one asynchronous area to another.

AC line emulation

For the AC line emulation, the Angle Difference Control (ADC) is used. As suggested in [64], the ADC in channel i-j achieved by applying a gain K_{POD} to the difference of the voltage angle θ_i and θ_j measured at the point of connection of the stations belonging to the channel.

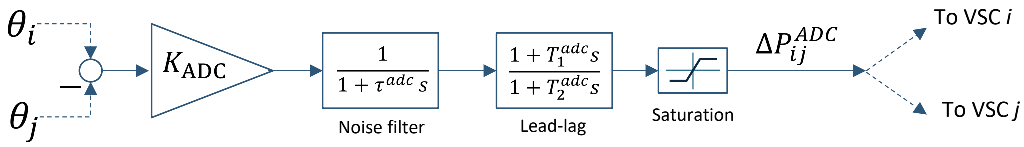

FIGURE 3.5: ADC IMPLEMENTATION IN CHANNEL I-J.

As firstly observed in [65] in real event in the European power system (reported also in [68]) and further analyzed in [69], the angle difference control with a filter to reduce measurements noise and delays is prone to affect the damping of interarea modes. To overcome this issue, [68] and [69] propose to increase the time constant of this filter. While a time constant of around 750ms is necessary for noise measurement and communication delays, [65] and [68] suggest increasing the time constant to approximately 50s. This slows the controller's action to stay outside the frequency range of interarea oscillations, avoiding their excitation. Therefore, ADC control is only used for static purposes (i.e., automatic power redispatch), reducing any potential contribution to dynamic phenomena.

To exploit the fast active power control of the HVDC link and make ADC useful for dynamic issues in the grid (such as first swing stability and active power oscillations), this report proposes a simple but effective solution. A lead-lag filter is added to the noise filter (whose time constant can remain in the range of milliseconds) to correct the phase of the injected active power, providing damping power to the AC grid. In this manner, ADC not only serves static purposes but also enhances the rotor angle stability of the grid.

Note that this implementation is only suitable if stations i and j belong to the same synchronous area.

Frequency control

The frequency control is based on the proposals in [71]. In an HVDC connecting two asynchronous areas, the frequency control can be applied in a bilateral manner [73]. This means the control reacts to the frequency deviation measured at both ends, but with different droop gains for each end. These droop gains can be tuned based on factors such as the size of each AC synchronous area or the allowable frequency deviation.

The same principle is applied here to a channel. For channel i-j, where VSC i is in a different asynchronous area than VSC j, the controller applies different frequency droop gains for the frequency deviations measured at each station belonging to the channel. For example, $(f^* - f_i) * K_{FCR}^{ij}$, represents the contribution demanded in the synchronous area where VSC i is connected, which will come from the area where VSC j is connected. Similarly, $(f^* - f_j) * K_{FCR}^{ji}$ applies to the area where converter j is connected. Having two different gains (K_{FCR}^{ij} and K_{FCR}^{ji}) allows for adjusting the priority between the pairs while considering the different frequency requirements of the AC zones.

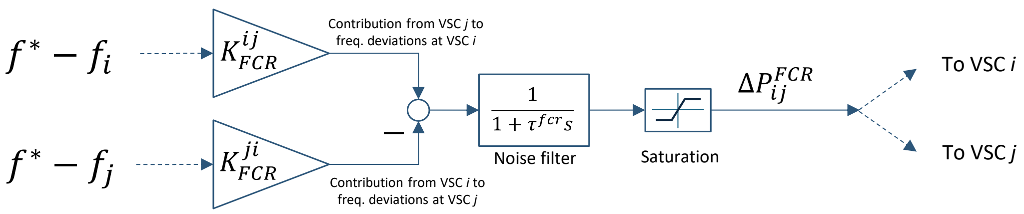

FIGURE 3.6: FREQUENCY CONTROL BASED ON BILATERAL EXCHANGES FOR CHANNEL I-J.

Note that frequency control is only suitable if stations *i* and *j* belong to different synchronous areas.

In the three different presented controls, it is noted that a **saturation block** is used per channel. This saturation serves to adjust the **power headroom** the converter can allocate for each service.

3.1.6 Benchmark Implementation

In order to test the proposed controllers, the Benchmark depicted in Figure 3.7 has been implemented using the Modelica Language. The system is composed of 6-terminal HVDC grid interconnecting two asynchronous systems (A1 and A2) together with some offshore production. This system can be seen as a very simplified version of a multiterminal DC grid interconnecting from example the continental Europe network with the GB network while importing offshore production. The objective of the test system is to be able to capture in simple but representative manner at the same time the frequency and the rotor-angle stability phenomena on the AC side and the dynamic behavior of the DC voltage.

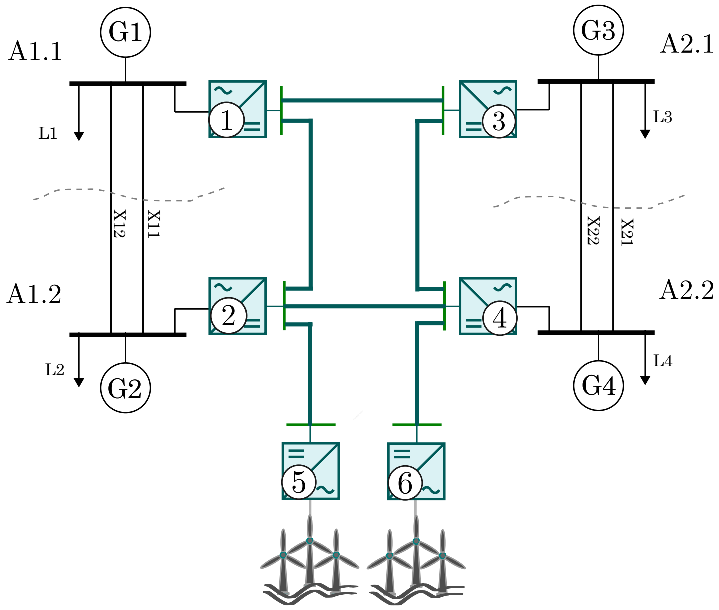

FIGURE 3.7: TEST SYSTEM FOR COORDINATED CONTROL.

Each asynchronous area is composed of 2 synchronous areas interconnected by an AC corridor, e.g. the asynchronous system A1 (A2) is composed of Areas A1.1 (A2.1) and A1.2 (A2.2) interconnected by the corridor composed of lines X11 (X21) and X12 (X22). This representation will allow to understand the behavior of the power exchanges inside a synchronous area following different disturbances.

Each area is composed by an equivalent synchronous generator that represents the installed synchronous generation in the area and an equivalent aggregated load. The generators are equipped with turbine governors and primary frequency control to capture the frequency dynamics of the systems. The important characteristics of the area are summarized in Table 3.2.

TABLE 3.2: CHARACTERISTICS OF EACH AREA

Area	Synchronous Capacity	Inertia	Equivalent Generator Droop	Situation
A1.1	10 GW	5s	0.2 pu/pu (P/f) in area capacity as base	Exporting 400MW to A1.2
A1.2	10 GW	5s	0.2 pu/pu (P/f) in area capacity as base	Importing 400MW from A1.1
A2.1	10 GW	5s	0.2 pu/pu (P/f) in area capacity as base	Exporting 400MW to A2.1
A2.2	10 GW	5s	0.2 pu/pu (P/f) in area capacity as base	Importing 400MW from A2.2

In each asynchronous system the areas are interconnected by AC corridors. In this test system, the AC lines (L11, L12, L21, L22) have an equivalent inductance of 1.25 pu (Base power = 1 GW, Base voltage = 320 kV).

The two asynchronous areas are interconnected by a 5-terminal DC grid. The control modes and the power setpoints of the different stations are summarized in Table 3.3.

TABLE 3.3: CHRACTERISTICS OF EACH VSC STATION

Station	Rating	Control mode	Active Power dispatch	Droop gain K_V
1	1 GW	Vdc droop	P = 200 MW, Q = 0	8 MW/kV
2	1 GW	Vdc droop	600 MW, Q = 0	10 MW/kV
3	1 GW	Vdc droop	200 MW, Q = 0	8 MW/kV
4	1 GW	Vdc droop	800 MW, Q = 0	10 MW/kV
5	1 GW	V/f	Non dispatchable; 900 MW injected by the offshore windfarms	N/A
6	1 GW	V/f	Non dispatchable; 900 MW injected by the offshore windfarms	N/A

All the cables in the DC grid are represented by a PI model and all the m represent a 100km cable sections. With $r = 0.02\ \Omega/\mathrm{km}$, $l = 1.4\ mH/km$. The capacitive effect on the cables is included in the DC capacitor of each VSC station ($195\mu F$). Other dynamic parameters of the VSC stations are summarized in Table 3.4.

TABLE 3.4: PARAMETERS OF VSC STATIONS

Parameter	Value
Base power	1 MVA
Base AC voltage	320 kV
Base DC voltage	640 kV
AC Connection resistance	0.001 pu
AC Connection inductance	0.18 pu
DC capacitor	195.31 μF
AC current loop time response	10 ms
Maximal current	1.2 pu
PLL time response	5 ms
SCR	>10

For the simulation, the models of the AC components are the ones from iPSL library presented in [74], and the HVDC components are the ones presented and used in [75].

From the proposed power flow situation in described in the tables below it can be observed that the offshore windfarms (Stations 5 and 6) are injecting 1800MW of offshore production to the AC systems (800 to A1 and 1000 to A2). It can be inferred that Areas A1.2 and A2.2 have important demand as they are importing power via the AC corridors from A1.1 and A2.1 respectively, and the power dispatch of stations 2 and 4 is higher than stations 1 and 3.

3.1.7 Results - POD

Case 0 – No supplementary control (or Constant power reference) in case of line tripping

As to understand the phenomena to be treated (electromechanical low frequency oscillations or inter-area oscillations), the disconnection of the line X12 at t=2s is simulated. In this first example, the active power references of the MTDC are not modified by any supplementary control as shown in Figure . Figure shows the active power on the two AC lines (X11 and X12) of the corridor. Before the event, both lines were loaded at 200 MW each, when the disconnection occurs, the power is reallocated on the remaining line X11 (from 200 MW to 400 MW), however badly damped oscillations are observed.

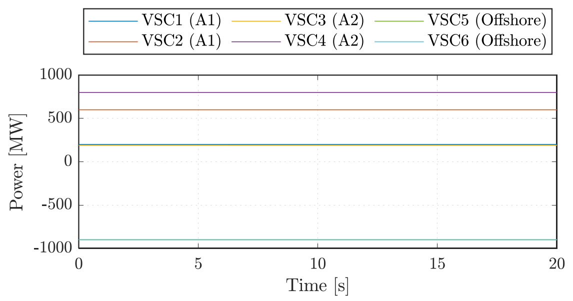

FIGURE 3.8: ACTIVE POWER OF STATIONS - CASE 0.

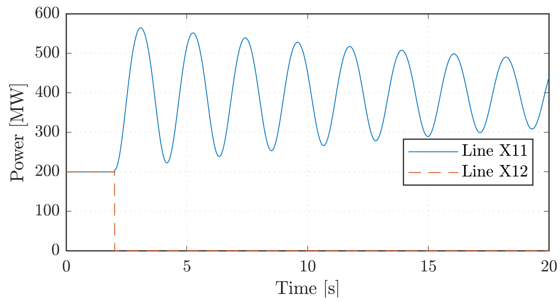

FIGURE 3.9: ACTIVE POWER IN THE AC CORRIDORS – CASE 0.

Figure 3.10 show the frequency of the areas in the system A1 and system A2. In system A1 (left plot) we can observe the inter-area oscillations are poorly damped. Since the active power references of the HVDC system are not modified, the system A2 is not disturbed. It can be stated that in this case the HVDC system works as a firewall between the two systems for this disturbance.

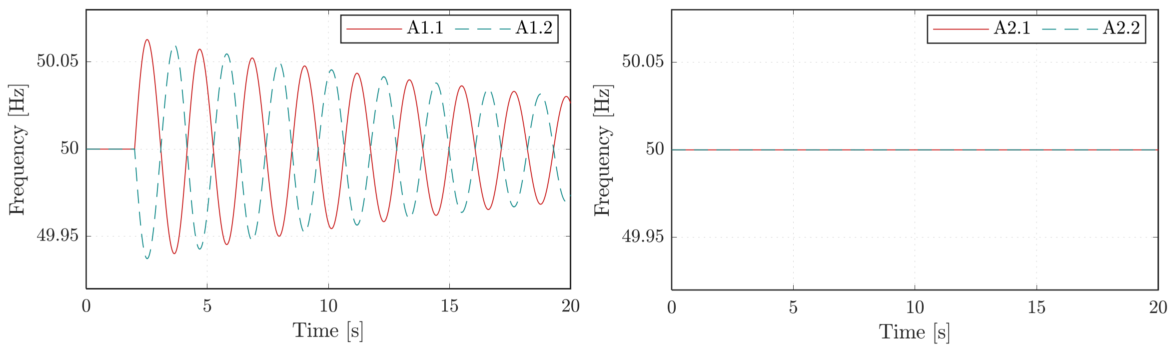

FIGURE 3.10: FREQUENCY OF SYSTEM A1 (LEFT) AND A2 (RIGHT) – CASE 0.

Case 1 - Understanding the issues of non-coordinated actions – Loss of firewall effect

In this example, a Local POD control is implemented as to understand the effect of non-coordinated active power modulations of the VCS stations. The tested controller modifies only the active power reference of VSC1 proportionally to the instantaneous frequency deviation measured at the point of connection of station 1 (i.e., $\Delta P_1 = k_{pod}^{local} * \Delta f_1$). The positive effect of the control can be observed in Figure , where the power of the AC corridor is plotted. Compared with the case where power constant reference was used, it can be observed that the power oscillation has been damped.

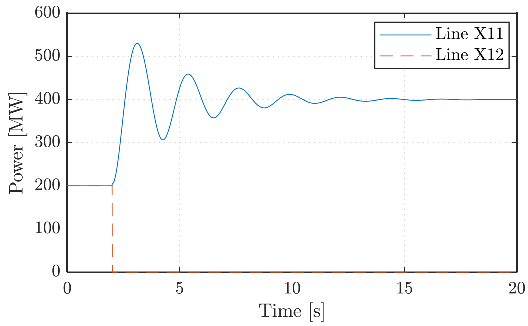

FIGURE 3.11: ACTIVE POWER IN THE AC CORRIDORS - CASE 1.

Figure shows the active power of the different stations. It is observed that the *local POD control* in VSC1, modulates the active power of VSC1 which contributes to the damping of the low frequency electro-mechanical oscillation. Additionally, because of the voltage droop control, when VSC1 modulates its power, the other dispatchable stations (VSC, VSC3, VSC4) will modulate their power as response to the DC voltage variations caused by the injection of power of VSC1. The extent of the power modulation of stations VSC2,3 and 4 depend on their droop gains and the characteristics of the DC grid.

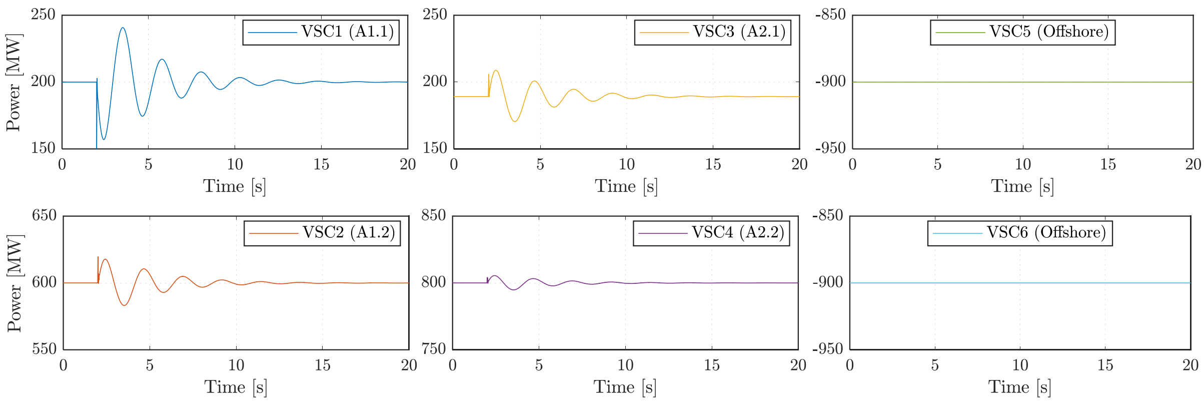

FIGURE 3.12: ACTIVE POWER OF STATIONS - CASE 1.

As the active power of stations VSC3 and VSC4 is modulated around their setpoint, the second AC system is excited as shown in Figure 3.13, where the frequencies of the areas A2.1 and A2.2 of the second asynchronous system are plotted. Therefore, while the *local POD control* damps a disturbance occurring in system A1, it also transmits the oscillation to the second asynchronous grid A2. **In this case the firewall capabilities observed in case 0 have been degraded.**

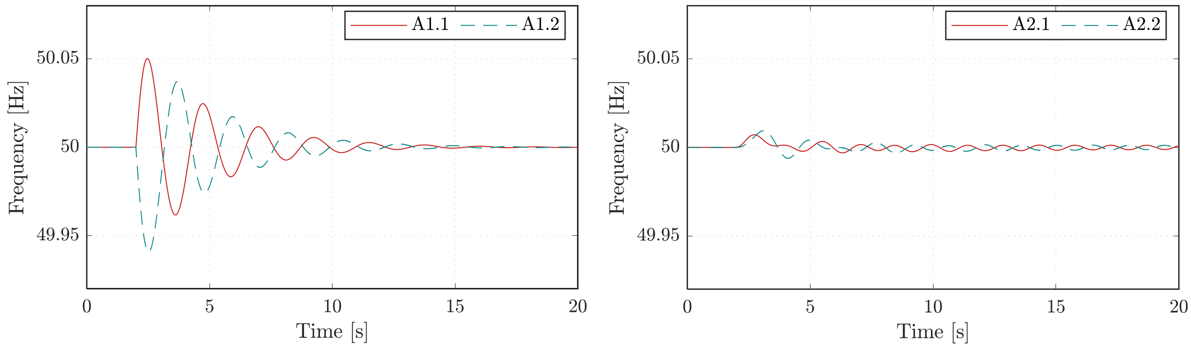

FIGURE 3.13: FREQUENCY OF SYSTEM A1 (LEFT) AND A2 (RIGHT) – CASE 1.

Case 2 – Proposed coordinated control – POD in channel 1-2

Here, the coordinated control described in Section 3.1.5 is applied in channel 1-2. This means that the active power of VSC1 and VSC2 are modified in a coordinated manner and proportionally to the difference of instantaneous frequencies measured at both points of connection (see Figure for the implementation). In Figure , we can observe that using the proposed control on channel 1-2 , the active power of VSC1 and VSC2 are modified in a complementary manner. As the active power injected by VSC1 is absorbed by station VSC2 at all instants, the sum of active power flowing inside the DC grid, are zero (neglecting losses), thus the voltage on the DC grid is barely modified (See Figure 3.15 where the DC voltage measured at the DC side of every station is plotted), thus the voltage droop control does not modulate the active power of the remaining stations.

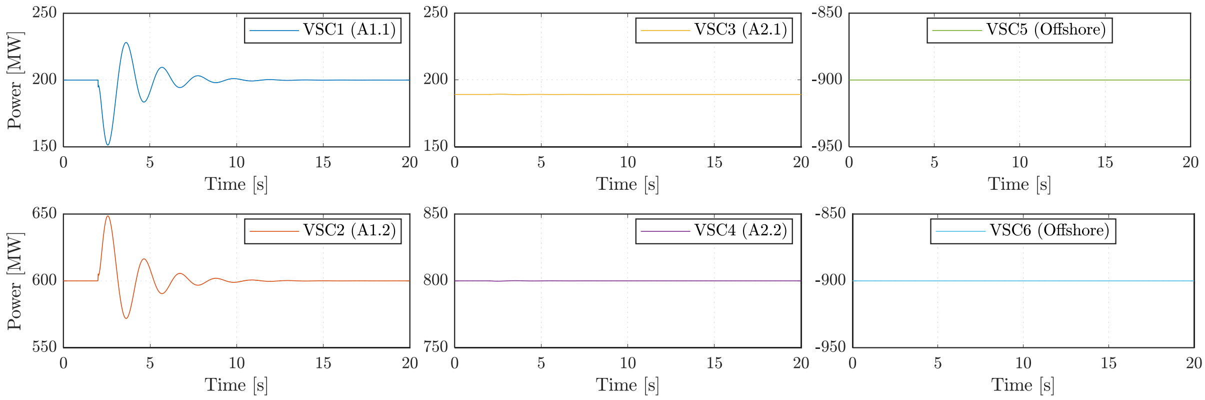

FIGURE 3.14: ACTIVE POWER OF STATIONS - CASE 2.

The effectiveness of the control to damp the oscillation is observed in Figure 3.16, where the power of the AC corridor is plotted. Compared with the Case 0, where constant power references are applied, it is observed that the oscillation has been damped.

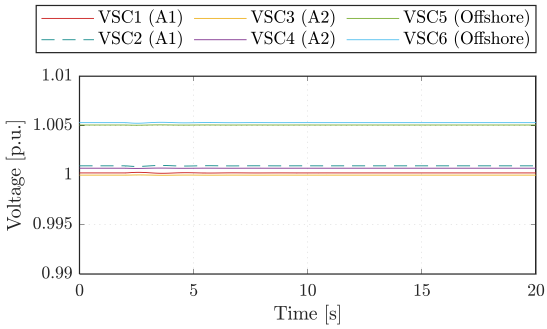

FIGURE 3.15: DC VOLTAGES - CASE 2.

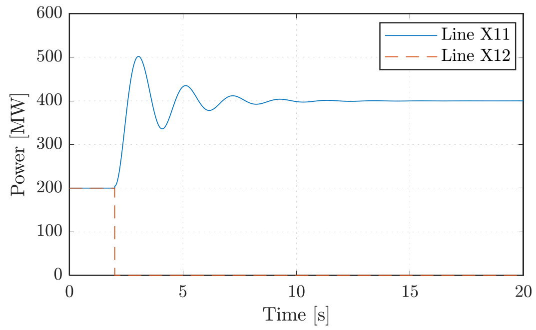

FIGURE 3.16: ACTIVE POWER IN AC CORRDIORS - CASE 2.

Moreover, using the proposed channeling concept, the firewall effect the HVDC system provides is kept. Figure 3.17 shows the frequencies of the different areas. It is observed that in area one, the oscillations are damped (with respect to Case 0), and contrary to Case 1, in this case the oscillations are not transmitted to area A2.

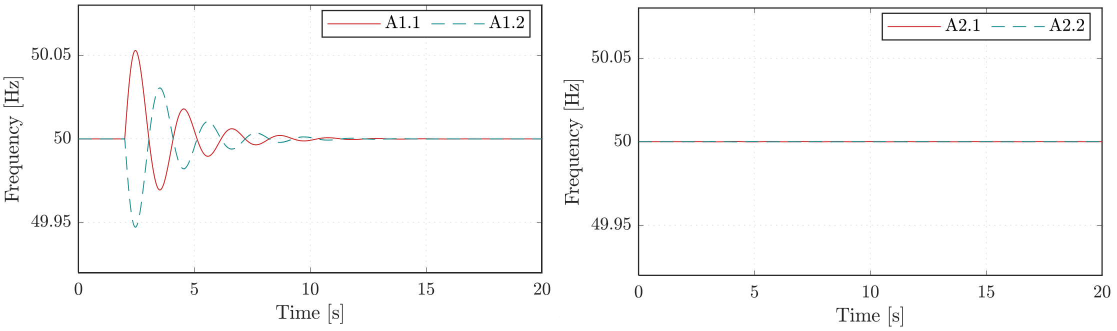

FIGURE 3.17: FREQUENCY OF SYSTEM A1 (LEFT) AND A2 (RIGHT) – CASE 2.

3.1.8 Results - AC line emulation

Case 3 – Proposed coordinated control – ADC in channel 1-2

In this example, the Angle difference control (ADC), presented in Figure 3.5, is activated in the *channel 1-2.* The same event is simulated: the tripping of line X11.

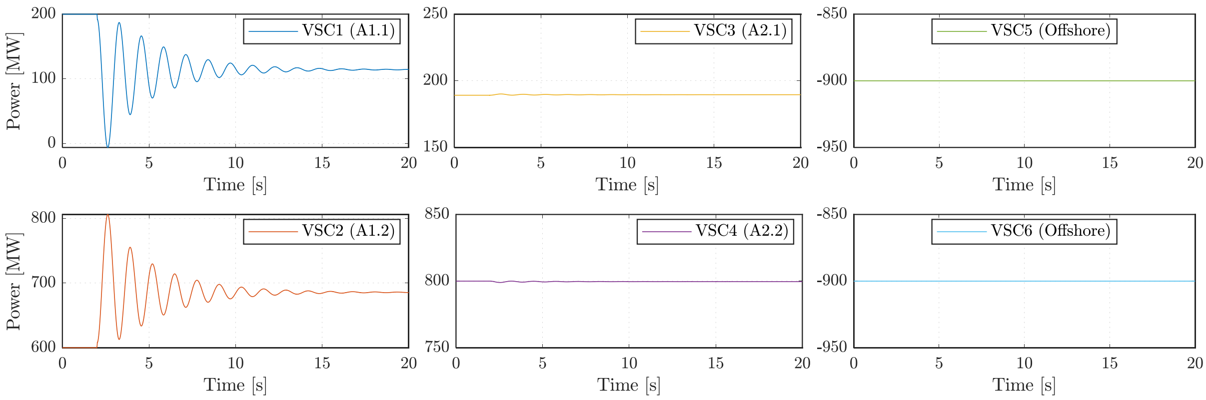

FIGURE 3.18: ACTIVE POWER OF STATIONS - CASE 3.

Since the ADC is implemented in channel 1-2 it is observed that active power injections of VSC1 and VSC2 are coordinated, barely disturbing the DC voltages of the stations (See Figure 3.19). Remark that the post fault steady state value of the active power has been modified of around 100 MW. As an AC line is emulated between the point of connection of VSC1 and VSC2; some power of the lost line has been reallocated in the emulated AC line, modifying therefore the post-fault steady state power of VS1 and VSC2.

To observe the positive effect of the ADC on the system, in Figure 3.20, the active power in lines X11 and X12 are plotted. Two cases are plotted, Case 2 (dashed yellow line: "POD") and Case 3 (blue solid line: "ADC"). Two main things are to be observed:

- By comparing Case 2 (dashed yellow line: "POD") and Case 3 (blue solid line: "ADC"), we observe the remaining AC line (X11) is less loaded in the post fault situation when we the ADC is applied (Case 3) than when only POD (Case 2) is used. Via de ADC, some transmitted power has been reallocated on the HVDC system as to unload the remaining corridor. This positive "static" effect can have a high impact on stopping cascading events as it represents an automatic mechanism to reduce overlading in AC lines in case or N-1 or N-k events.

- By comparing Case 2 with Case 0, it is observed that, not only the static situation is enhanced (as in the previous comparison), but also the interarea oscillation has been damped. This is achieved thanks to the lead lag filter added in the ADC that corrects the phase of the power injections as to increase the damping of the system.

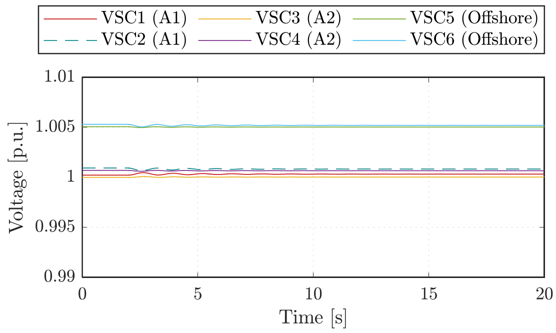

FIGURE 3.19: DC VOLTAGES - CASE 3.

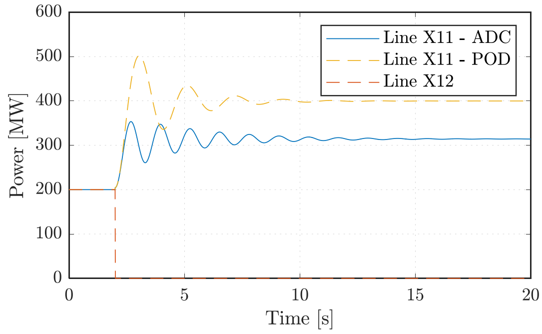

FIGURE 3.20: ACTIVE POWER IN AC CORRIDORDS - CASE 2 AND CASE 3.

Furthermore, by analyzing the frequencies of the different areas (Figure 3.21), it is shown that the disturbance has not been propagated to the second area, thus keeping the firewall effect the HVDC system can provide.

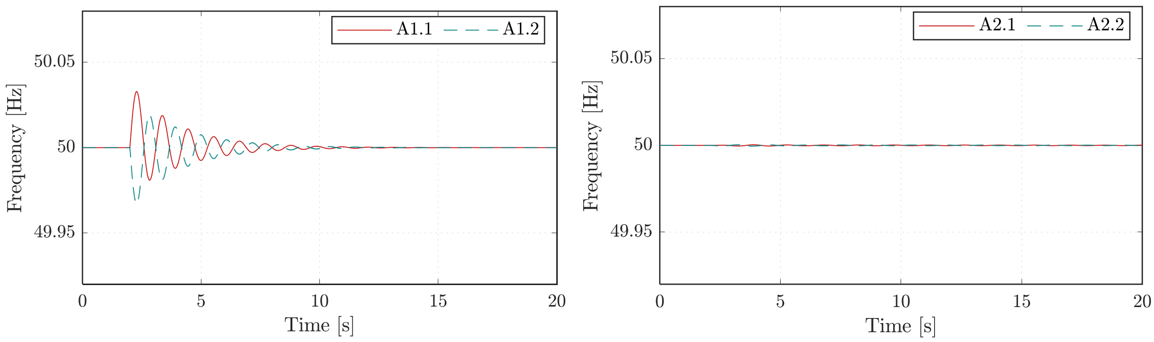

FIGURE 3.21: FREQUENCY OF SYSTEM A1 (LEFT) AND A2 (RIGHT) – CASE 3.

3.1.9 Results - Frequency control

In the following cases, the simulated event is a load step of 200 MW in Area A2.2, representing 10% of the installed synchronous capacity in System A2.

Case 4 – No supplementary control in case of frequency event

Figure 3.22 shows the frequency of both System, A1 and A2 in this base scenario (no frequency control). It is observed that, the frequency of the system where the load step is simulated drops, presenting a nadir of approximately 49.6 Hz and a post-fault steady state frequency of 49.8 Hz. Moreover, it is observed that the frequency of system A2 is not disturbed as the HVDC link did not participate in supporting the exchanges of reserves between systems.

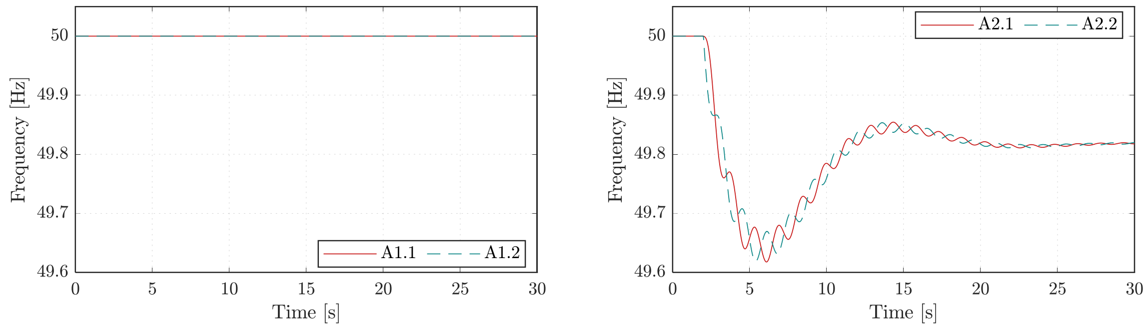

FIGURE 3.22: FREQUENCY OF SYSTEM A1 (LEFT) AND A2 (RIGHT) – CASE 4.

Case 5 – Frequency control in channel 1-4

The HVDC system represent a means to share frequency reserves from system A1 to system A2 in a controlled manner. To do so, the frequency control depicted in Figure 3.6 is **activated in channel 1-4**. Figure 3.23, shows the active power of the different stations. It is observed that via channel 1-4 n frequency reserves are sent from VSC1 to VSC4 (approximately 70 MW in steady state).

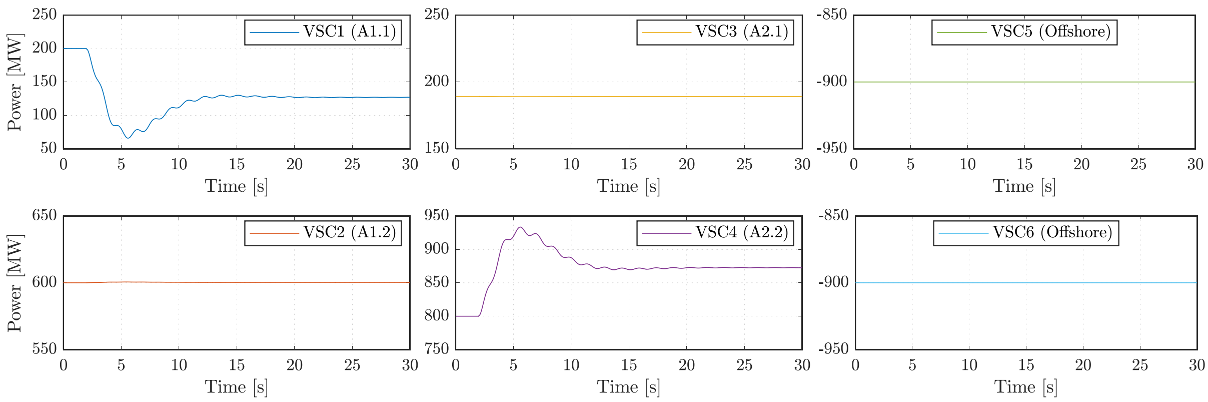

FIGURE 3.23: ACTIVE PWOER OF STATIONS - CASE 4.

As observed in Figure 3.24, this allows the frequency of area A2 to reach a nadir of around 49.7 Hz and a steady state frequency of 49.85 Hz by taking frequency reserves from area A1.

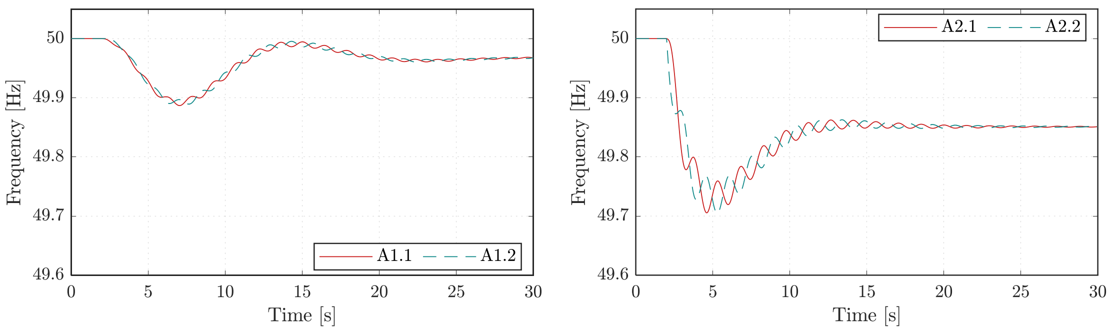

FIGURE 3.24: FREQUENCY OF SYSTEM A1 (LEFT) AND A2 (RIGHT) – CASE 5.

Case 6 – FCR in channel 1-4 and 2-4 with limits

In this case, the frequency control is **activated in channels 1-4 and 2-4**. To limit the frequency reserves shared from A1 to A2 to 100 MW, the active power limits of each channel can be limited (as shown in the control scheme in Figure 3.25). In this example the contribution of channel 1-4 is limited to 60 MW and the contribution of channel 2-4 is limited to 40 MW.

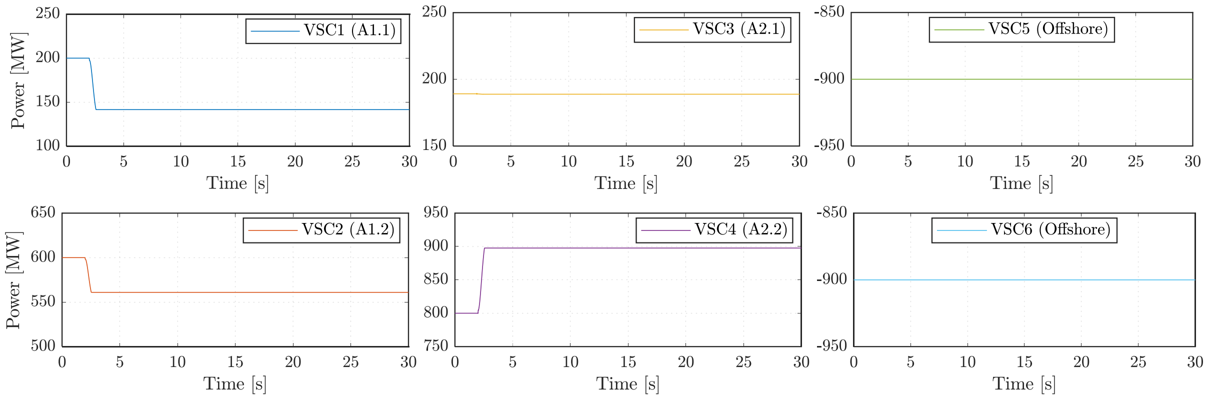

FIGURE 3.25: ACTIVE POWER OF STATIONS - CASE 6.

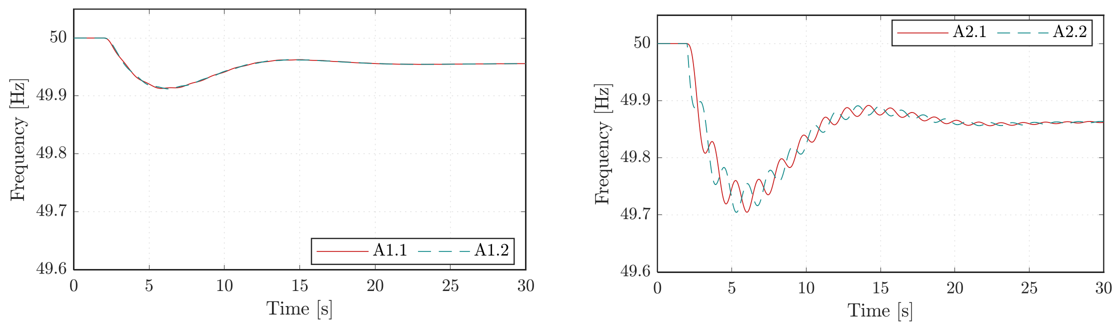

FIGURE 3.26: FREQUENCY OF SYSTEM A1 (LEFT) AND A2 (RIGHT) – CASE 6.

The advantage of this approach is that the operator of the system can decide how much available headroom can be used in each channel to provide frequency services, similar to how generators allocate power reserves to participate in the Frequency Containment Reserves market [71]. Following the channelling approach, the HVDC system can allocate a specific headroom per channel to be used in case of a frequency disturbance. Reference [71] discusses such possibility.

3.1.10 Results - Combination of different services

Case 7 – POD + ADC + Frequency control

In this final example, the presented different services are combined in the 6 possible channels. The different control gains and the allocated headrooms are summarized in Table 3.5.

TABLE 3.5: CONTROL GAINS AND ALLOCATED HEADROOMS

Channel	POD	ADC	Frequency control	Headroom for POD+ADC	Headroom for FCR
1-2	K_{POD}^{12} =1GW/Hz	K_{ADC}^{12} = 20MW/deg	N/A	±100MW	N/A
2-3	N/A	N/A	K_{FCR}^{23} = 0 K_{FCR}^{32} = 500MW/Hz	N/A	±60MW
3-4	K_{POD}^{34} =1GW/Hz	K_{ADC}^{34}=20MW/deg	N/A	±100MW	N/A
4-1	N/A	N/A	K_{FCR}^{41} = 500MW/Hz K_{FCR}^{14}=0	N/A	±40MW
1-3	N/A	N/A	K_{FCR}^{13} =0 K_{FCR}^{31}= 500MW/Hz	N/A	0MW
2-4	N/A	N/A	K_{FCR}^{24} =0 K_{FCR}^{42} = 500MW/Hz	N/A	0MW

Note that channels embedded in one synchronous system (e.g., 1-2 and 3-4) are suitable to provide AC line emulation and POD services. While channels that interconnect asynchronous systems can provide frequency support (e.g., 2-3, 4.1, 1-3 and 2-4).

The simulated disturbance is a load step of 200 MW in A2.2. Figure 3.27 shows the active power in the different stations, Figure 3.28 shows the frequency in both areas and Figure 3.29 shows the active power in the line X21 for Case 4, Case5 and Case 7.

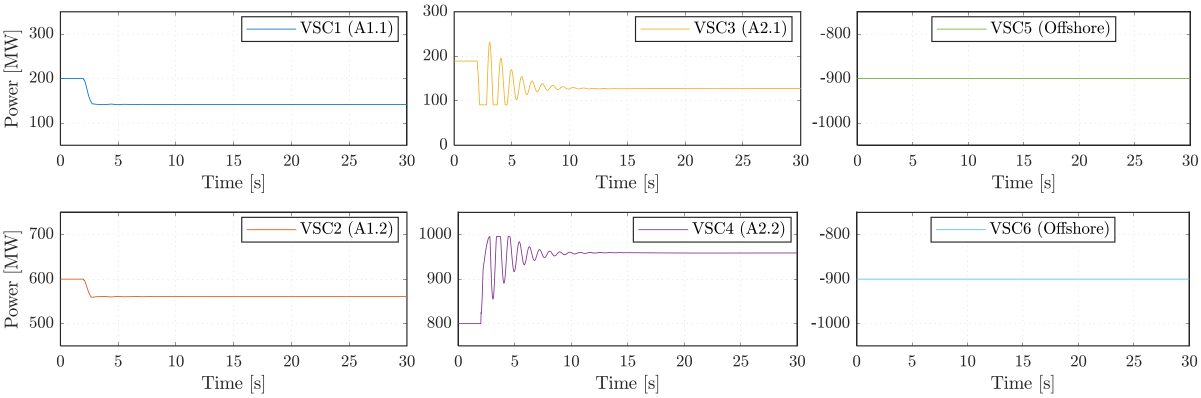

FIGURE 3.27: ACTIVE POWER OF STATIONS - CASE 7.

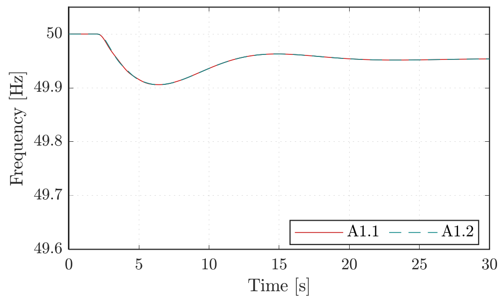

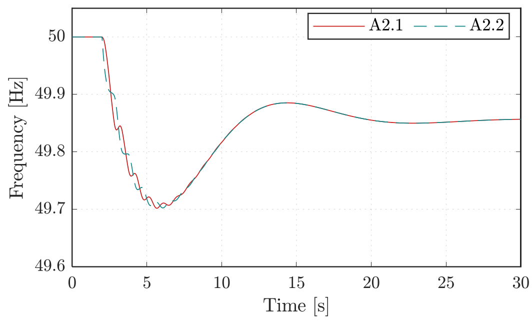

FIGURE 3.28: FREQUENCY OF SYSTEM A1 (LEFT) AND A2 (RIGHT) – CASE 7.

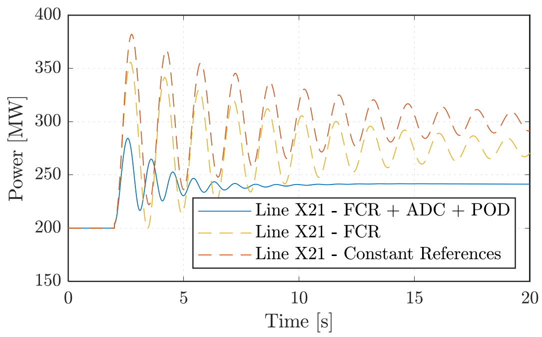

FIGURE 3.29: ACTIVE POWER IN THE AC CORRIDOR - CASE 4, 6 AND 7.

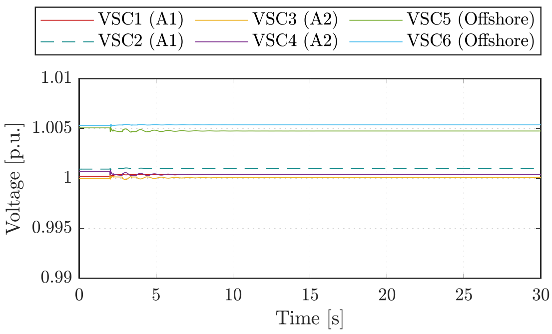

FIGURE 3.30: DC VOLTAGE OF STATIONS - CASE 7.

Different observation to understand the effect of the control scheme can be made:

- Regarding frequency stability, it is observed that VSC1 and VSC2 send active power to system A2 (60 MW and 40 MW respectively). This helps the system to have a frequency nadir of 49.7 Hz (which is better compared with case 4)

- In terms of the low frequency oscillations excited by the disturbance (generator tripping), compared with case 5, oscillations in both areas have been damped. This has been achieved mainly thanks to the action of the POD activated in channels 1-2 and 3-4.

- The positive impact of the ADC in channel 2-3 can be observed in Figure 3.29. As the frequency event occurs, the primary control from the generator is activated, to cope with the power imbalance generators in A2.1 need to increase their power reference and start sending more power to A2.2. In case 0 and case 4, this power is shared via the AC corridors. When the AC line emulation is activated, this power can be automatically reallocated on the HVDC system.

Finally, Figure 3.30 shows the DC voltage of the different stations as to show that the DC voltage have been barely disturbed despite the fast power modulations of the converters.

3.1.11 Conclusions on primary coordinated controls for AC grid support

This section focuses on the services provided by Multi-Terminal Direct Current (MTDC) systems to AC systems, which can be enhanced through coordination and communication between different stations. The targeted services are **Power Oscillation Damping (POD), AC line emulation, and Frequency Control.** This section proposed a coordinated control layer (based on communication between stations of measurements at the station level) for the "autonomous adaptation" of the HVDC system to support the "absorption" phase of the R&R trapezoid by providing the services (see D2.1 for the explanation of the different phases). The rationale behind this proposal is that if a critical service (such as AC line emulation) requires communication, other services can also benefit from this communication system. The proposed control layer uses the ***channelling*** concept.

The following conclusions can be derived from this chapter:

- **On the Low-frequency power oscillation damping:**
  - HVDC links are already required to damp power oscillations by injecting active or reactive power. This capability is also expected for multi-terminal systems. POD can be done locally without coordination using these power injections. However, using active power injections changes the DC voltage levels, causing other stations to adjust their power accordingly. When HVDC systems connect multiple asynchronous grids, oscillations in one area can be transmitted to other areas through these power changes.
  - Our proposal involves using the channelling concept to modulate power injections only within stations in one synchronous area. This prevents oscillations from propagating to other asynchronous areas, ensuring a firewall effect. To damp oscillations with active power injections without transmitting them to other asynchronous areas, there must be at least two converters in the targeted synchronous area.
  - **Impact on R&R:** In the event of a disturbance, poorly damped oscillations in the grid can cause transient overloading of AC corridors, potentially leading to line tripping. POD can reduce transient overloading, thereby decreasing the likelihood of overloads and disconnections.

- **On the AC line emulation:**
  - The AC line emulation service has proven highly beneficial for embedded HVDC links, as it removes the need for operators to manually dispatch HVDC power. With an AC line emulation controller, also known as angle difference control (ADC), the HVDC system adjusts its power reference to follow the natural power flow direction of the grid. This adaptation occurs not only for minor power fluctuations but also during N-1 events, such as generator or line trips.
  - AC line emulation has been applied to HVDC links. This report utilizes the channelling concept to implement the ADC in multi-terminal HVDC systems. It is possible to emulate the behaviour of an AC line per channel. To provide this service to one area, at least two terminals of the MTDC must be connected within that area.

    - Furthermore, real events have shown that ADC, depending on the HVDC topology and control filters, can negatively affect the damping of interarea oscillations. To mitigate these adverse effects, a simple solution is proposed: the implementation of a lead-lag filter. This filter will adjust the phase and provide the necessary damping to the system.
    - **Impact on R&R:** By redirecting power through the HVDC system during N-1 contingencies to support the AC system and avoid overloading of surrounding AC lines, the ADC controller significantly reduces the likelihood of line tripping due to overloading. Consequently, it helps prevent and stop cascading failures, enhancing the overall resilience and reliability of the grid.

- **Frequency control:**
    - Frequency reserves can be shared between asynchronous grids via HVDC systems. If this service is provided without coordination between stations, the power needed at the receiving terminals will be supplied by the sending terminals based on the DC voltage droop gains, which are not designed for this purpose. Coordination is necessary to determine from which sending stations the power will come.
    - The proposals presented in this report allow for coordinated frequency support between stations using the *channeling* concept. This enables the operator to decide from which stations these reserves will come, through control design. Additionally, the operator can predetermine the available headroom (or reserve) of each sending station to participate in the frequency regulation of the receiving AC system, like how operators allocate headroom in their generators for the frequency containment reserve market.
    - **Impact on R&R:** By sharing frequency reserves via the HVDC system, in the event of a contingency in one area, another asynchronous area can support the affected area, reducing the likelihood of load disconnections. This service is particularly useful in stopping cascading events following system splitting, when the imbalance between generation and load in each island is very high.

3.2 Supervisory Control and Coordination with AC-DC Grid Control

3.2.1 State of the art and identified gaps – Global DC grid control

Following the structure presented in the introductory chapter presenting the hierarchical control structure proposed by the IEC standard IEC TS 63291-1:2023, this section tackles the functions that can be included at the "Global DC grid control" and the ones that can be included in the "AC/DC grid control".

Global DC grid control

The IEC standard IEC TS 63291-1:2023 has listed the following main functions for the DC grid control:

- continuous processing of initial converter schedules dispatched by the AC/DC Grid control
- ensuring a secure steady-state operation of the HVDC Grid System within defined safety limits (i.e. consistency checks, set value modifications etc.)
- optimizing DC network operation (e.g. after unscheduled events) and reacting on occurring deviations from the anticipated power injections with new DC node voltage control mode setup (if some degrees of freedom are tolerated)
- managing the control modes of all converter stations in the DC node voltage control layer
- provision of operational simplifications for the HVDC Grid System by "default scenarios" (e.g. pre-defined energisation sequences, response to usual/frequent contingencies etc.)

Additional (supplementary) functions have also been listed, but not further detailed here. They can be found in IEC TS 63291-1:2023.

As its name suggests, the global DC grid control should have a global view of the MTDC grid and its status. To this purpose, it receives various measurements from all converters, nodes, and branches and sends back commands. These commands could be either setpoint changes (e.g., DC power, DC voltage) mode changes, or even topological changes (e.g., open close switching devices).

Several ways to achieve the above have been proposed in the literature. The authors of [76] and [77] propose an Optimal Power Flow (OPF) to determine the setpoints of the VSCs, updated at regular time intervals, with the objective of minimizing losses. The work in [78] computes the power and voltage setpoints by solving a multi-objective optimization. The coordinated control detailed in [79] uses simple DC power flow computations to update the voltage and power setpoints at regular time intervals. A similar method is proposed in [80] estimating setpoint corrections for the VSCs to restore the power flows through selected converters. Various re-dispatch schemes are compared in [81] with the objective of correcting the voltage offset left by voltage droop control after a disturbance. The ability of the schemes to track the desired power setpoints is also assessed.

Reference [82] proposes a three-level control structure inspired of AC frequency control practice. Primary control consists of a simple current-based droop scheme. The secondary level involves a slow Proportional-Integral (PI) control to reset the VSC powers to their reference values, if possible, and a redispatch scheme updating the power references at regular time intervals. An OPF as tertiary control is referenced. A hierarchical control structure with three levels has also been proposed in [4]. The secondary control [83] is based on Model Predictive Control to smoothly steer the HVDC grid between operating points, restore the DC voltage inside limits, and alleviate overloads after DC grid outages, while accounting for model and measurement inaccuracies. The tertiary level was based on a SC-OPF formulation, that was providing references to the secondary control, ensuring that the system variables (i.e., DC voltages and currents) remain between limits following N-1 outages. The above schemes focus on balanced HVDC grids, i.e., either symmetric monopole configurations or balanced bipole configurations. The works in [84, 85], focusing on HVDC grid interoperability, make reference to a central controller also addressing unbalanced operation, although the actual formulation is not detailed.

Other alternatives not based on DC voltage droop control have been also proposed. The work in [86] relies on multiple “master” converters whose voltage setpoints are determined by solving a SCOPF. The latter minimizes MTDC grid losses while keeping DC voltages within limits after the outage of a VSC. The pilot voltage droop concept is introduced in [87]. The strategy is to communicate a common DC voltage to all converters to share the powers more efficiently. In addition, two methods are used for power setpoint tracking, namely a simple PI controller and a setpoint redispatching by a central entity. A different approach is followed in [88] where fast communication is used to match at each time step the sum of DC currents injected by wind farms with the sum of DC currents of the grid-side converters.

AC/DC grid control

This control level provides the scheduled powers to the coordinated DC grid control based on energy prices, renewable energy forecasts and security criteria applied by each relevant TSO of the adjacent AC areas.

The schedules for each converter terminal can be obtained by the application of a combined AC/DC SC-OPF including AC and DC contingencies. Applications of SC-OPF to HVDC grids have received significant attention in the literature.

In terms of **control strategies**, some references propose preventive solutions, i.e., the sought operating state must exhibit no violations either in “N” conditions (namely, with all components available) or in case of any contingency from a suitably defined contingency set [89] [90] [91] [92]. Other works jointly address preventive and corrective solutions, i.e., the initial state is accompanied by corrective solutions to be implemented after contingency occurrence, aimed to restore compliance with operating quantities constraints [93] [94] [95] [96] [97] [98] [99] [100]. A specific set of corrective control actions is determined for each contingency leading to violations.

Preventive-corrective formulations can be simplified to address preventive-only problems, by setting to empty the set of corrective actions. The strategy of pursuing corrective actions alone, i.e. a “purely” corrective strategy starting from a given operating condition, is not represented in the literature. In fact, on the one hand it is not so meaningful as the joint optimisation of preventive and corrective actions; on the other, the problem of identifying corrective actions without preventive ones can be reduced to a set of independent OPF problems, one for each contingency, possibly with suitable constraints on the maximum deviations of the control variables from their initial states to account for the operational constraints of the resources engaged in the control actions.

The **SC-OPF problem** can be formulated either as a *dispatch* or a *redispatch* problem. In the former case [93] [89] [96] [97] [98] [99] [100], the set-points of the controllable quantities are fed into the objective function of the optimisation in absolute terms; in the latter case [94] [95] [90] [91] [92], the objective function of the optimisation depends on the set-point variations with respect to an initial operating condition given in input, hence the solution is expressed in terms of deviations with respect to the initial set-points. The dispatch approach simulates an energy market integrated with an ancillary service market. The redispatch approach is consistent with an ancillary service market, where the operating state resulting from the energy market is modified to guarantee security, and costs incur from the deviations of the quantities from the original values.

The **objective** of the optimization is linked to the above dispatch/redispatch alternative. In the dispatch approach, whether corrective actions are included or not, the objective is the minimisation of the energy production costs for the operation of the system in N conditions. The typical cost model of fossil-fuelled power plants is generally applied, i.e. quadratic with respect to the generated power. On the other hand, when considering the redispatch approach, the objective is related to the minimisation of the costs of the set-point deviations from the original values, which are often defined with a proportionality law. In particular, complex objective functions have been applied in [95] [90] [91], in terms of linear combinations of several weighted objectives that include the number of contingencies that could not be secured after preventive/corrective action identification, and other objectives, such as generation costs or deviations of power or voltage set-points of VSCs from their initial values. When contingencies are modelled in probabilistic terms, the objective function can be adapted accordingly. For example, in [94], the objective function to be minimised is the total expected cost (referred to as *risk* in the paper) of operation, defined as the sum of preventive redispatch cost and of corrective expected costs (risk); in turn, the latter are defined as the sum, for all contingencies, of contingency probability multiplied by the total corrective redispatch cost and demand curtailment cost associated to the contingency itself. In [92], the objective function combines squared redispatch powers and a risk index, the latter depending on contingency probability and a contingency impact metric. In general, when corrective actions are available the need for preventive actions is reduced, with consequent reduction in operating costs.

The **control variables** available for dispatch, redispatch, and/or corrective actions typically include generators' and VSCs' active power. Sometimes other components are also dealt with, such as phase-shifting transformers [98]. VSCs are often regarded as the only resource available in corrective control, due to their fast activation time compared to that of generators [93] [95] [97] [100]. In [94], load change is encompassed within the corrective actions. Where voltage is explicitly accounted for, voltage control resources are used as control variables, such as VSCs (for the voltage control of the DC or AC side) and generators. In [98], ULTCs and DC/DC converters are also mentioned. Technical constraints of the control resources are accounted for in the optimisation problem, such as generator and VSC capability. Additional constraints are considered in some cases, such as maximum realistic deviation of the control variables from their pre-contingency values in corrective control [96] [98], and voltage difference limits across the VSC converters in order to avoid over-modulation [98].

Controlled variables are operational quantities that need to remain within upper / lower limits in the N and N-1 state, thus impose constraints to the optimisation problem. The major controlled variables are AC and DC branch power flows (or currents, according to the formulation), often accompanied by AC and DC bus voltages [94] [95] [90] [91] [96] [97] [98]. AC bus phase angle differences, as well, are considered in [94]. In [90] [91], the list of constraints varies according to the contingency elements: because AC contingencies essentially only affect the AC grid, only AC quantities are included as constraints; conversely, for DC contingencies both AC and DC quantities are set as constraints. In [92], AC overloads are indirectly addressed via the minimisation of an overload index. The constraints related to the control variables of the problem, in particular SVC and generator limits, are always accounted for.

The **contingencies** always regard AC and DC branches[1]. Generators and VSCs are often dealt with, as well. As to the order, only N-1 contingencies are considered[1]. In [95], the loss of individual poles of DC components in bipolar configuration is included. In terms of contingency list, some works specify selection criteria to limit the amount of contingencies to analyse, such as considering the outage of lines whose loading is higher than 90% of the nominal value [90] [91]. In [98], filtering is based on a severity index threshold, where the index is defined from the ratio between the optimum values of the OF computed considering only one contingency and the base case, respectively.

The HVDC **configuration** is always modelled with monopolar equivalent but in [95], where a detailed model of bipolar configuration with metallic return is considered.

SC-OPF applications consider purely **static** security constraints. The compliance with dynamic stability constraints could be inserted by synthesizing stability limits into static constraints, identified via offline dynamic simulation. Moreover, in the SC-OPF formulations that do not account for the steady state before the implementation of corrective actions, detailed simulations of the contingencies should be carried out ex-post, to check not only if the post-contingency evolution is stable, but also if the resulting "immediate" steady state is acceptable (at least until corrective actions are implemented).

In terms of **grid model complexity**, both non-linear and linear [93] [89] [95] [100] [92] approaches can be found. In [95] a linearized grid model is adopted for corrective actions, which are checked ex-post with a non-linear model. In [99] the grid is non-linear, but linear factors are used to describe the effect of one line outage on the other lines' flows. In [92] linear sensitivities are employed to compute risk indices.

As for the **optimisation**, both non-linear and linear approaches are adopted, depending on the involved functions. Reference [89] employs a linear programming approach with piecewise linear functions for generation cost and AC/DC transmission losses. In [95] [90] [91], the optimisation is carried out via a differential evolution algorithm in turn relying on power flow calculations. In [100] the problem is in terms of stochastic programming with chance constraints and a quadratic objective function, solved via scenario approach followed by robust optimisation. In [96] the optimisation is based on the application of a primal-dual interior point for local search (based on MATPOWER) combined with differential evolution method for global search.

It is worth pointing out that the SC-OPF problem is generally **deterministic**, with exceptions of considering the probability of contingencies [94] [92] or of power injections [100].

The management of **operational constraints in post-contingency situations** deserves a more in-depth discussion. It is interesting to observe that the loss of AC or DC branches does not significantly affect the active power balance of the system (apart from the case of separation into islands), in fact the only imbalance is associated to a change in power losses. On the other hand, AC generator contingencies and VSC contingencies do alter the power balance: a generator contingency causes a frequency perturbation in the AC system, which activates the frequency regulation of the AC interconnected system and possibly (in case a frequency support control logic is operating) of HVDC grids connecting the affected AC island with other AC islands, thus the perturbation propagates to the HVDC grid and the healthy AC grids.

In case a VSC is lost, an imbalance within the HVDC grid is triggered, that is faced by the other converters' control logics such as PV droop. If the DC grid is fully embedded within a single AC island,

[1] apart from an early application that addresses only AC branches but includes AC busbar faults leading to N-k contingencies.

the VSC loss will cause power flow redistributions but (apart from a change in the losses) no power imbalance in the AC grid. If the HVDC grid connects more than one AC island, the loss of a converter may alter the power injection in the AC grids thus creating frequency perturbations.

From the above remarks, it follows that in case contingencies cause power unbalances, the frequency and/or the DC power-voltage regulation schemes will act, leading to different conditions respectively in the immediate aftermath of contingency clearing (possibly accounting for fast, automatic actions of defence schemes acting on VSCs) and at the steady state of (automatic) FCR and automatic FRR reserve deployment, before manual FRR and RR are eventually applied. The acceptability of these intermediate states, in terms of frequency, branch loading and voltage magnitude should be verified and possibly enforced as constraints in the SC-OPF. However, this would by far increase the optimisation problem complexity and related computational burden. Therefore, the typical approach for the SC-OPF with corrective control in the literature is to enforce the operating constraints in the stage after the full deployment of the corrective control actions, which can be regarded within the scope of manual frequency regulation (manual Frequency Restoration Reserve, m-FRR, or Replacement Reserve, RR). Only in [96], out of the consulted references, where the optimisation relies on instances of power flow problems, a feasibility check is carried out to assure the existence and viability (in terms of maximum allowed violations) of the post-contingency short-term operating condition, before application of the corrective actions. Moreover, [96] considers two stages of corrective control, i.e. fast and slow actions, respectively by VSCs and by generators.

Within the applications just dealing with preventive control, only in [89] among the analysed works, the frequency response of AC grids to imbalances is considered, as well as the possible support by VSCs equipped with frequency support logics such as power/frequency droop. In this case, the power flow operating quantities (for which constraints are checked) are those established in the post-fault primary frequency steady state, and the post-fault steady state frequency is included as a constraint in the optimisation.

3.2.2 Problem Statement

As discussed in sub-section 3.2.1, most of the work in the literature has focused on supervisory control of HVDC grids operating in balanced conditions, where loss of one pole of a VSC meant the complete outage of power at that terminal. This is the case, for example, with symmetric monopole configuration.

However, following the emergence of bipole configurations, either with dedicated metallic return (DMR) or ground return, unbalanced conditions can arise following the outage of a pole of a VSC terminal or cable. In such cases, the remaining “healthy” pole of the terminal can still transfer up to half of the rated power of the terminal. As a result, current will flow even in steady-state conditions through the return path, leading to an imbalance between the positive and negative poles of the HVDC grid. Therefore, the following considerations have to be addressed:

- How to re-distribute the power of the tripped pole to the rest of the converters in the HVDC grid? For instance, in point-to-point connections it is rather obvious that following the outage of one pole at one end, the healthy pole power should be set to compensate the lost power, up to its rated capability. In MTDC grids, there are more options (e.g., the lost power could be re-distributed to other healthy terminals), but it should also take into account the different strategy for DC voltage control and power sharing (i.e., droop control instead of Master-Slave)
- How to ensure that the return path electrical variables (i.e., neutral point voltages and neutral path currents) remain between acceptable limits.

- Ground/sea return paths have the advantage that the neutral voltages remain close to zero, hence there is limited need to monitor and control them (assuming sufficient design of the electrodes). However, earth/sea return currents might have to be controlled between very strict limits.
- The use of DMR cables allows high return current (up to the rated current of the DMR). Nevertheless, depending on its design characteristics, the voltage drop through its resistance may be significant, leading to deviation of the neutral point voltages from zero. This can impose challenges on the control of the converters and must be limited.

The subsequent sections propose a control method that expands the work in the literature in order to address the above considerations.

3.2.3 Proposed Control Method

Overall control structure

This chapter discusses the higher levels of control of an HVDC grid, namely the AC/DC grid control and the coordinated DC grid control. These two schemes are closely interrelated and need to exchange information in regular intervals. The AC/DC grid controls focuses on the combined AC/DC system (which can involve more than one AC and or HVDC grids) in order to ensure its optimal and secure operation. Figure 3.31 gives an overview of the connections between the two higher levels, to be further detailed in the sub-sequent control actions.

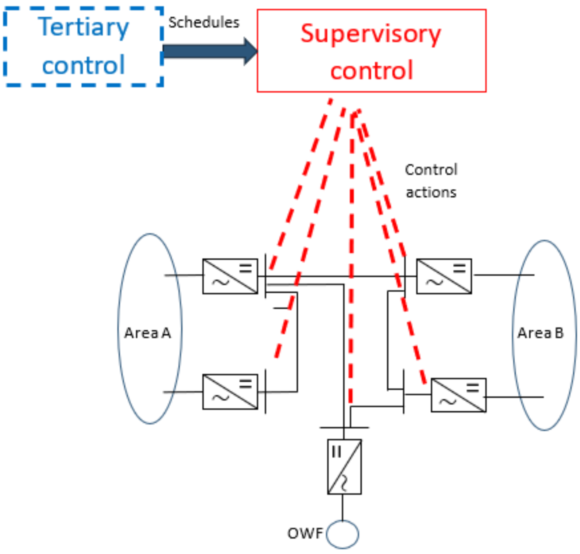

FIGURE 3.31: OVERVIEW OF CONTROL STRUCTURE

Tertiary control - SC-OPF for AC/DC grid control

This sub-section describes the AC-DC grid control. It focuses on its main functions and its interactions with the supervisory control.

A SC-OPF application for AC/DC grids was developed within WP5 of the project, in order to compute security indices and to feed the resilience analysis module with N-1 secure operating conditions, in the context of planning studies. The same SC-OPF application can be thought as applicable in the operational planning and operation process. In fact, as recalled above, the SC-OPF can be seen as a function to be performed in operational planning and in quasi-real time, as a tertiary level of control, updated on the basis of the latest market outcomes. A SC-OPF instance could also be run in real time in the control room, fed with real time operation data and operating costs from the latest available market outcome, to continuously update the converter set-points as the operating condition changes, either slowly or due to events such as contingencies. The SC-OPF can compute corrective actions to be implemented in case an analysed contingency occurs, thus building a look-up table of manual or automatic actions. In the latter case, they need to be integrated in the high-level control system of the HVDC grid, providing an event-based defence functionality.

The SC-OPF is formulated as a two-stage N-1 security-constrained redispatching (SC-R) approach:

1. solve active power related issues,
2. solve reactive power related issues.

The SC-R exploits both preventive and corrective control actions. The preventive actions include the redispatching of active power setpoints and AC voltage setpoints for AC conventional generators, the curtailment of renewable generators, the variation of shift angle of PSTs (Phase Shifting Transformers) as well as the power and DC voltage setpoints for DC grid converters with constant power and PV droop controls. The corrective actions include the load shedding, the corrective variations of active power and AC voltage setpoints for dispatchable AC generators, the corrective variations of DC voltage and power setpoints for embedded DC converters.

The advantage of the proposed SC-R approach is that both stages are formulated as Linear Programming problems, where AC load flow equations are linearised: this makes the algorithm efficient to solve large power systems. Also, active/reactive decoupling techniques are used, so that two separate problems can be solved in a cascaded way. The first stage is modelled using a conventional formulation based on Power Transfer Distribution Factors (PTDF) and provides the preventive variations of active power setpoints for AC generators and for AC/DC converters. The second stage is modelled based on a suitable decoupled formulation of reactive power/voltage problem [101] and provides the variations of AC voltage setpoints for the conventional AC generators and for converters, as well as the DC voltage setpoints for the converters.

The sets of contingencies which can currently be analysed are:

- N-1 contingencies of AC branches,
- N-1 contingencies of DC branches,
- N-1 contingencies of converters,
- N-1 contingencies of AC generators (including equivalent renewable injections).

The SC-OPF is detailed in D6.1.

Supervisory HVDC grid control

Main objectives

The control developed in this work is inspired from the work in [83], where the concept of MPC was used. Hence, the main objectives of this controller, as listed in [83], are preserved and repeated also below:

- The controller can accommodate the varying power injections by renewable sources.

- It is robust with respect to model inaccuracies as well as disturbances, such as outages of AC/DC converters or DC cables/lines.
- It can prevent or correct DC voltage and current violations.
- It can smoothly drive the system from the current to a desired operating point.
- It can avoid excessive impact on the adjacent AC systems and facilitate the provision of additional services (such as frequency support).
- It avoids extensive communication requirements between controllers.

In addition to the above, the proposed controller addresses the problems listed before, i.e.:

- Redistribution of power among converters and among poles during unbalanced operation.
- Regulation of neutral currents in the DMR or ground return paths, as well as regulation between limits of neutral point voltages.

As in [83], the supervisory controller should make a distinction between dispatchable and non-dispatchable VSCs. Dispatchable VSCs can receive a power setpoint that can be set depending on market agreements and they can also participate to the DC voltage control through a P −V droop characteristic. Typically, they are connected to strong AC areas, however this is not necessary. The non-dispatchable VSCs, on the other hand, have their power varied by external factors. For instance, a converter connecting an offshore wind farm is considered non-dispatchable, since it simply collects and injects into the MTDC grid the power produced by the WF. Hence, they are assumed to not participate in DC voltage control. The proposed supervisory control acts primarily on dispatchable terminals. Nevertheless, control actions on the non-dispatchable terminals can still be actuated, if a limit violation cannot by alleviated otherwise.

The subsequent subsections will describe the principle of MPC, the control formulation and the behaviour of the control following MTDC grid outages.

Brief description of MPC

MPC consists of computing a sequence of control changes which minimizes a multi-time-step objective and satisfies constraints in the future [102]. This optimization relies on a model of the system evolution. At a given discrete time k, using the latest available measurements, the controller computes a sequence of optimal control actions to be applied from k to $k + N_c - 1$, so that the system meets a desired target at $k + N_p$, where $N_p \geq N_c$. N_c and N_p are referred to as control and prediction horizons, respectively. Out of this sequence, only the first component is applied. Then, at the next time instant $k + 1$, the procedure is repeated for the updated control and prediction horizons, using the newly received measurements. This yields a closed-loop behaviour, that can account for unexpected behaviour and approximation of the system model.

Control formulation

The objective of the supervisory control is to steer the VSCs of the HVDC grids to their reference powers while obeying various constraints:

- lower and upper limits on DC node voltages;
- lower and upper limits on the power of each VSC;
- limit on the rate of change of each VSC power;
- upper limit on each DC branch current ;

- average DC voltage constraint;
- upper limit on DMR or ground return currents;
- upper limit on neutral DC node voltages.

To achieve the above, the supervisory controller collects from the HVDC grid measurements at regular time intervals. Hence. at time k the following latest measurements are available:

- $\boldsymbol{P}_{\boldsymbol{m}}^{+}(k)$ and $\boldsymbol{P}_{\boldsymbol{m}}^{-}(k)$ the vectors of positive pole and negative pole VSC power measurements, respectively.
- $V_{\boldsymbol{m}}^{+}(k)$ and $V_{\boldsymbol{m}}^{-}(k)$ the vectors of pole-to-neutral DC node voltages (positive and negative pole, respectively)
- $\boldsymbol{I}_{\boldsymbol{m}}^{+}(k)$ and $\boldsymbol{I}_{\boldsymbol{m}}^{-}(k)$ the vector of DC branch currents.

Based on these measurements, a reference trajectory [103] is defined with the objective of steering the VSC powers at each terminal to the reference values $\boldsymbol{P}^{ref}$, as provided by the AC-DC grid control for each VSC terminal (i.e. for both poles), in N_c control steps. That trajectory is linear and defined as follows ($j = 1, \ldots, N_c$):

$$\boldsymbol{P}^{ref}(k+j) = \left(\boldsymbol{P}_{\boldsymbol{m}}^{+}(k) + \boldsymbol{P}_{\boldsymbol{m}}^{-}(k)\right) + \frac{j}{N_c}\left[\boldsymbol{P}^{ref} - \left(\boldsymbol{P}_{\boldsymbol{m}}^{+}(k) + \boldsymbol{P}_{\boldsymbol{m}}^{-}(k)\right)\right] \tag{3-1}$$

An illustration of the reference trajectory for a single converter and $N_c = 3$ steps is given in Figure 3.32.

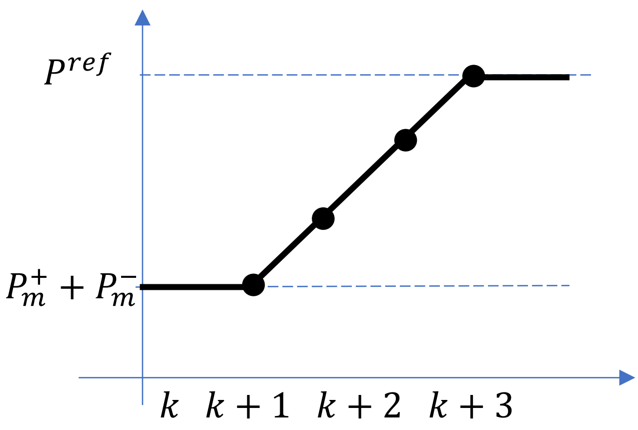

FIGURE 3.32: EXAMPLE OF REFERENCE TRAJECTORY FOR $N_c = 3$ FOR A SINGLE TERMINAL

At this point, it is important to highlight the difference in the calculation of the power references between non-dispatchable and dispatchable terminals. The non-dispatchable terminals are injecting/exporting power from the MTDC grid as dictated by external factors (e.g., wind speed for offshore wind farms). Hence their power reference should be taken equal to their latest measured power.

In contrast, the power references of the dispatchable terminals are provided in regular intervals by the AC-DC grid control, which has assumed a specific production of the non-dispatchable terminals. To cope with the variability of the non-dispatchable VSC powers, it is necessary to adjust the power references of the dispatchable VSCs. This can be achieved through a variety of procedures. A simple option has been proposed in [83] and is not further elaborated here.

As discussed, an optimization problem is at the heart of the MPC scheme. This consists of minimizing the deviations of the predicted VSC powers with respect to that reference trajectory. In order to ensure that the MPC prefers a balanced operating point when the MTDC grid is balanced, a second term involving the DMR currents is added, as follows:

$$min \sum_{j=1}^{N_c} \left\| \boldsymbol{P}^{ref}(k+j) - \left(\boldsymbol{P}^{+}(k+j) + \boldsymbol{P}^{-}(k+j)\right) \right\|_{W}^{2} + \sum_{j=1}^{Nc} \left\| \boldsymbol{I}^{0} \right\|_{W_0}^{2} \tag{3-2}$$

where: $\boldsymbol{W}$ is a diagonal weighting matrix assigned to the deviations of total (i.e., sum of both poles) VSC terminal powers from their references $\boldsymbol{P}^{ref}$. Non dispatchable terminals are assigned a higher weight than the dispatchable VSCs in order to resort to them when actions on dispatchable VSCs only are not sufficient. The weighting matrix $\boldsymbol{W_0}$ has in general a much smaller weight, only to enable the solution to move towards balanced operating points in balanced configurations.

The minimization is subject to various constraints which are listed below.

- For the positive and negative poles (for $j = 1, \dots, N_c$):
  - DC voltage contraint :

$$\boldsymbol{V}_{\boldsymbol{min}}^{\pm} \leq \boldsymbol{V}^{\pm}(k+j) \leq \boldsymbol{V}_{\boldsymbol{max}}^{\pm} \tag{3-3}$$

  - VSC power constraint:

$$\boldsymbol{P}_{\boldsymbol{min}}^{\pm} \leq \boldsymbol{P}^{\pm}(k+j) \leq \boldsymbol{P}_{\boldsymbol{max}}^{\pm} \tag{3-4}$$

  - Change of power constraint:

$$\boldsymbol{\Delta P}_{\boldsymbol{min}}^{\pm} \leq \boldsymbol{P}^{\pm}(k+j) - \boldsymbol{P}^{\pm}(k+j-1) \leq \boldsymbol{\Delta P}_{\boldsymbol{max}}^{\pm} \tag{3-5}$$

  - Branch power constraint:

$$-\boldsymbol{I}_{\boldsymbol{max}}^{\pm} \leq \boldsymbol{I}^{\pm}(k+j) \leq \boldsymbol{I}_{\boldsymbol{max}}^{\pm} \tag{3-6}$$

  - Average voltage constraint (one constraint for each pole):

$$\boldsymbol{V}_{\boldsymbol{avg}}^{\pm}(k+j) = \boldsymbol{V}_{\boldsymbol{avg}}^{\pm}(k) + \frac{j}{N_c}\left[\boldsymbol{V}_{\boldsymbol{avg}}^{\boldsymbol{ref}} - \boldsymbol{V}_{\boldsymbol{avg}}^{\pm}(k)\right] \tag{3-7}$$

The average voltage of the positive pole is defined as $\boldsymbol{V}_{\boldsymbol{avg}}^{+}(k+j) = \frac{\sum_{i=1}^{n_t} V_i^{+}(k+j)}{n_t}$, where $n_t$is the number of terminals. Similar equations hold for the negative pole.

- For the ground or DMR currents ($\boldsymbol{I^0}$) and neutral voltages ($\boldsymbol{V^0}$) (for $j = 1, \dots, N_c$):
  - Neutral point voltage constraint:

$$\boldsymbol{V^0_{min}} \leq \boldsymbol{V^0}(k+j) \leq \boldsymbol{V^0_{max}} \tag{3-8}$$

  - Return path (DMR or ground) constraint:

$$-\boldsymbol{I^0_{max}} \leq \boldsymbol{I^0}(k+j) \leq \boldsymbol{I^0_{max}} \tag{3-9}$$

- Equality constraints giving the predicted evolution of the various variables in response to the control actions $\Delta\boldsymbol{P^{\pm}_{set}}(k+j-1)$ for $j = 1, \dots, N_c$:
  - DC voltage prediction:

$$\Delta\boldsymbol{P^{\pm}_{set}}(k+j-1) = \boldsymbol{S^{\pm}_{P}}[\boldsymbol{V^{\pm}}(k+j) - \boldsymbol{V^{\pm}}(k+j-1)] \tag{3-10}$$

  - Active power prediction:

$$\Delta\boldsymbol{P^{\pm}_{set}}(k+j-1) = \boldsymbol{P^{\pm}}(k+j) - \boldsymbol{P^{\pm}}(k+j-1) + \boldsymbol{K^{\pm}_{V}}[\boldsymbol{V^{\pm}}(k+j) - \boldsymbol{V^{\pm}}(k+j-1)] \tag{3-11}$$

  - Branch current prediction**:**

$$\boldsymbol{I^{\pm}}(k+j) = \boldsymbol{I^{\pm}}(k+j-1) + \boldsymbol{S^{\pm}_{I}}\Delta\boldsymbol{P^{\pm}_{set}}(k+j-1) \tag{3-12}$$

  - Neutral current prediction:

$$\boldsymbol{I^0}(k+j) = \boldsymbol{I^+}(k+j) - \boldsymbol{I^-}(k+j) \tag{3-13}$$

  - Neutral voltage prediction**:**

$$\boldsymbol{I^0}(k+j) = \boldsymbol{G^0}\,\boldsymbol{V^0}(k+j) \tag{3-14}$$

It is important to note that the formulation has been kept as simple as possible in this report to ease understanding. However, it can be further enriched in order to satisfy various performance targets. The following are noted:

- The prediction horizon N_p has been taken equal to the control horizon N_c
- The rate of change of power constraint can include constraints per converter or even per AC area. Here, the constraints have been listed per converter.
- To avoid abrupt corrections following a limit violation, the values of the voltage and current limits ($\boldsymbol{V^{\pm}_{max,min}}$ and $\boldsymbol{I^{\pm}_{max,min}}$) can be progressively tightened, as described in [83].
- Slack variables can be added in some constraints to relax them in case of infeasibility. These slack variables should be heavily penalized in the objective function.
- The matrices $\boldsymbol{S^{\pm}_{P}}$, $\boldsymbol{S^{\pm}_{I}}$ are sensitivity matrices depending on the topology of the system, the resistances of the poles and the DC voltage droop gains of the converters.

- The $\boldsymbol{K_V^{\pm}}$ matrix is a diagonal matrix whose entries are equal to the droop gains of the dispatchable converters (or 0 for non-dispatchable converters).
- The $\boldsymbol{G^0}$ matrix is the admittance matrix of the neutral points of the VSCs. Clearly, the rows and columns corresponding to grounded points (where the neutral voltage is by default equal to 0) should be removed.
- The aforementioned sensitivity matrices should be updated following a topological change in the MTDC grid. To some extent, the MPC scheme, due to its closed-loop behaviour, can cope with outdated models, however this will have an impact on the response time of the controller.
- Following outages of converters, the power references of the converters have to be updated, e.g., by setting the reference of the tripped converter to 0. The adjustment of the remaining converters should be in line with the N-1 security of the combined AC/DC grid and should come from the AC-DC grid control.

Tuning and response time

The control horizon is chosen to obtain a desired 5% settling time as in [83]. The latter can be easily calculated by neglecting the losses of the MTDC grid and assuming no voltage or current limit is reached. From the VSC powers after one control step of the MPC will be:

$$\boldsymbol{P}\,(k+1) = \boldsymbol{P}\,(k) + \frac{\boldsymbol{P}^{ref} - \boldsymbol{P}\,(k)}{N_c} \tag{3-15}$$

Therefore, the error δP after one step will be:

$$\delta\boldsymbol{P}\,(k+1) = \boldsymbol{P}^{ref} - \boldsymbol{P}\,(k+1) = \frac{N_c - 1}{N_c}\left(\boldsymbol{P}^{ref} - \boldsymbol{P}\,(k)\right) \tag{3-16}$$

Following the same logic for the next steps, the error at the n-th step will be:

$$\delta\boldsymbol{P}\,(k+n) = \left(\frac{N_c - 1}{N_c}\right)^n \left(\boldsymbol{P}^{ref} - \boldsymbol{P}\,(k)\right) \tag{3-17}$$

A settling time of 40 s has been chosen, which translates to a total of 8 steps for the chosen sampling time of 5 s. Therefore, by substituting n = 8 the maximum control horizon Nc is found as follows:

$$\left(\frac{N_c - 1}{N_c}\right)^8 \leq 0.05 \Rightarrow N_c^{max} = 3\;steps \tag{3-18}$$

3.2.4 Implementation and Results

Test system description

In order to test the proposed MPC scheme the HVDC grid shown in Figure 3.33 is set-up. It consists of two asynchronous AC areas and an offshore wind farm interconnected via a 5-terminal MTDC grid. Each AC area is connected to two converters. For all connections, the bipole configuration with a DMR has been adopted. Note that only one pole is shown in Figure 3.33. The neutral point of T1 has been selected as the grounding point.

The relevant parameters of the VSCs are given in Table 3.6, whereas Table 3.7 gives the DC cable parameters. The DMR resistances of each section have been taken as 20% higher than the pole resistances.

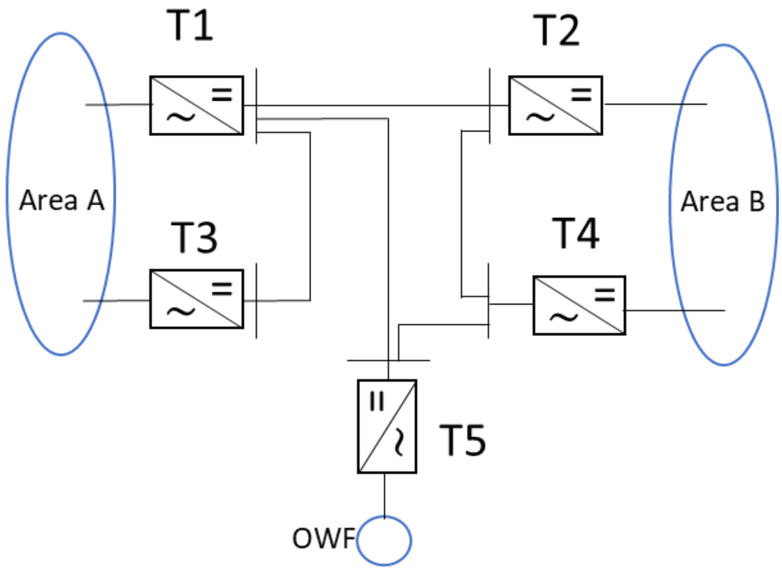

FIGURE 3.33:5-TERMINAL HVDC TEST SYSTEM.

TABLE 3.6: VSC PARAMETERS (POSITIVE AND NEGATIVE POLES)

VSC Name	Rating (MW)	K_V (MW/kV)	Dispatchable?
T1	1000	10	Yes
T2	1000	10	Yes
T3	1000	10	Yes
T4	1000	10	Yes
T5	350	0	No

TABLE 3.7: DC CABLE PARAMETERS (POSITIVE AND NEGATIVE POLES)

Name	Rating (MW)	Resistance (Ω)
T1-T2	1000	1.5
T1-T3	1000	3.5
T1-T5	350	2.5
T2-T4	1000	4.0
T4-T5	350	1.5

As far as the MPC parameters are concerned, they are listed below:

- The active power limits have been set to $P_{min} = -10$ and $P_{max} = +10$ pu for all VSCs, except for the ones connected to T5, for which the limits are $P_{min} = -3.5$ and $P_{max} = +3.5$ pu (on a 100 MW base);
- The DC voltage limits to $V_{min} = 0.96$ and $V_{max} = 1.04$ pu;
- The rate of change limits have been neglected by setting them to very large values;

- The DC branch current limits have been set to I_{max} = 10 pu, except for both branches connected to T5, which have a lower capacity with $I_{max} = 3.5\,pu$.

The focus is on the response of the MTDC grid, hence the AC areas are modelled as infinite grids.

Implementation

The proposed controller has been implemented in Python using standard functions. The MTDC grid has been implemented in PowerFactory. Figure 3.34 shows the interaction between the two platforms. PowerFactory is used to calculate the MTDC grid load flow, thus providing the necessary measurements. Using the Python interface of PowerFactory, the measurements are collected and used to initialize the MPC scheme. After the solution of the optimization problem in Python, the new converter setpoints are provided to PowerFactory in order to calculate the new load flow. Given the relatively slow response time of the proposed scheme, sequential static load flows are sufficient to capture the behaviour of the controller.

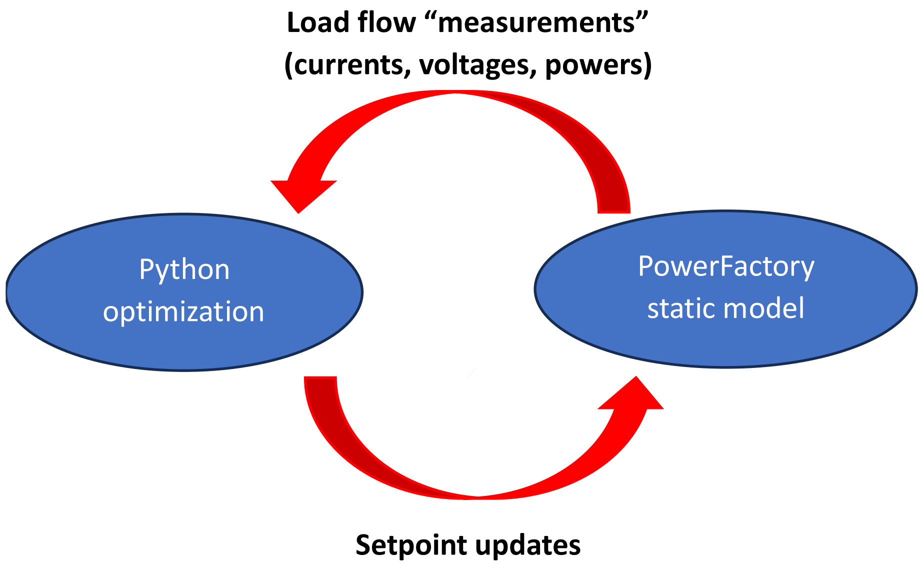

FIGURE 3.34: IMPLEMENTATION OF PROPOSED CONTROL.

Results for balanced operation

The capability of the proposed scheme to effectively manage a balanced MTDC system is first demonstrated in a balanced system. The controller is expected to progressively steer the system from one operating point to the other and ensure its balanced operation. In addition, system constraints should be respected throughout such transitions or promptly corrected after outages.

The following cases are presented:

- Change of power and average voltage references of supervisory control;
- Outage of full terminal (both poles).

Change of power and voltage references of supervisory control

Figure 3.31, showing the interactions between the supervisory MTDC grid control and the AC-DC grid control, the latter is expected to provide the supervisory control with hourly (or mid-hourly, etc.) power schedules, based on market agreements, forecasted RES production, etc. In addition, the average voltage reference setpoint of the converter can be utilized to optimize the losses in the MTDC grid, as discussed in [104]. On its turn, the MTDC grid supervisory controller receives the new references and calculates the necessary actions to reach the new desired reference schedule.

In this example, the power and average DC voltage references of the supervisory controller are changed at $t = 15$ s. Figure 3.35 shows the active power transfer through each terminal (sum of positive and negative poles) and the pole-to-neutral DC voltages. It is shown that the MPC can successfully deal with both these objectives and steer the active powers and the average DC voltage to their reference values[2]. The settling time of the control is around 40 s, as anticipated from the selection of the sampling time (5s) and the control horizon ($N_c = 3$ steps).

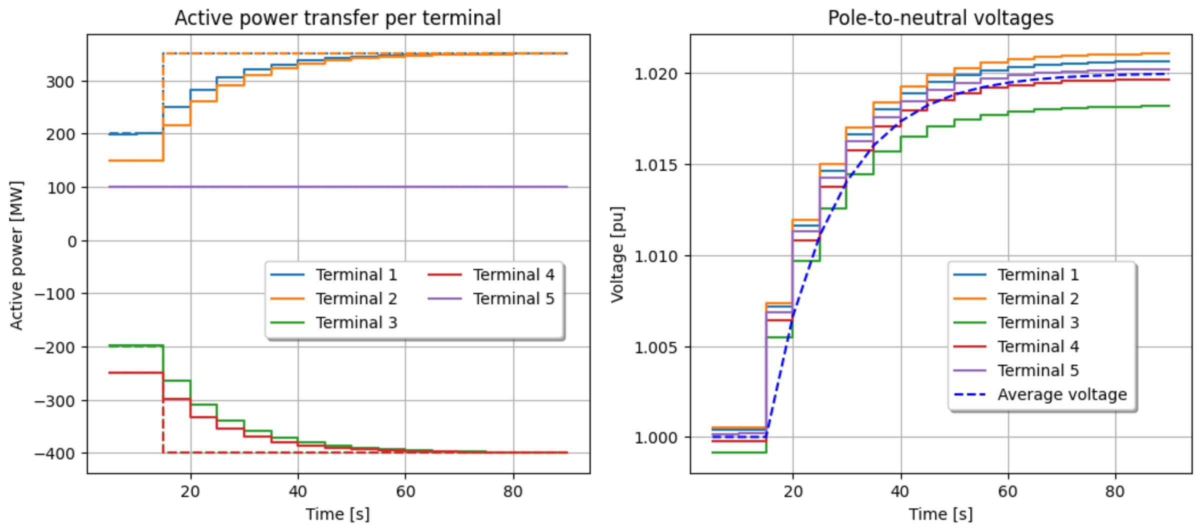

FIGURE 3.35: ACTIVE POWER TRANSFER PER TERMINAL AND POLE-TO-NEUTRAL VOLTAGES WHEN THE MPC RECEIVES NEW POWER AND AVERAGE VOLTAGE SETPOINTS.

Outage of a VSC terminal (both poles)

This sub-section illustrates the behaviour of the proposed supervisory controller following the loss of both poles of a VSC terminal. Note that following this outage, the MTDC grid will still be balanced. Following the outage, the supervisory control is updated of the status of the tripped converter, which does not participate anymore in the power dispatch. The following events are simulated:

- At $t = 5$ s, both poles of terminal T3 trip. T3 is injecting power into the AC system. Hence, this outage leads to a surplus of power injected into the MTDC grid.
- At $t = 90$ s, new power references are sent to the remaining terminals. These new references could emanate from the AC-DC grid control taking into account the N-1 security of the AC systems. In fact, these references could be pre-calculated and pre-programmed in the supervisory control and applied immediately after the outage. Nevertheless, here a delay is assumed to also demonstrate the behaviour of the supervisory control with outdated power references.

The response of the VSC terminal powers and the DC voltages are shown in Figure 3.36. Right after the disturbance, all terminals operating in droop control mode are sharing the power surplus by increasing their power export. Since they have the same droop value, terminals T1, T2 and T4 take up approximately a third of the power previously transferred through terminal T3. Terminal T5 does not participate in DC voltage control, hence its power output does not change. This is desirable and

[2] Note that in these and similar figures the active power references of the converters are denoted with dashed lines in the left figure.

demonstrates the capability of the proposed scheme to still take meaningful action even with outdated references. The pre-disturbance power references of the converters are not anymore physically feasible, hence the MPC cannot track them. Nevertheless, it settles at an operating point until the new (feasible) references are received at $t = 90$ s. Then, it successfully steers the system to the new desired operating point.

Regarding the DC voltages, a significant increase is observed immediately after the disturbance. This is due to the loss of terminal T3 and the proportional nature of the droop control. This voltage deviation depends on the values of the DC voltage droop gains. These gains can be tuned based on static and dynamic performance characteristics, however this is not further elaborated here. Some of the DC voltages violate the voltage limits set in the MPC. The supervisory control though promptly restores them between limits and brings the average DC voltage to 1 pu. It is highlighted that the DC voltages are correctly corrected by the proposed scheme even before the new power references are received.

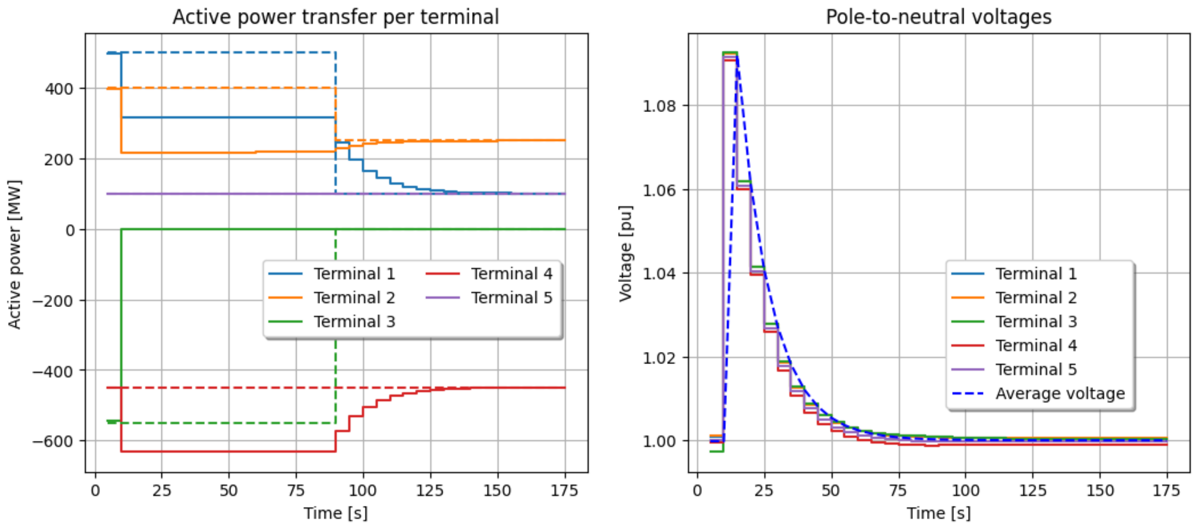

FIGURE 3.36: SYSTEM RESPONSE TO OUTAGE OF BOTH POLES OF VSC TERMINAL.

Results for unbalanced operation

This section will demonstrate the behaviour of the proposed scheme during unbalanced operation of the MTDC grid. Following the outage of a single pole of a VSC terminal, it should be demonstrated that the controller can automatically re-dispatch the power between the positive and negative poles in order to satisfy as much as possible the desired power references, while also respecting voltage and current constraints in the neutral part of the MTDC grid.

To illustrate the above, results are presented for two cases:

- Unconstrained neutral voltage case: in this case there is no constraint on the deviation of the voltage at the neutral points of the MTDC grid.
- Constrained neutral voltage case: the limit of the neutral voltage is set such as it becomes active during the simulation. Then the impact of this constraint is investigated.

Case of unconstrained neutral voltage

In this case, the neutral voltage is unconstrained and can vary freely as a consequence of the unbalanced operation of the MTDC. The positive pole of terminal T3 is tripped at $t = 5$ s.

As shown in Figure 3.37, the first reaction of the MTDC after the loss of the VSC on the positive pole of terminal 3 is to compensate the lost power. This is done through the droop control of the remaining dispatchable VSCs of the positive-pole part of the MTDC grid. After this initial reaction, the MPC-based controller automatically takes the necessary corrective actions in order to restore the VSC powers to their pre-contingency reference values, as shown in Figure 3.38. However, this requires to unevenly split the powers between positive and negative poles, as shown in Figure 3.38, most notably in terminal 1 where the positive and negative pole power are in opposite direction. Although this is physically possible (especially if the converters are coupled on the AC side), it can be prevented through additional constraints in the formulation, if desired. At $t = 90$ s, new power and average DC voltage references are provided to the supervisory controller. The MPC successfully steers the system to the new reference operating point, demonstrating its capability to track them even in unbalanced mode.

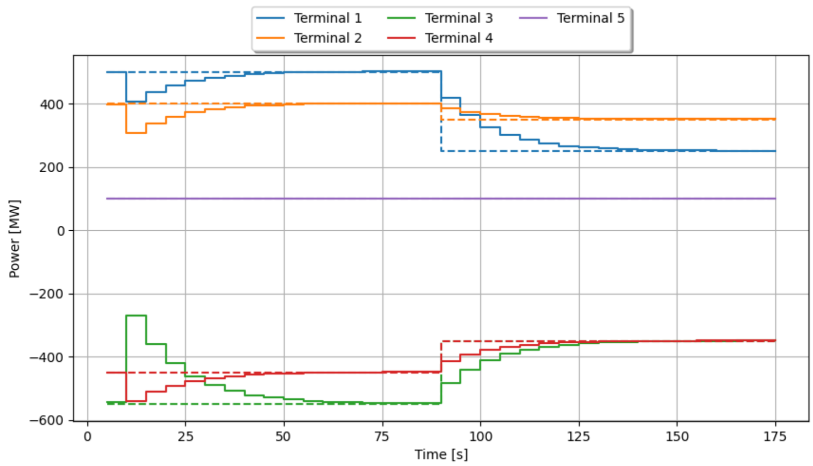

FIGURE 3.37: ACTIVE POWER TRANSFERS PER TERMINAL.

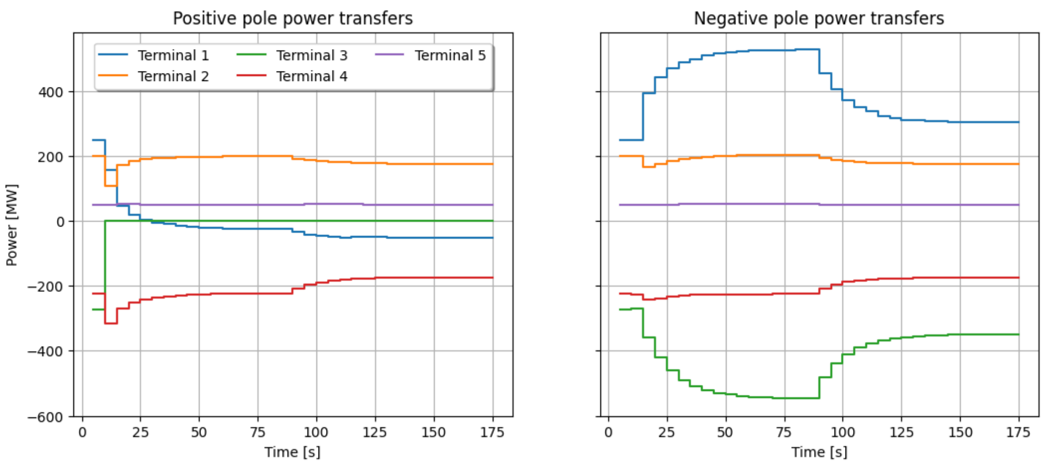

FIGURE 3.38 : ACTIVE POWER TRANSFERS PER POLE.

Figure 3.39 shows the pole-to-neutral DC voltages in the MTDC system. As expected, these are no further balanced. In particular, the impact of the pole outage at $t = 5$ s is observed only in the positive pole-to-neutral voltages. Instead, the observed deviations in the negative pole voltages are due to the subsequent MPC actions. In both cases, the proposed scheme successfully restores the DC voltages to 1 pu. After $t = 90$ s, both positive and negative pole-to-neutral voltages are adjusted so that the average DC voltage settles to the new reference of 1.02 pu.

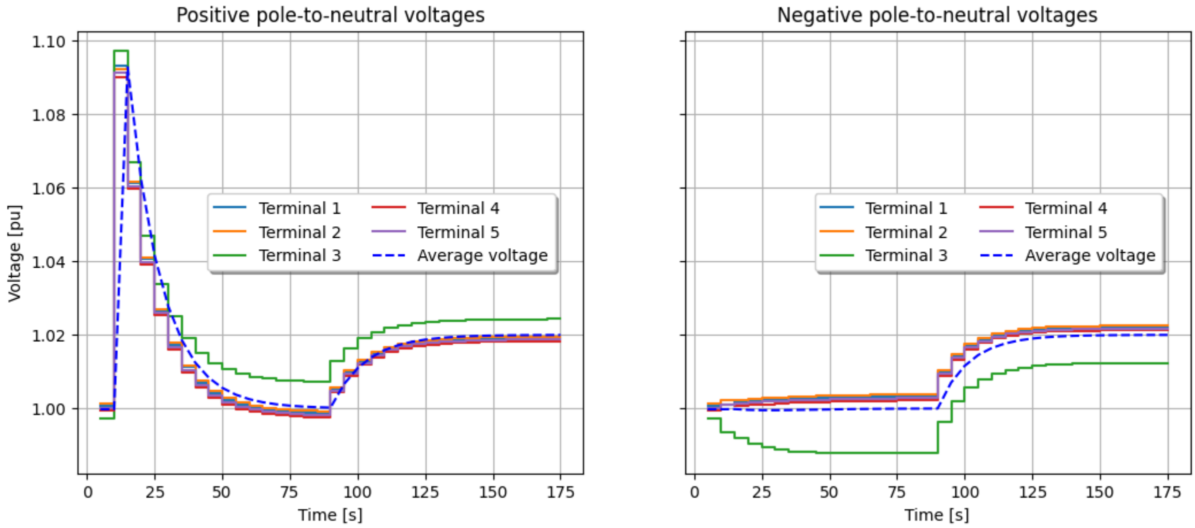

FIGURE 3.39: POLE-TO-NEUTRAL VOLTAGES PER POLE.

Figure 3.40 shows the currents flowing through the DMR cables of the system and the resulting neutral point DC voltages. Clearly, since the powers are not anymore balanced there will be current flowing in some parts of the DMRs of the MTDC grid. In particular, the highest DMR current is observed in DMR between T1 and T3, as expected, since the positive pole of T3 is the initiating disturbance. In the rest of the DMR cables, the proposed scheme manages successfully to limit as much as possible the neutral currents. The same is observed in the neutral point voltages. Note that the maximum observed DC voltage is relatively low (i.e., 4.46 kV). This value depends heavily on the design of the DMR. In this case the cable resistance of the DMR is relatively low (120% of the pole resistance).

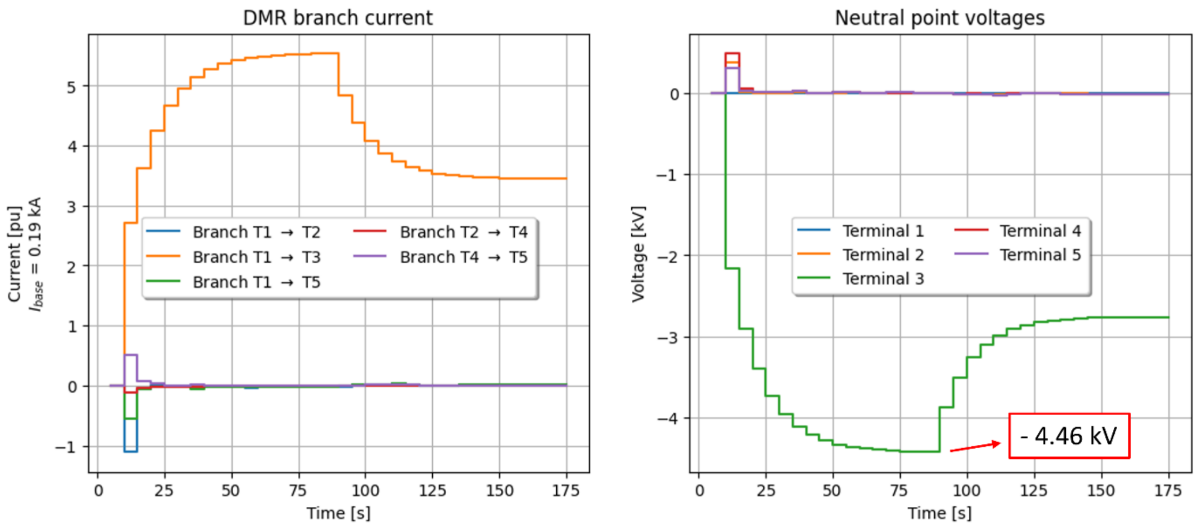

FIGURE 3.40: DMR BRANCH CURRENT AND NEUTRAL POINT VOLTAGES.

However, more significant deviations could be observed if the DMR design resulted in a higher resistance. For example, the work in [105] assumed a much higher resistance (10 times the pole resistance), which would undoubtedly lead to higher neutral voltage deviations.

Case of constrained neutral voltage

The aim of this sub-section is to illustrate the effectiveness of the proposed scheme to respect constraints in the neutral part of the MTDC grid. To this purpose, the outage of the positive pole of T3 is simulated again, however a constraint of 3.15 kV is included for the neutral point voltages.

Figure 3.41 compares the neutral point voltages without constraint (left) and with constraint (right) on the neutral point voltages. As expected, the MPC is able to respect the constraint and limit the neutral voltage at T3 to 3.15 kV.

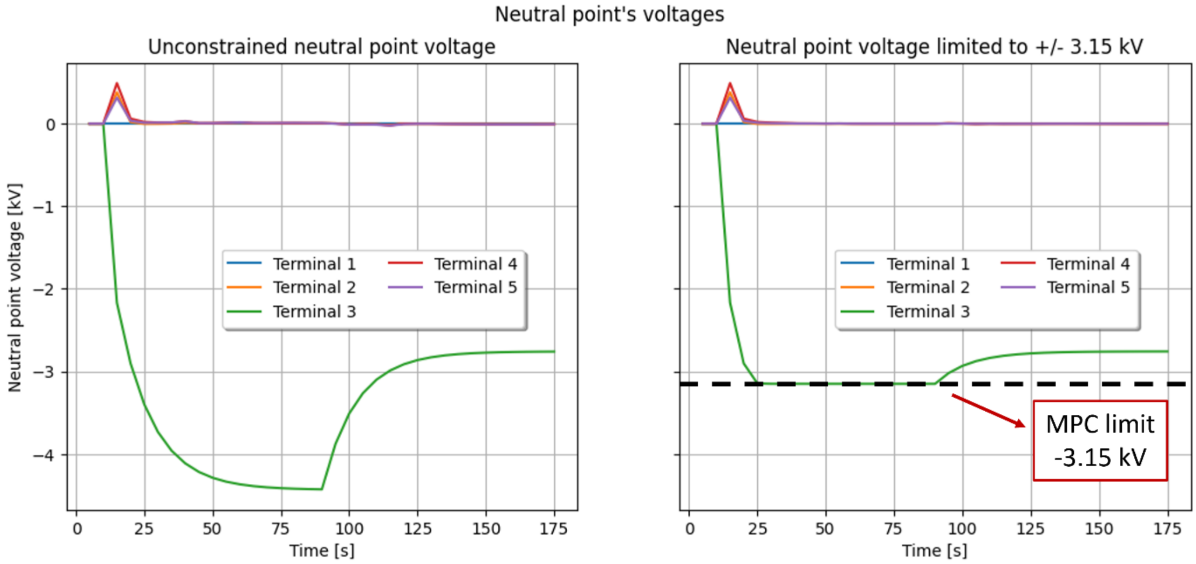

FIGURE 3.41: NEUTRAL POINT VOLTAGES WITHOUT AND WITH CONSTRAINT.

However, respecting the neutral voltage constraint comes at the expense of reaching the desired power reference, as shown in Figure 3.42. In practice, the voltage constraint prevents T3 from reaching its power reference before $t = 90$ s.

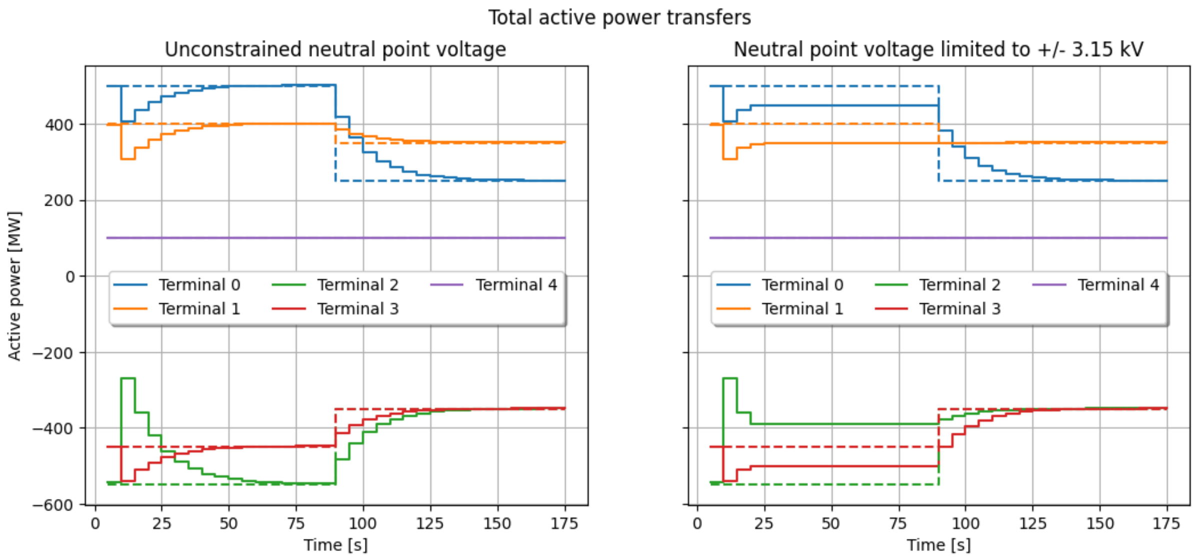

FIGURE 3.42: TERMINAL POWERS WITHOUT AND WITH CONSTRAINT ON NEUTRAL VOLTAGES.

3.2.5 Conclusions on the supervisory control

This functionality has focused on the higher and slower levels of control that dictate the operation and performance of an HVDC grid, the tertiary control (or AC/DC grid control) and the supervisory HVDC grid control (or global HVDC grid control).

The tertiary control level concerns the actual operation of the combined AC/DC grid control. Its aim is to choose an appropriate dispatch of the generating units in the system and the HVDC converters, taking into account the renewable production, and the desired power exchanges, as well as ensuring that security criteria of the system are respected following predefined N-1 (and higher order) contingencies. This level must consider AC and DC contingencies and their impact on both AC and DC systems. In addition, the task of this level is to identify the necessary corrective actions (e.g., HVDC grid setpoint adjustments) that can be taken following an AC or DC contingency. An SC-OPF could be applied to fulfil these objectives, which can even be ran in real-time, using the latest market data and available forecasts, thus updating in regular time intervals (e.g., hourly) the dispatch of the HVDC grid converters. In this document, only a high-level description of the functionality and of the existing work in the literature is provided. A more detailed description of the SC-OPF is described in Deliverable D6.1.

The aim of the supervisory control is to continuously monitor the state of the HVDC grid, ensure an acceptable voltage profile, alleviate violations that might appear following contingencies and steer the system between operating points in a coordinated manner. In addition, it effectively manages unbalanced operation following the outage of a single pole by appropriately redistributing the power between the positive and negative poles in the system. This allows to control and limit the currents going through the DMR or ground, as well as the neutral point voltages. The control scheme receives new HVDC grid measurements and components states at regular intervals and solves a constrained optimization problem to calculate the necessary control actions to satisfy the objective of bringing the converters powers as close as possible to their references. These references emanate from the aforementioned tertiary control level. Simulation results on a five-terminal MTDC grid have demonstrated the effectiveness of the controller to satisfy the above objectives.

4. Conclusions

The HVDC-WISE Project Task 3.2 provides insights into the future challenges of AC/DC grids regarding the control actions and proposes enhancements to existing control strategies across various layers of the AC/DC grid as to enhance the reliability and resilience of the integrated system.

These control proposals are organized into core functions and supplementary control functions. The main contributions of this report are summarized as follows:

Chapter 2 – Core functions

- **Understanding of the challenges and opportunities of combining inertia provision and DC voltage control within the same station**.
    - The virtual inertia support from stations controlling DC voltage in HVDC systems is commonly regarded as a design trade-off problem – larger virtual inertia leads to better frequency stability but deteriorates DC voltage stability. The optimal inertia constant should be the highest value that maintains DC voltage stability.
    - For systems with only one DC voltage control (DVC) station (e.g., a Master Station in Master-Slave configurations), applying GFM control can worsen both frequency and DC voltage stability.
    - On the other hand, distributed DC voltage droop control allows more dynamic energy sharing by dispatching power across terminals, with effective inertia determined by droop gains, inertia constants, and the number of participating terminals. This setup ensures predictable contributions from each terminal, enabling clearer reserve sharing among different AC areas.
- **Control proposal to combine GFM and DC voltage control:** A novel improved GFM-based DC voltage droop control has been proposed for enhanced DC voltage stability while retaining the functionality of inertia support by sharing reserves across different AC areas.
- **Understanding on the firewall capability of GFM converters**. Firewall capability is considered “inherent” to HVDC systems due to the controllability of grid-following converters. Replacing GFL with GFM control, however, can reduce this capability, as GFM controllers prioritize supporting the directly connected AC grid. Analytical small-signal models have been developed to assess firewall capability as a function of key parameters such as short-circuit ratio (SCR), damping, and DC voltage control.
- **Control proposal for damping DC oscillations on the post-fault recovery.** This report addresses oscillations on the DC side of an MTDC system following converter deblocking. A fuzzy logic-based controller is proposed for improved damping during post-fault recovery compared with classical PI approaches.

Chapter 3 – Supplementary control functions

- **Understanding the need of coordination for provision of active power-based services in MTDC grids**. Different services the MTDC can provide are based on active power injection (this report focused on low frequency power oscillation damping, AC line emulation and frequency reserves sharing), while the control of the DC voltage also depends on the balance of active power in the MTDC grid. It has been shown in this report coordination is essential to deliver these services effectively while minimizing interactions with DC voltage control.

- **Proposal of a coordinated control layer provide active power-based services.**
    - The proposal is based on the channel concept: If converter i modulates its power by ΔP_{ij}, converter j modulates the same amount of power in the opposite direction, thus $-\Delta P_{ji}$ (this coordination is achieved using communication).
    - It has been shown how the different analysed services (low frequency power oscillation damping, AC line emulation and frequency reserves sharing) can be implemented in a channel and combined. Their effectiveness was demonstrated via time domain simulations.
    - The AC line emulation service has shown significant potential to enhance system resilience by automatically redistributing active power references to reduce the load on surrounding AC lines following an N-1 disturbance. This automatic adjustment, which does not require operator intervention, can help prevent line overloading and reduce the risk of cascading failures.
- **Proposal of a supervisory control for a MTDC grid.** The proposed supervisory control continuously monitors the state of the HVDC grid to ensure an acceptable DC voltage profile, address potential violations following contingencies, and guide the system between operating points in a coordinated and optimized manner. It also manages unbalanced operations due to single pole outages by redistributing power between the positive and negative poles, thereby controlling and limiting currents through the DMR, ground, and neutral point voltages.

The HVDC-WISE project aims to provide new insights into power system reliability and resilience, reflecting the evolving nature of the grid—particularly with the large-scale integration of HVDC systems—and addressing new and emerging threats to system integrity. **This report demonstrates how the various proposals and control strategies contribute to strengthening resilience and reliability by enhancing the grid's ability to respond effectively to events and disturbances**. In future work packages, these control strategies will be tested in realistic use cases, where their impact on resilience and reliability will be quantified, and their potential interactions when combined will be thoroughly assessed.

TABLE 4.1: CONVERTER STATION PARAMETERS

Parameters	Onshore converter station per MMC	Offshore converter station per MMC
Rated Power	2000 MVA	2000 MVA
Fundamental Frequency	50 Hz	50 Hz
AC Grid Voltage	400 kV	220 kV
AC Converter Bus Voltage	275 kV	275 kV
DC Link Voltage	525 kV	525 kV
Transformer Reactance	0.18 pu	0.15 pu
MMC Arm Inductance	0.025 mH	0.0497 mH
MMC Arm Resistance	0.0785	0.0785
Capacitor Energy in Each Submodule (SM)	30 MJ	30 MJ
Number of Submodules per valve	240	200
Rated Voltage and Current of Each Submodule (SM)	2.5 kV/2 kA	2.5 kV/2 kA
Conduction Resistance of Each IGBT/Diode	$5.44 * 10^{-4}$	$5.44 * 10^{-4}$

The HVDC cable is modelled using Frequency Dependent (Phase) model. The data for the cable model is based on the experience of 2 GW [107] Offshore Interconnection projects in the North Sea and has been listed in Table 4.2 and Table 4.3.

TABLE 4.2: RELEVANT GEOMETRICAL AND MATERIAL DATA OF GENERIC 525 KV HVDC LAND CABLE

Main Layers	Properties	Unit	Parameter Data (Nominal)
Core Conductor	Metallic Cross-Sectional Area	[mm2]	3000
	Outer Diameter	[mm]	68
	DC Resistivity (max.) at 20° C	[Ωm]	$1.7241 * 10^{-8}$
Main Insulation (XLPE)	Conductor Screen Thickness	[mm]	1.8
	Main Insulation Thickness	[mm]	26.5
	Insulation Screen Thickness	[mm]	1.5
	Relative Permittivity	-	2.4
Metallic Screen	Screen Thickness	[mm]	1.2
	Diameter Over Screen	[mm]	1.38
	DC Resistivity (max.) at 20° C	[Ωm]	$2.8264 * 10^{-8}$
Outermost Jacket	HDPE Jacket Thickness	[mm]	5.0
	External Semiconductor Skin Thickness	[mm]	0.3
	Relative Permittivity	-	2.5
Overall Cable	Diameter	[mm]	153

TABLE 4.3: RELEVANT GEOMETRICAL AND MATERIAL DATA OF GENERIC 525 KV HVDC SUBSEA CABLE

Main Layers	Properties	Unit	Parameter Data (Nominal)
Core Conductor	Metallic Cross-Sectional Area	[mm2]	2500
	Outer Diameter	[mm]	60
	DC Resistivity (max.) at 20° C	[Ωm]	$1.7241 * 10^{-8}$
Main Insulation (XLPE)	Conductor Screen Thickness	[mm]	2.0
	Main Insulation Thickness	[mm]	26.0
	Insulation Screen Thickness	[mm]	1.8
	Relative Permittivity	-	2.4
Metallic Sheath	Material	-	Lead
	Thickness	[mm]	3.2

	DC Resistivity (max.) at 20º C	[Ωm]	2.14* 10^{-7}
Armour	Material at Armour Wires	[mm]	Galvanized Steel
	Thickness of Single Armour Wire	[mm]	6.0
Overall Cable	Diameter	[mm]	161

5. References

[1] IEC, "IEC 62747:2014 Terminology for voltage-sourced converters (VSC) for high-voltage direct current (HVDC) systems," 2014.

[2] IEC, "IEC TS 63291-1:2023 High voltage direct current (HVDC) grid systems and connected converter stations - Guideline and parameter lists for functional specifications - Part 1: Guideline," 2023.

[3] InterOPERA, "D2.1 Functional requierments for HVDC grid systems and subsystems," 2024.

[4] L. Papangelis, Local and centralized control of multi-terminal DC grids for secure operation of combined AC/DC systems (Doctoral Thesis), Liege: Université de Liège, 2018.

[5] T. M. Haileselassie, Control, Dynamics and Operation of Multi-terminal VSC-HVDC Transmission Systems (PhD Thesis), Trondheim: Norwegian University of Science and Technology, 2012.

[6] F. D. Bianchi, J. L. Domínguez-García and O. Gomis-Bellmunt, "Control of multi-terminal HVDC networks towards wind power integration: A review," *Renewable and Sustainable Energy Reviews 55,* pp. 1055-1068, 18 May 2016.

[7] D. Pattabiraman, R. H. Lasseter and T. M. Jahns, "Comparison of Grid Following and Grid Forming Control for a High Inverter Penetration Power System," 2018.

[8] N.-B. Lai, A. Tarraso, G. N. Baltas, L. V. Marin Arevalo and P. Rodriguez, "External Inertia Emulation Controller for Grid-Following Power Converter," *IEEE Transactions on Industry Applications,* vol. 57, no. 6.

[9] T. &. W. X. Liu, "Physical Insight Into Hybrid-Synchronization-Controlled Grid-Forming Inverters Under Large Disturbances," *IEEE Transactions on Power Electronics,* vol. 37, no. 10, pp. 11475-11480, 2022.

[10] R. Rosso, X. Wang, M. Liserre, X. Lu and S. Engelken, "Grid-Forming Converters: Control Approaches, Grid-Synchronization, and Future Trends—A Review," *IEEE Open Journal of Industry Applications,* vol. 2, pp. 93-109, 2021.

[11] R. Ghosh, N. R. Tummuru and B. S. Rajpurohit, "A New Virtual Oscillator-Based Grid-Forming Controller with Decoupled Control Over Individual Phases and Improved Performance of Unbalanced Fault Ride-Through," *IEEE Transactions on Industrial Electronics,* vol. 70, no. 12, pp. 12465-12474, 2023.

[12] E. Rokrok, T. Qoria, A. Bruyere, B. Francois and X. Guillaud, "Effect of Using PLL-Based Grid-Forming Control on Active Power Dynamics Under Various SCR,," in *IECON 2019 - 45th Annual Conference of the IEEE Industrial Electronics Society*, Lsibon, 2019.

[13] National Renewable Energy Laboratory, "Virtual Oscillator Control Maintains Grid Operations with High Inverter Penetrations," Denver, 2016.

[14] S. D'Arco and J. Suul, ""Virtual synchronous machines — Classification of implementations and analysis of equivalence to droop controllers for microgrids,," in *IEEE Grenoble Conference*, Grenoble, 2013.

[15] J. Roldán-Pérez, A. Rodríguez-Cabero and M. Prodanovic, "Design and Analysis of Virtual Synchronous Machines in Inductive and Resistive Weak Grids," *IEEE Transactions on Energy Conversion,* vol. 34, no. 4, pp. 1818-1828, 2019.

[16] X. Gao, D. Zhou, A. Anvari-Moghaddam and F. Blaabjerg, "A Comparative Study of Grid-Following and Grid-Forming Control Schemes in Power Electronic-Based Power Systems," *Power Electronics and Drives,* vol. 8, no. 1, pp. 1-20, 2023.

[17] A. Tayyebi, F. Kupzog, F. Dörfler and W. Hribernik, "Grid-Forming Converters - Inevitability, Control Strategies and Challenges in Future Grid Applications," in *CIRED Workshop 2018*, Ljubljana, 2018.

[18] Q. C. Zhong and G. Weiss, "Synchronverters: Inverters that mimic synchronous generators," *IEEE Transactions on Industrial Electronics,* vol. 58, no. 4, p. 1259–1267, 2011.

[19] H. Bevrani, T. Ise and Y. Miura, "Virtual synchronous generators: A survey and new perspectives," *International Journal of Electrical Power & Energy Systems,* vol. 54, p. 244–254, 2014.

[20] S. D'Arco, J. A. Suul and O. B. Fosso, "A Virtual Synchronous Machine implementation for distributed control of power converters in SmartGrids," *Electric Power Systems Research,* vol. 122, p. 180–197, 2015.

[21] A. Abdalrahman, Y. -J. Häfner, M. K. Sahu, K. K. Nayak and A. Nami, "Grid Forming Control for HVDC Systems: Opportunities and Challenges," in *2022 24th European Conference on Power Electronics and Applications (EPE'22 ECCE Europe)*, Hanover, Germany, 2022.

[22] C. Henderson, D. Vozikis, D. Holliday, X. Bian and A. Egea-Àlvarez, "Assessment of Grid-Connected Wind Turbines with an Inertia Response by Considering Internal Dynamics," *Energies,* vol. 13, no. 5, p. 1038, 2020.

[23] K. Shinoda, A. Benchaib, J. Dai and X. Guillaud, "Over- and Under-Voltage Containment Reserves for Droop-Based Primary Voltage Control of MTDC Grids," *IEEE Trans. on Power Del.,* vol. 37, no. 1, pp. 125-135, 2022.

[24] Y. Pang, A. Egea-Alvarez, J. C. Gonzalez-Torres, K. Shinoda, F. Perez and A. Benchaib, "DC Voltage Stability Analysis and Enhancement for Grid-Forming-Based MTDC Systems," *IEEE Transactions on Power Electronics,* vol. Early Access, 2024.

[25] L. Carlsson, "HVDC A "firewall" against disturbances in high-voltage grids," ABB, 2005.

[26] C. Spallarossa, Y. Pipelzadeh and T. C. Green, "Influence of Frequency-Droop Supplementary Control on Disturbance Propagation through VSC HVDC Links," in *General Meeting of the IEEE-Power-and-Energy-Society (PES)*, 2013.

[27] L. Lourenço, F. Perez, A. Iovine, G. Damm, R. Monaro and M. Salles, "Stability Analysis of Grid-Forming MMC-HVDC Transmission Connected to Legacy Power Systems," *Energies,* vol. 14, p. 8017, 2021.

[28] C. M. Freitas, E. H. Watanabe and M. L. F. C., "d-q Small-Signal Model for Grid-Forming MMC and Its Application in Electromagnetic-Transient Simulations," *Energies,* vol. 6, p. 2195, 2023.

[29] J. Arévalo-Soler, E. Sánchez-Sánchez, E. Prieto-Araujo and O. Gomis-Bellmunt, "Impact analysisof energy-based control structures for grid-forming and grid-following MMC on power system dynamics based on eigen properties indices," *Electrical Power and Energy Systems,* 022.

[30] Q. Tu, Z. Xu and L. and Xu, "Reduced switching-frequency modulation and circulating current suppression for modular multilevel converters," *IEEE Transactions on Power Delivery,* vol. 26, no. 3, pp. 2009-2017, 2011.

[31] W. Wang, L. Jiang, Y. Cao and Y. Li, "A Parameter Alternating VSG Controller of VSC-MTDC Systems for Low Frequency Oscillation Damping," *IEEE Trans on Power Syst.,* vol. 35, no. 6, pp. 4609-4621, 2020.

[32] P. W. Sauer and M. A. Pai, Power System Dynamics and Stability, Illinois, 1997, p. 230.

[33] X. Wang, J. Liu, J. Hu, Y. Meng and C. Yuan, "Frequency Characteristics of the Synchronous-Frame Based D-Q Methods for Active Power Filters," *Journal of Power Electronics (JPE),* 2007.

[34] O. Cwikowski, A. Wood, A. Miller, M. Barnes and R. and Shuttleworth, "Operating DC circuit breakers with MMC," *IEEE Transactions on Power Delivery,* vol. 33, pp. 260--270, 2017.

[35] O. Cwikowski, H. Wickramasinghe, G. Konstantinou, J. Pou, M. Barnes and R. and Shuttleworth, "Modular multilevel converter DC fault protection," *IEEE Transactions on Power Delivery,* vol. 33, pp. 291--300, 2017.

[36] T. Li and C. and Zhao, "Recovering the modular multilevel converter from a cleared or isolated fault," *IET generation, transmission & distribution,* vol. 9, pp. 550--559, 2015.

[37] R. Damas, Y. Son, M. Yoon, S. Kim and S. and Choi, "Subsynchronous oscillation and advanced analysis: A review," *IEEE Access,* vol. 8, pp. 224020--224032, 2020.

[38] V. Virulkar and G. and Gotmare, "Sub-synchronous resonance in series compensated wind farm: A review," *Renewable and Sustainable Energy Reviews,* vol. 55, pp. 1010--1029, 2016.

[39] A. Shetgaonkar, L. Liu, A. Lekić, M. Popov and P. and Palensky, "Model predictive control and protection of MMC-based MTDC power systems," *International Journal of Electrical Power & Energy Systems, Elsevier,* vol. 146, p. 108710, 2023.

[40] H. Oruganti, S. Dash, C. Nallaperumal and S. and Ramasamy, "A proportional resonant controller for suppressing resonance in grid tied multilevel inverter," *Energies,* vol. 11, p. 1024, 2018.

[41] S. D'Arco, J. Suul and M. and Molinas, "mplementation and analysis of a control scheme for damping of oscillations in VSC-based HVDC grids," in *In 2014 16th International Power Electronics and Motion Control Conference and Exposition*, Antalya, Turkey, 2014.

[42] C. Li, Y. Li, Y. Cao, H. Zhu, C. Rehtanz and U. and Häger, "Virtual synchronous generator control for damping DC-side resonance of VSC-MTDC system.," *IEEE Journal of Emerging and Selected Topics in Power Electronics,* vol. 6, no. 3, pp. 1054-1064, 2018.

[43] Y. Liu, A. Raza, K. Rouzbehi, B. Li, D. Xu and B. and Williams, "Dynamic resonance analysis and oscillation damping of multiterminal DC grids," *EEE Access,* vol. 5, pp. 16974-16984, 2017.

[44] M. Abedrabbo, F. Dejene, W. Leterme and D. and Van Hertem, "HVDC grid post-DC fault recovery enhancement," *IEEE Transactions on Power Delivery,* vol. 36, no. 2, pp. 1137-1148, 2020.

[45] J. Pou, S. Ceballos, G. Konstantinou, V. Agelidis, R. Picas and J. and Zaragoza, "Circulating Current injection methods based on instantaneous information for the modular multilevel converter," *IEEE Transactions on Industrial Electronics,* vol. 62, no. 2, pp. 777-78, 2014.

[46] J. Qin and M. and Saeedifard, "Predictive control of a modular multilevel converter for a back-to-back HVDC system," *IEEE Transactions on Power delivery,* vol. 27, no. 3, pp. 1538-1547, 2012.

[47] X. She, A. Huang, X. Ni and R. and Burgos, "AC circulating currents suppression in modular multilevel converter," in *In IECON 2012-38th Annual Conference on IEEE Industrial Electronics Society* , Montreal, QC, Canada, 2012.

[48] Z. Li, P. Wang, Z. Chu, H. Zhu, Y. Luo and Y. and Li, "An inner current suppressing method for modular multilevel converters," *IEEE Transactions on Power Electronics,* vol. 28, no. 11, pp. 4873-4879, 2013.

[49] J. Freytes, G. Bergna, J. Suul, S. D'Arco, F. Gruson, F. Colas, H. Saad and X. and Guillaud, "Improving small-signal stability of an MMC with CCSC by control of the internally stored energy," *IEEE Transactions on Power Delivery,* vol. 33, no. 1, pp. 429-439, 2017.

[50] J. Pou, S. Ceballos, G. Konstantinou, V. Agelidis, R. Picas and J. and Zaragoza, "Circulating current injection methods based on instantaneous information for the modular multilevel converter," *IEEE Transactions on Industrial Electronics,* vol. 62, no. 2, pp. 777-788, 2014.

[51] O. Cwikowski, H. Wickramasinghe, G. Konstantinou, J. Pou, M. Barnes and R. and Shuttleworth, " Modular multilevel converter DC fault protection," *IEEE Transactions on Power Delivery,* vol. 33, no. 1, pp. 291-300, 2017.

[52] C. S. &. ENGINEERING, "CSE NO32 Feburary 2024," URL: New Settlement Procedure for Unintended Exchange in Continental Europe | CSE (cigre.org)., 2024.

[53] C. W. G. B4.62, "Connection of Wind Farms to Weak AC networks," CIGRE Technical Brochure, vol. 671, 2016.

[54] J. Dawson, "Fuzzy logic control of linear systems with variable time delay," in *In Proceedings of 1994 9th IEEE International Symposium on Intelligent Control*, Columbus, OH, USA, 1994.

[55] C. Lee, "Fuzzy logic in control systems: fuzzy logic controller," *IEEE Transactions on systems, man, and cybernetics,* vol. 20, no. 2, pp. 404-418, 1990.

[56] S. Arunprasanth, U. Annakkage and R. and Kuffel, "Real time digital simulation of a static var compensator with fuzzy supervisory control," in *In 2013 IEEE 8th International Conference on Industrial and Information Systems*, Peradeniya, Sri Lanka, 2013.

[57] P. Dash, A. Routray and A. and Liew, "Design of an energy function based fuzzy tuning controller for HVDC links," *International Journal of Electrical Power & Energy Systems,* vol. 21, no. 5, pp. 337-347, 1999.

[58] A. Nguyen, T. Taniguchi, L. Eciolaza, V. Campos, R. Palhares and M. and Sugeno, "Fuzzy control systems: Past, present and future," *IEEE Computational Intelligence Magazine,* vol. 14, no. 1, pp. 56-68, 2019.

[59] A. Ofoli, "Fuzzy-logic applications in electric drives and power electronics," in *In Power electronics handbook*, Elsevier, 2024, pp. 1233--1260.

[60] ENTSOE, "HVDC links in system operations," cite, 2019.

[61] M. Elizondo, R. Fan, H. Kirkham, M. Ghosal, F. Wilches-Bernal, D. Schoenwald and J. Lian, "Interarea oscillation damping control using high-voltage dc transmission: A survey," *IEEE Transactions on Power Systems,* vol. 33, no. 6, pp. 6915--6923, 2018.

[62] F. Errigo, J. C. Gonzalez-Torres, A. Benchaib, L. Chédot, A. Sari, P. Venet and F. Morel, "Errigo, Florian, et al. "Modular Multilevel Converter with Embedded Energy Storage for Power Oscillation Damping and Fast Frequency Response-A case study." 41. CIGRE International Symposium. 2021.," in *41. CIGRE International Symposium*, Ljubljana, 2021.

[63] J. Renedo, A. Garcia-Cerrada, L. Rouco and L. Sigrist, "Coordinated design of supplementary controllers in VSC-HVDC multi-terminal systems to damp electromechanical oscillations," *IEEE Transactions on Power Systems,* vol. 36, no. 1, pp. 712--721, 2020.

[64] J. C. Gonzalez-Torres, G. Damm, V. Costan, A. Benchaib and F. Lamnabhi-Lagarrigue, "A novel distributed supplementary control of Multi-Terminal VSC-HVDC grids for rotor angle stability enhancement of AC/DC systems," *IEEE Transactions on Power Systems,* vol. 36, no. 1, pp. 623-634, 2020.

[65] L. Coronado, C. Longas, R. Rivas, S. Sanz, J. Bola, P. Junco and G. Perez, "INELFE: main description and operational experience over three years in service.," in *AEIT HVDC International Conference (AEIT HVDC)*, Florence, Italy, 2019.

[66] J. C. Gonzalez-Torres, G. Damm, V. Costan, A. Benchaib and F. Lamnabhi-Lagarrigue, "Transient stability of power systems with embedded VSC-HVDC links: Stability margins analysis and Control," *IET Generation, Transmission & Distribution,* vol. 14, no. 17, pp. 3377 - 3388, 2020.

[67] J. C. Gonzalez-Torres, G. Damm, V. Costan, A. Benchaib and F. Lamnabhi-Lagarrigue, "Dynamic control of embedded HVDC to contribute to transient stability enhancement," in *CIGRE*, Paris, Fr, 2020.

[68] C. Cardozo, A. Diaz-Garcia, G. Giannuzzi, G. Torresan, F. Xavier, A. Cordon, L. Coronado, R. Zaottini and C. Pisiani, "Small Signal Stability Analysis of the Angle Difference Control on a HVDC Interconnection Embedded in the CE Synchronous Power System," in *2020 IEEE/PES Transmission and Distribution Conference and Exposition (T&D)*, 2020.

[69] J. Renedo, L. Rouco, L. Sigrist and G.-C. Aurelio, "Impact of AC-line-emulation controllers of VSC-HVDC links on inter-area-oscillation damping," in *IECON 2019-45th Annual Conference of the IEEE Industrial Electronics Society*, Lisbon, Portugal, 2019.

[70] O. H. project, "D3.3 Analysis of the synchronisation capabilities of BESS power converters," 2022.

[71] K. Shinoda, J. Dai, G. Bakhos, J. C. Gonzalez-Torres, A. Benchaib and S. Bacha, "Design consideration for frequency containment reserve provisions by a multi-terminal HVDC system," *IET Generation, Transmission & Distribution,* vol. 17, no. 18, pp. 4024--4037, 2023.

[72] G. BAKHOS, S. BACHA, J.-C. Gonzalez-Torres, L. Vanfretti, A. BENCHAIB, J. DAI and K. SHINODA, "Hybrid AC/DC Power System Stability: An Attempt of Global Approach," *Preprint Available at SSRN 4704802,* 2024.

[73] L. Harnefors, N. Johansson and L. Zhang, "Impact on interarea modes of fast HVDC primary frequency control," *IEEE Transactions on Power Systems,* vol. 32, no. 2, pp. 1350--1358, 2016.

[74] L. Vanfretti, T. Rabuzin, M. Baudette and M. Murad, "iTesla Power Systems Library (iPSL): A Modelica library for phasor time-domain simulations," *SoftwareX,* vol. 5, pp. 884--88, 2016.

[75] J. C. Gonzalez-Torres, R. Mourouvin, K. Shinoda, A. Benchaib and A. Zama, "A simplified approach to model grid-forming controlled MMCs in power system stability studies," in *2021 IEEE PES Innovative smart grid technologies Europe (ISGT Europe)*, 2021.

[76] M. Aragues-Penalba, A. Egea-Alvarez, S. G. Arellano and a. O. Gomis-Bellmunt, "Droop control for loss minimization in HVDC multi-terminal transmission systems for large offshore wind farms," *Electric Power Systems Research,* 2014.

[77] C. Gavriluta, I. Candela, A. Luna, A. Gomez-Exposito and P. Rodriguez, "Hierarchical Control of HV-MTDC Systems With Droop-Based Primary and OPF-Based Secondary," *IEEE Transactions on Smart Grid,* 2015.

[78] S. Nanou, O. Tzortzopoulos and S. Papathanassiou, "Evaluation of an enhanced power dispatch control scheme for multi-terminal HVDC grids using Monte-Carlo simulation," *Electric Power Systems Research,* 2016.

[79] P. Rault, "Dynamic Modeling and Control of Multi-Terminal HVDC Grids," Ecole Centrale de Lille, 2014.

[80] T. M. Haileselassie, A. G. Endegnanew and K. Uhlen, "Secondary control in multi-terminal VSC-HVDC transmission system," in *IEEE PES General Meeting*, 2015.

[81] J. Beerten and D. V. Hertem, " Analysis of power redispatch schemes for HVDC grid secondary voltage control," in *IEEE PES General Meeting*, 2015.

[82] A. Egea-Alvarez, J. Beerten, D. V. Hertem and O. Gomis-Bellmunt, "Hierarchical power control of multiterminal HVDC grids," *Electric Power Systems Research,* 2015.

[83] L. Papangelis, M.-S. Debry, P. Panciatici and T. Van Cutsem, "Coordinated supervisory control of multi-terminal HVDC grids: A model predictive control approach," *IEEE Transactions on Power Systems,* 2017.

[84] D. Chen and B. Marshall, "Modelling Asymmetrical HVDC Transfer Network for Multi-Vendor-Multi-Terminal Interoperability," in *Renewable Power Generation and Future Power Systems Conference*, Glasgow, 2023.

[85] D. Chen, B. Marshall, C. Foote, S. Rangasamy and S. Tian, "Towards HVDC interoperability-assessing existence of equilibrium with reference to converter terminal behaviour," in *19th International Conference on AC and DC Power Transmission*, Glasgow, 2023.

[86] R. T. Pinto, "Multi-Terminal DC Networks System Integration, Dynamics and," Delft University of Tech, 2014.

[87] B. Berggren, K. Linden and R. Majumder, "DC Grid Control Through the Pilot Voltage Droop Concept - Methods for Establishing Set-Point Tracking," in *IEEE International Energy Conference*, 2014.

[88] J. Zhu, C. D. Booth, G. P. Adam and A. J. Roscoe, "Coordinated direct current matching control strategy for multi-terminal DC transmission systems with integrated wind farms," *Electric Power Systems Research,* 2015.

[89] J. S. Guzmán-Feria, L. M. Castro, N. González-Cabrera and J. H. Tovar-Hernández, "Security constrained OPF for AC/DC systems with power rescheduling by power plants and VSC stations," *Sustainable Energy, Grids and Networks,* vol. 27, 2021.

[90] F. S. a. D. W. T. Sennewald, "Active and Reactive Power PSCOPF for Mixed AC- HVDC-Systems," in *2018 IEEE PES Innovative Smart Grid Technologies Conference Europe (ISGT-Europe)*, Sarajevo, 2018.

[91] T. S. a. D. W. T. Sennewald, "A preventive security constrained optimal power flow for mixed AC-HVDC-systems," in *13th IET International Conference on AC and DC Power Transmission*, Manchester, 2017.

[92] E. Ciapessoni, D. Cirio, S. Massucco and A. Pitto, "A Probabilistic Risk Assessment and Control methodology for HVAC electrical grids connected to multiterminal HVDC networks," in *IFAC Proceedings Volumes, Volume 44, Issue 1, Pages 1727-1732*, 2011.

[93] C. Fu and et al. , "VSC-HVDC Incorporated Corrective Security-Constrained Optimal Power Flow," *Journal of Physics: Conference Series, Volume 2320, 2022, The 15th International Conference on Computer and Electrical Engineering (ICCEE 2022) 24/06/2022 - 26/06/2022.*

[94] V. Bhardwaj, H. Ergun and D. Van Hertem, "Risk-based preventive-corrective security constrained optimal power flow for ac/dc grid," in *2021 IEEE Madrid PowerTech Conference*.

[95] F. L. a. D. W. T. Sennewald, "Preventive and Curative Actions by Meshed Bipolar HVDC-Overlay-Systems," *IEEE Transactions on Power Delivery,* vol. 35, no. 6, pp. 2928-2936, 2020.

[96] J. Cao, W. Du and H. F. Wang, "An Improved Corrective Security Constrained OPF for Meshed AC/DC Grids With Multi-Terminal VSC-HVDC," *IEEE Tr. on Power Systems,* vol. 31, no. 1, 2016.

[97] R. Teixeira Pinto, M. Aragues-Penalba, O. Gomis-Bellmunt and A. Sumper, "Optimal Operation of DC Networks to Support Power System Outage Management," *IEEE Transactions on Smart Grid,* vol. 7, no. 6, p. 2953–2961, 2016.

[98] V. Saplamidis, R. Wiget and G. Andersson, "Security constrained Optimal Power Flow for mixed AC and multi-terminal HVDC grids," in *2015 IEEE Eindhoven PowerTech*.

[99] S. C. a. G. Andersson, "Security constrained OPF incorporating corrective control of HVDC," 2014 Power Systems Computation Conference, Wroclaw, Poland.

[100] R. Wiget, M. Vrakopoulou and G. Andersson, "Probabilistic security constrained optimal power flow for a mixed HVAC and HVDC grid with stochastic infeed," 2014 Power Systems Computation Conference, Wroclaw, Poland.

[101] E. Ciapessoni, D. Cirio, F. Conte, A. Pitto, S. Massucco and M. Saviozzi, "Probabilistic Security-Constrained Preventive Control under Forecast Uncertainties Including Volt/Var Constraints," *Energies,* vol. 16, no. 1812, 2023.

[102] J. M. Maciejowski, Predictive control: with constraint, Pearson education, 2002.

[103]]. S. J. Qin and T. A. Badgwel, "A survey of industrial model predictive control technology," *Control Eng. Practi,* pp. 733-764, 2003.

[104] L. Papangelis, "Local and centralized control of multi-terminal DC grids for secure operation of combined AC/DC systems.," University of Liege, 2018.

[105] C. K. Jat, J. Dave, D. V. Hertem and H. Ergun, "Hybrid AC/DC OPF Model for Unbalanced Operation of Bipolar HVDC Grids," *IEEE Transactions on Power Systems,* 2023.

[106] C. W. G. B4.57, "Guide for the Development of Models for HVDC Converters in a HVDC Grid," CIGRE Technical Brochure, 2014.

[107] C. Electra, "ELECTRA N ° 321 April 2022," 2023.

[108] C. Brantl, R. Puffer, P. Tünnerhoff and P. Ruffing, "Impact of the HVDC system configuration on DC line protection," 2019.

[109] CIGRÉ Working Group B4.70, "Brochure 832- Guide for electromagnetic transient studies involving VSC converters," CIGRÉ, Paris, France, 2021.

[110] ENTSO-E: RG-CE System Protection & Dynamics Sub Group, "HVDC Links in System Operations," ENTSO-E, Brussels, Belgium, 2019.

[111] D. Van Hertem, O. Gomis-Bellmunt and J. Liang, HVDC Grids: For Offshore and Supergrid of the Future, Wiley, 2016.

[112] Shu Wang, Jinxiang Zhu, Lan Trinh and Jiuping Pan, "Economic assessment of HVDC project in deregulated energy markets," in *Third International Conference on Electric Utility Deregulation and Restructuring and Power Technologies*, Nanjing, 2008.

[113] C. Hahn, "Modellierung und Regelung selbstgeführter, höherstufiger Multiterminal-HGÜ-Systeme mit Gleichspannungszwischenkreis," Friedrich-Alexander-Universität (FAU), Erlangen-Nürnberg, 2018.

[114] D. Larruskain, V. Valverde, E. Torres, G. Buigues and M. Santos, "Protection Systems for Multi-Terminal HVDC Grids," *Renewable Energy and Power Quality Journal,* vol. 1, pp. 310-315, 4 2018.

[115] M. Muniappan, "A comprehensive review of DC fault protection methods in HVDC transmission systems," *Protection and Control of Modern Power Systems,* vol. 6, no. 1, p. 1, 12 2021.

[116] I. Cowan, G. Chaffey, B. Ponnalagan, M. Rahman, O. Adeuyi, D. Van Hertem, I. Jahn, F. Page, K. Ishida, K. Kuroda and L. Kunjumuhammed, "Demonstration of partially selective HVDC grid protection system with hardware-in-the-loop IEDs," in *15th International Conference on Developments in Power System Protection (DPSP 2020)*, Liverpool, UK, 2020.

[117] M. Wang, G. Chaffey, D. Van Hertem, I. Jahn, F. Page, K. Ishida, K. Kuroda, L. Kunjumuhammed, I. Cowan, B. Ponnalagan, M. Rahman and O. Adeuyi, "Multi-vendor interoperability tests of IEDs for HVDC grid protection," in *15th International Conference on Developments in Power System Protection (DPSP 2020)*, Liverpool, UK, 2020.

[118] M. Wang, W. Leterme, G. Chaffey, J. Beerten and D. Van Hertem, "Multi-vendor interoperability in HVDC grid protection: State-of-the-art and challenges ahead," *IET Generation, Transmission & Distribution,* vol. 15, no. 15, pp. 2153-2175, 8 2021.

[119] Q. Yang, S. Le Blond, R. Aggarwal, Y. Wang and J. Li, "New ANN method for multi-terminal HVDC protection relaying," *Electric Power Systems Research,* vol. 148, pp. 192-201, 7 2017.

[120] Y. Li, Y. Gong and B. Jiang, "A novel traveling-wave-based directional protection scheme for MTDC grid with inductive DC terminal," *Electric Power Systems Research,* vol. 157, pp. 83-92, 2018.

[121] H.-x. Ha and S. Subramanian, "Implementing the protection and control of future DC Grids," Innovation and Technology Department, SAS, Alstom Grid, 2014.

[122] M. Abedrabbo, W. Leterme and D. Van Hertem, "Systematic Approach to HVDC Circuit Breaker Sizing," *IEEE Transactions on Power Delivery,* vol. 35, no. 1, pp. 288-300, 2 2020.

[123] K. Sharifabadi, L. Harnefors, H.-P. Nee, S. Norrga and R. Teodorescu, Design, Control and Application of Modular Multilevel Converters for HVDC Transmission Systems, John Wiley & Sons, Ltd., 2016.

[124] N. A. Belda, C. A. Plet and R. P. P. Smeets, "Analysis of Faults in Multiterminal HVDC Grid for Definition of Test Requirements of HVDC Circuit Breakers," *IEEE Transactions on Power Delivery,* vol. 33, no. 1, pp. 403-411, 2 2018.

[125] M. K. Bucher and C. M. Franck, "Contribution of Fault Current Sources in Multiterminal HVDC Cable Networks," *IEEE Transactions on Power Delivery,* vol. 28, no. 3, pp. 1796-1803, 7 2013.

[126] PROgress on Meshed HVDC Offshore Transmission Networks (PROMOTioN), "D4.2 – Broad comparison of fault clearing strategies for DC grids," 29 November 2019. [Online]. Available: https://www.promotion-offshore.net/fileadmin/PDFs/D4.2_Broad_comparison_of_fault_clearing_strategies_for_DC_grids.pdf. [Accessed 3 February 2023].

[127] A. Schön, A. Lorenz and R. A. A. Valenzuela, "Impedance-based analysis of HVDC converter control for robust stability in AC power systems," in *2022 24th European Conference on Power Electronics and Applications (EPE'22 ECCE Europe)*, Hanover, Germany, 2022.

[128] M. Quester, F. Loku, O. El Azzati, L. Noris, Y. Yang and A. Moser, "Investigating the Converter-Driven Stability of an Offshore HVDC System," *Energies,* vol. 14, no. 8, p. 2341, 4 2021.

[129] CLC/TS 50654-1, "HVDC Grid Systems and connected Converter Stations - Guideline and Parameter Lists for Functional Specifications—Part 1: Guidelines’," CENELEC, 2020.

[130] P. Düllmann, "European offshore grid: On protection system design for radial bipolar multi-terminal HVDC networks," in *CIGRE Session 2022*, Paris, 2022.

[131] CIGRE WG B4.55, "HVDC connection of offshore wind power plants: Technical Brochure 619," CIGRE, Paris, 2015.

[132] VDE Verband der Elektrotechnik, Elektronik, Informationstechnik e.V., "Technical rules for the connection of HVDC systems and generation systems connected via HVDC systems (VDE-AR-N 4131)," Frankfurt am Main, Germany, 2019.

[133] F. Loku, "On converter control interoperability in multi-terminal HVDC networks," RWTH Aachen University, Aachen, 2022.

[134] F. Loku, M. Quester, C. Brantl and A. Monti, "MMC control optimization approach to facilitate DC-side interoperability in MTDC networks," *Electric Power Systems Research,* vol. 203, p. 107639, 2022.

[135] S. D. Tavakoli, E. Sánchez-Sánchez, E. Prieto-Araujo and O. Gomis-Bellmunt, "DC Voltage Droop Control Design for MMC-Based Multiterminal HVDC Grids," *IEEE Transactions on Power Delivery,* vol. 35, no. 5, pp. 2414-2424, 2020.

[136] CIGRÉ JWG B4/B5.59, "TB739: Protection and local control of HVDC-grids," CIGRÉ, 2018.

[137] O. Antoine, L. Papangelis, P. Tielens, K. Karoui, H. Ergun, G. Bastianel, A. Agbemuko, J. Beerten, W. Leterme and D. Van Hertem, "AC/DC hybrid grid modelling enabling a high share of Renewables," European Commission, November 2022.

[138] P. Aristidou, L. Papangelis, X. Guillaud and T. & Van Cutsem, "Modular modelling of combined AC and DC systems in dynamic simulations," in *2015 IEEE PowerTech*, Eindhoven , 2015.

[139] T. V. Cutsem, "Classification of power system stability," University of Liege.

[140] N. Hatziargyriou and e. al, "Definition and Classification of Power System Stability – Revisited & Extended," *IEEE Transactions on Power System,* vol. 36, no. 4, pp. 3271-3281, 2021.

[141] P. Ruffing, N. Collath, C. Brantl and A. Schnettler, "DC Fault Control and High-Speed Switch Design for an HVDC Network Protection Based on Fault-Blocking Converters," *IEEE Transactions on Power Delivery,* vol. 34, no. 1, pp. 397-406, 2019.

[142] CIGRÉ, "Technical Brochure 804: DC grid benchmark models for system studies," CIGRÉ, Paris, 2020.

[143] Ofgem, "Grid Code (GC) GC0137: Minimum Specification Required for Provision of GB Grid Forming (GBGF) Capability (formerly Virtual Synchronous Machine (VSM) Capability) (GC0137)," january 2022.

[144] R. H. Renner, Interaction of HVDC grids and and AC power systems - Operation and Control (Doctoral Thesis), Leuven: KU Leuven – Faculty of Engineering Science, 2016.

[145] B. Johnson, R. Lasseter, F. Alvarado and R. Adapa, "Expandable multiterminal DC systems based on voltage droop," *IEEE Transactions on Power Delivery ,* pp. 1926 - 1932, 1 Oktober 1993.

[146] P. Rault, Dynamic Modeling and Control of Multi-Terminal HVDC Grids, PhD Thesis, Lille: Ecole Centrale de Lille, 2014.

[147] A. Egea-Alvarez, J. Beerten, D. Van Hertem and O. Gomis-Bellmunt, "Hierarchical power control of multiterminal HVDC grids," *Electric Power Systems Research,* vol. 121, no. 1, p. 1–7, 2015.

[148] C. Dierckxsens, K. Srivastava, M. Reza, S. Cole, J. Beerten and R. Belmans, "A distributed DC voltage control method for VSC MTDC systems," *Electric Power,* vol. 82, no. 1, p. 54–58, 2012.

[149] F. Thams, S. Chatzivasileiadis, E. Prieto-Araujo and R. Eriksson, "Disturbance attenuation of DC voltage droop control structures in a multi-terminal HVDC grid," in *2017 IEEE Manchester PowerTech*, Manchester, UK, 2017.

[150] F. Thams, S. Chatzivasileiadis, E. Prieto-Araujo and R. Eriksson, "Disturbance attenuation of DC voltage droop control structures in a multi-terminal HVDC grid," in *IEEE Manchester PowerTech*, 2017.

[151] K. Vrana, J. Beerten, R. Belmans and O. B. Fosso, "A classification of DC node voltage control methods for HVDC grids," *Electric Power Systems Research,* vol. 103, no. 1, pp. 137-144, 2013.

[152] L. Xu, L. Yao and M. Bazargan, "DC grid management of a multi-terminal HVDC transmission system for large offshore wind farms," in *2009 International Conference on Sustainable Power Generation and Supply*, Nanjing, China, 2009.

[153] J. Liang, T. Jing, O. Gomis-Bellmunt, J. Ekanayake and N. Jenkins, "Operation and Control of Multiterminal HVDC Transmission for Offshore Wind Farms," *IEEE Transactions on Power Delivery,* vol. Volume 26, no. 4, pp. 2596 - 2604, 2011.

[154] A. Egea-Alvarez, S. Fekriasl, F. Hassan and O. Gomis-Bellmunt, "Advanced Vector Control for Voltage Source Converter Connected to Weak Grids," *IEEE Transactions on Power Systems,* vol. 30, no. 6, 2015.

[155] Y. Gu and T. C. Green, "Power System Stability With a High Penetration of Inverter-Based Resources," *Proceedings of the IEEE,* vol. 111, no. 7, pp. 832-853, 2023.

[156] R. Musca, A. Vasile and G. Zizzo, "Grid-forming converters. A critical review of pilot projects and demonstrators," *Renewable and Sustainable Energy Reviews,* 2022.

[157] Y. Chen, R. Hesse, D. Turschner and H. P. Beck, "Dynamic properties of the virtual synchronous machine (VISMA)," *Renewable Energy and Power Quality Journal,,* vol. 1, no. 9, p. 755–759, 2011.

[158] J. Suul and S. D’Arco, "GRID-FORMING CAPABILITIES OF HVDC CONVERTERS Overview of concepts, motivations and challenges,”," SINTEF Energy Research, Trondheim, 2021.

[159] E. Rokrok, T. Qoria, A. Bruyere, B. Francois and X. Guillaud, "Effect of Using PLL-Based Grid-Forming Control on Active Power Dynamics Under Various SCR," in *IECON 2019 - 45th Annual Conference of the IEEE Industrial Electronics Society*, 2019.

[160] A. Belila, Y. Amirat, M. Benbouzid, E. M. Berkouk and G. Yao, "Virtual synchronous generators for voltage synchronization of a hybrid PV-diesel power system," *International Journal of Electrical Power and Energy Systems,* vol. 117, January 2019.

[161] A. Jain, J. N. Sakamuri and N. A. Cutululis, "Grid-forming control strategies for black start by offshore wind power plants," *Wind Energy Science,* vol. 5, no. 4, p. 1297–1313, 2020.

[162] E. Rokrok, "Grid-forming control strategies of power electronic converters in transmission grids: application to HVDC link," 2022.

[163] C. Collados-Rodriguez, "Integration of an MMC-HVDC Link to the Existing LCC-HVDC Link in Balearic Islands Based on Grid-Following and Grid-Forming Operation," *IEEE Transactions on Power Delivery,* vol. 37, no. 6, p. 5278–5288, 2022.

[164] R. Yang, G. Shi, X. Cai, C. Zhang and G. Li, "Internal Energy Based Grid-Forming Control for MMC-HVDC Systems with Wind Farm Integration," in *2021 IEEE 12th Energy Conversion Congress & Exposition - Asia (ECCE-Asia)*, 2021.

[165] T. M. Haileselassie, "Dynamics and Operation of Multi-terminal VSC-," NTNU, 2012.

[166] C. Dierckxsens, K. Srivastava, M. Reza, S. Cole, J. Beerten and a. R. Belmans, "A distributed DC voltage control method for VSC MTDC systems," *Electric Power Systems Research,* 2012.

[167] T. K. Vrana, "System Design and Balancing Control of the North Sea Super Grid," NTNU, 2013.

[168] Abdalrahman, Pagnani, Mirtaheri, Soløst, C. Ramos, Dall, Zou, Lu, Ndreko, Baranski, Bogner, Karrari, Qoria, Tveit and Costan, "Grid-Forming Functional Requirements for HVDC Converter Stations and DC-Connected PPMs in Multi-terminal Multi-vendor HVDC systems," EU Project InterOPERA —101095874 — HORIZON-CL5-2022-D3-01, Brussels, 2024.

[169] A. Jain, Ö. Göksu and N. Cutululis, "Control Solutions for Blackstart Capability and Islanding Operation of Offshore Wind Power Plants," in *17th International Workshop on Large-Scale Integration of Wind Power into Power Systems as well as on Transmission Networks for Offshore Wind Power Plants*, Energynautics GmbH, 2018.

[170] D. Pagnani, F. Blaabjerg, C. Leth Bak, F. Faria da Silva, L. Kocewiak and J. Hjerrild, "Offshore wind farm black start service integration: Review and outlook of ongoing research," *Energies,* vol. 13, no. 23, pp. -, 2013.

[171] J. Sakamuri, Ö. Göksu, Bidadfar, O. Saborío-Romano, A. Jain and N. Cutululis, "Black Start by HVdc-connected Offshore Wind Power Plants," in *IECON 2019 - 45th Annual Conference of the IEEE Industrial Electronics Society*, Lisbon, Portugal, 2019.

[172] C. Klein, P. Düllmann, L. Osterkamp, N. Corte, P. Ruffing, S. Iftekharul Huq, A. Ahmedi, D. Yates and W. Leterme, "Black start of HVDC links via grid-forming wind turbines: sensitivity analysis and technical requirements," p. 266 – 273, 26-28 September 2023.

[173] CENELEC, *CLC/TS 50654-1:2020 : HVDC Grid Systems and connected Converter Stations - Guideline and Parameter Lists for Functional Specifications - Part 1: Guidelines,* CENELEC, 2020.

[174] M. Pertl, T. Weckesser, M. Rezkalla and M. Marinelli, "Transient stability improvement: a review and comparison of conventional and renewable-based techniques for preventive and emergency control," *Electrical Engineering,* vol. 100, pp. 1701-1718, 2018.

[175] R. Shah, J. C. Sánchez, R. Preece and M. Barnes, "Stability and control of mixed AC-DC systems with VSC-HVDC: a review," *IET Generation Transmission and Distribution,* vol. 12, pp. 2207-2219, 2017.

[176] S. Johansson, G. Asplund, E. Jansson and R. Rudervall, "Power system stability benefits with VSC DC-transmission systems," in *CIGRE Session*, Paris (France), 2004.

[177] L. Zhang, "Power System Reliability and Transfer Capability Improvement by VSC- HVDC (HVDC Light)," in *Cigr\'{e} Conference in Estonia*, 2007.

[178] H. F. Latorre, M. Ghandhari and L. Söder, "Active and reactive power control of a VSC-HVdc," *Electric Power Systems Research,* vol. 78, pp. 1756-1763, 2008.

[179] A. Fuchs, M. Imhof, T. Demiray and M. Morari, "Stabilization of Large Power Systems Using VSC - HVDC and Model Predictive Control," *IEEE Transactions on Power Delivery,* vol. 29, pp. 480-488, 2014.

[180] L. Sigrist, F. Echavarren, L. Rouco and P. Panciatici, "A fundamental study on the impact of HVDC lines on transient stability of power systems," in *Proc. IEEE/PES PowerTech Conference, Eindhoven, Netherlands*, 2015.

[181] J. Machowski, P. Kacejko, L. Nogal and M. Wancerz, "Power system stability enhancement by WAMS-based supplementary control of multi-terminal HVDC networks," *Control Engineering Practice,* vol. 21, pp. 583-592, #may# 2013.

[182] R. Eriksson, "Coordinated Control of Multiterminal DC Grid Power Injections for Improved Rotor-Angle Stability Based on Lyapunov Theory," *IEEE Transactions on Power Delivery,* vol. 29, pp. 1789-1797, 2014.

[183] G. Tang, Z. Xu, H. Dong and Q. Xu, "Sliding Mode Robust Control Based Active-Power Modulation of Multi-Terminal HVDC Transmissions," *IEEE Transactions on Power Systems,* vol. 31, pp. 1614-1623, 2016.

[184] O. Kotb, M. Ghandhari, R. Eriksson, R. Leelarujic and V. K. Sood, "Stability enhancement of an interconnected AC/DC power system through VSC-MTDC operating point adjustement," *Electric Power Systems Research,* vol. 151, pp. 308-318, 2017.

[185] J. Renedo, A. García-Cerrada and L. Rouco, "Active Power Control Strategies for Transient Stability Enhancement of AC/DC Grids With VSC-HVDC Multi-Terminal Systems," *IEEE Transactions on Power Systems,* vol. 31, pp. 4595-4604, 2016.

[186] T. M. Haileselassie and K. Uhlen, "Primary frequency control of remote grids connected by multi-terminal HVDC," in *Proc. IEEE/PES General Meeting, Providence, RI, USA*, 2010.

[187] N. R. Chaudhuri, R. Majumder and B. Chaudhuri, "System Frequency Support Through Multi-Terminal DC (MTDC) Grids," *IEEE Transactions on Power Systems,* vol. 28, pp. 347-356, 2013.

[188] M. H. Haque, "Improvement of First Swing Stability Limit by Utilizing Full Benefit of Shunt FACTS Devices," *IEEE Transactions on Power Systems,* vol. 19, pp. 1894-1902, 2004.

[189] M. H. Haque and P. Kumkratug, "Application of Lyapunov stability criterion to determine the control strategy of a STATCOM," *IEE Proc. Gener. Transm. Distrib.,* vol. 151, pp. 415-420, 2004.

[190] M. A. Abido, "Power system enhancement using FACTS controllers: A review," *The Arabian Journal for Science and Engineering,* vol. 34, pp. 153-172, 2009.

[191] I. Martnez Sanz, B. Chaudhuri and G. Strbac, "Coordinated Corrective Control for Transient Stability Enhancement in Future Great Britain Transmission System," in *Proc. 19th Power Systems Computation Conference (PSCC), Genoa, Italy*, 2016.

[192] N. R. Trinh, I. Erlich, M. Zeller and K. Wuerflinger, "Enhancement of grid transient stability using MMC-VSCH-VDC control," in *Proc. 11th IET Conference on AC and DC Power Transmission, Birmingham, UK*, 2015.

[193] J. Renedo, A. García-Cerrada and L. Rouco, "Reactive-Power Coordination in VSC-HVDC Multi-Terminal Systems for Transient Stability Improvement," *IEEE Transactions on Power Systems,* vol. 32, pp. 3758-3767, 2016.

[194] J. Renedo, L. Rouco, A. Garcia-Cerrada and L. Sigrist, "A communication-free reactive-power control strategy in VSC-HVDC multi-terminal sytems to improve transient stability," *Electric Power Systems Research,* vol. 174, pp. 105854-(1-13), 2019.

[195] R. Rosso, X. Wang, M. Liserre, X. Lu. and S. Engelken, Grid-Forming Converters: Control Approaches,Grid-Synchronization, and Future Trends—A Review, ,: IEEE, 2021, pp. 93-109.

[196] Y. -J. H. M. K. S. K. K. N. a. A. N. A. Abdalrahman, "Grid Forming Control for HVDC Systems: Opportunities and Challenges," in *2022 24th European Conference on Power Electronics and Applications (EPE'22 ECCE Europe)*, Hanover, Germany, 2022.

[197] M. Panteli, P. Mancarella, D. Trakas, E. Kyriakides and N. and Hatziargyriou, "Metrics and quantification of operational and infrastructure resilience in power systems," *IEEE Transactions on Power Systems,* vol. 32, pp. 4732--4742, 2017.

[198] German TSO, "Netzentwicklungsplan Strom 2037/2045," www.netzentwicklungsplan.de, Berlin, 2023.

[199] NationalGridESO, "NatNGESO NIA Black Start Tech - Capability and Readiness," NationalGridESO, 2019.

[200] J. Rimez, K. Geens, L. Schyvens and L. a. P. T. Yang, "Black start and system restoration utilizing a the NEMO Modular Multilevel Converter – a practical test in the Belgium transmission system," Cigré, Cigre Session 48, 2020.

[201] Ö. Göksu, "Black Start and Island Operation Capabilities of Wind Power Plants," in *Wind Integration Workshop (proceedings)*, Berlin, 2017.

[202] C. Klein, "Abschlussbericht: HVDC BLADE, Demonstration der Schwarzstartfähigkeit von über HGÜ-angebundenen Offshore Windparks," Leibnitz- Inforamtionszentrum Technik und Naturwissenschaften Universitätsbibliothek (TIB), Hannover, 2024.

[203] O. S. J. N. S. a. N. A. C. A. Jain, "Blackstart from HVDC-connected offshore wind: Hard versus soft energization," in *IET Renewable Power Generation*, doi: 10.1049/rpg2.12010, IET, 2020, pp. 127-138.

[204] O. S. J. N. S. a. N. A. C. A. Jain, "Blackstart from HVDC-connected offshore wind: Hard versus soft energization," in *IET Renewable Power Generation*, doi: 10.1049/rpg2.12010., IET, 2020, pp. vol. 15, no. 1,127-138.

[205] S. Bolik and e. al., "HVDC connection of offshore wind power plants - TB 619," CIGRÉ, Paris, 2015.

[206] J. C. Gonzalez-Torres, R. Mourouvin, K. Shinoda, A. Benchaib and A. Zama, "A simplified approach to model grid-forming controlled MMCs in power system stability studies," in *2021 IEEE PES Innovative smart grid technologies Europe (ISGT Europe)*, 2021.

[207] ENTSOE, "Anslysis of CE inter-area oscillations of 1st december 2016," 2017.

[208] T. Q., X. Z. and X. L., "Reduced Switching-Frequency Modulation and Circulating Current Suppression for Modular Multilevel Converters," *IEEE Trasactions on Power Delivery,* vol. 26, no. 3, pp. 2009-2017, 2011.

[209] L. K. J. R. M. H. M. &. W. X. Harnefors, "A Universal Controller for Grid Connected Voltage-Source Converters.," *IEEE Journal of Emerging and Selected Topics in Power Electronics,,* vol. 9, no. 5, pp. 5761 - 5770, 2021.

[210] Y. Lamrani, F. Colas, T. Van Cutsem and e. al, "On the Stabilizing Contribution of Different Grid-Forming Controls to Power Systems," *TechRxiv,* 2024.

[211] I. Sadeghkhani, M. E. Hamedani Golshan, J. M. Guerrero and A. Mehrizi-Sani, "A Current Limiting Strategy to Improve Fault Ride-Through of Inverter Interfaced Autonomous Microgrids," *IEEE Transactions on Smart Grid,* vol. 8, no. 5, pp. 2138-2148, 2017.

[212] S. P. Me, S. Zabihi, F. Blaabjerg and B. Bahrani, "Adaptive Virtual Resistance for Postfault Oscillation Damping in Grid-Forming Inverters," *IEEE Transactions on Power Electronics,* vol. 37, no. 4, pp. 3813-3824, 2022.

[213] Z. Zeng, P. Bhagwat, M. Saeedifard and D. Groß, " "Hybrid Threshold Virtual Impedance for Fault Current Limiting in Grid-Forming Converters,," in *IEEE Energy Conversion Congress and Exposition (ECCE)*, Nashville, 2023.

A. Details about simulations of post-fault recovery process

A four-terminal MMC-based MTDC network with a DC voltage rating of ±525 kV is discussed in Figure 2.31 of section 2.3. The offshore AC system consists of converter stations and aggregated average-value model wind farms. In the applied networks, offshore converters are labelled MMC1 and MMC2. The offshore converter is connected to the offshore AC system via D-Y transformers. The rating of this transformer is 275 kV/220 kV, 2 GVA. Besides, this converter transformer is connected to a wind turbine transformer. This transformer has a voltage ratio of 220 kV/66 kV and acts as a VA scaled-up transformer. Thus, a power rating of 2 GW can be achieved by choosing the proper scaling factor. The lower voltage end of this transformer is connected to the wind turbine.

In each network topology, the converter station per pole (i.e., positive and negative pole) comprises four key elements: converter transformer, startup insertion resistor, arm reactor, and valve. The converter transformer is a two winding, star-delta configuration. A tertiary winding may provide auxiliary power to the converter station from the AC system. However, in this study, the tertiary winding is absent. The AC grid side is connected to the transformer's star side, and the DC grid side to the delta side. The delta connection prevents the low-frequency zero sequence voltage from being injected into the AC system.

Furthermore, the leakage inductance of the transformer and the arm rector provide sufficient reactance between the AC-side voltage and the valve required to control the AC grid current. Due to the near-pure sinusoidal waveform of the converter's voltage, a standard AC transformer is adopted. This transformer also provides galvanic isolation between the AC and DC grids.

The pre-insertion resistors are placed between the AC bus and the converter transformer. To limit the inrush current produced by charging the sub-module (SM) capacitors, DC filters, DC line/cable, and the remote station, the resistor is switched on for a few seconds and bypassed after a dedicated set period. The arm reactor is connected in series with a converter valve. In this work, the arm reactor is placed on the AC side of the converter. The arm reactor limits the circulating current between the converter valves.

Furthermore, it also limits the rate of rise of the fault current. Each converter valve consists of n SMs. In the presented networks, the number of SMs is selected based on the geographical location. For the studied cases, a half-bridge (HB) topology of the SM is selected, which consists of three main states: Bypass, Blocked, and Inserted state. However, the voltage across the SM is determined by the current direction.

With the high number of SMs, the AC side of the valve provides a smooth AC waveform. The Type 5, i.e., Average Value Models (AVM) [106] based on switching functions, converter model is used in these networks. To capture the accurate dynamics of the converter station, it is modelled by using small time steps of RTDS.

Table 4.1 lists the converter station parameters with associated values used in this work. Further, to reduce the tedious modelling time, control, electrical parameters, and limits values are scripted using draft variables. These draft variables are controlled via a script at the start simulation. This script is written in C++ in an RSCAD /RTDS environment.